IMPULSE VOLTAGE DISTRIBUTION AND TRANSFER IN MINERAL OIL AND RTEmp-FILLED BARREL-TYPE TRANSFORMERS

by

full name of author
Wilson Elzaer Kazibwe

A thesis
presented to the University of Manitoba
in partial fulfillment of the
requirements for the degree of
Master of science
in
Department of Electrical Engineering

Winnipeg, Manitoba

✓(c) full name of author, 1984

1984

IMPULSE VOLTAGE DISTRIBUTION AND TRANSFER IN MINERAL OIL AND RTEmp-FILLED BARREL-TYPE TRANSFORMERS

BY

WILSON ELZAER KAZIBWE

A thesis submitted to the Faculty of Graduate Studies of the University of Manitoba in partial fulfillment of the requirements of the degree of

MASTER OF SCIENCE

© 1984

Permission has been granted to the LIBRARY OF THE UNIVERSITY OF MANITOBA to lend or sell copies of this thesis, to the NATIONAL LIBRARY OF CANADA to microfilm this thesis and to lend or sell copies of the film, and UNIVERSITY MICROFILMS to publish an abstract of this thesis.

The author reserves other publication rights, and neither the thesis nor extensive extracts from it may be printed or otherwise reproduced without the author's written permission.

ABSTRACT

A barrel-type distribution transformer has been represented by lumped circuit parameters. The responses of the impulsed and non-impulsed windings to surges originating from either the low- or the high-voltage side have been predicted through the use of the Electromagnetics Transients Program. Theoretical and experimental results have been found to be in good agreement. The relative importance of various winding parameters has been determined. Reduction of the equivalent network of the transformer has been carried out. Its use has been found to yield results of good accuracy. An alternative design of the same transformer has been considered. The effect of change, in the winding design, on the response to surges has been evaluated. The results have revealed that the new design exhibits a more uniform distribution of surge voltage and is less susceptible to failure due to transferred surges. The breakdown and conduction characteristics of RTEmp, an alternative transformer oil, have been experimentally studied. Theoretical evaluation of stress distribution in an RTEmp-filled transformer has been carried out. The studies have revealed that there is no significant difference between the voltage stress distribution of an RTEmp-filled and that of the mineral oil transformer.

ACKNOWLEDGEMENTS

The author wishes to express his appreciation to his supervisor, Prof. M.R. Raghuveer, for the invaluable guidance during the course of this work.

Special thanks go to Carte Electric ltd., Winnipeg, for financial support; together with the fruitful discussions with Messrs. T. Bialek, J. Cross and B. Klaponski.

The technical assistance of G.H. Toole is gratefully acknowledged. Gratitude is extended to R. Kuffel for his help with RTEmp experiments.

Dr. A.M.S. Katahoire deserves thanks for his inspiration.

To date, the author continues to incur indebtedness to his mother, Mrs. Mary Kaate for her love and support; brother, Prof. H.M Sendaula, for his encouragement and generosity.

CONTENTS

ABSTRACT iv

ACKNOWLEDGEMENTS v

Chapter page

I. INTRODUCTION 1

Format of Dissertation 5

II. MODELLING OF TRANSFORMER WINDINGS 6

Transformer Description 6
Determination of the Electrical Circuit Equivalent of the Transformer 7

III. DETERMINATION OF WINDING CONSTANTS 13

Winding Resistance 13
Direct-current Resistance 13
Impulse Resistance 15
Interturn Capacitance 18
Layer-to-Layer Capacitance 21
Capacitance between the Innermost High-voltage Layer and the Outermost Low-voltage Layer . . 22
Capacitance between the Outermost High-voltage layer and Tank and the Capacitance between Sections on different Limbs 22
Coil-to-tank Capacitance 23
Coil-to-coil Capacitance 24
Section-to-section Capacitance 26
layer-to-earth capacitance 27
Computation of Self-inductance 29
Calculation of Self-inductance using the Hexagonal shape 34
Computation of Self-inductance of a Straight Conductor Segment 37
Determination of Layer-to-layer Mutual-inductance 42
Section-to-section Mutual-inductance 44

IV. EXPERIMENTAL DETERMINATION OF IMPULSE VOLTAGE DISTRIBUTION 48

V. METHOD OF SOLUTION AND COMPUTATION OF IMPULSE VOLTAGE DISTRIBUTION 52

The Electromagnetic Transients Program 52
Computation of Impulse Voltage Distribution 54
Simplification of the Transformer Models and an Alternative to the EMTP Solution Technique . . 66
Simplification of Transformer Models 67
An Alternative to the EMTP Solution Technique . . 72

VI. STUDY OF THE BREAKDOWN AND CONDUCTION CHARACTERISTICS OF RTEmp AND THE SIMULATION OF AN RTEmp-FILLED TRANSFORMER 75

Test Chamber and Electrodes 75
Breakdown Tests 77
Determination of Conduction Characteristics of RTEmp 79
Computation of Impulse Voltage Distribution Along the Windings of an RTEmp-filled Transformer . . 86

VII. VARIATION OF DESIGN PARAMETERS 94

Thickness of Formel Coating 94
Clearance of Coils from the Tank Wall 97
Number of Sections per High-voltage Coil 99

VIII. SURGE TRANSFERENCE FROM AN IMPULSED TO A NONIMPULSED WINDING 113

IX. CONCLUSIONS AND FUTURE RESEARCH 135

Appendix page

A. THE FORTRAN COMPUTER PROGRAM USED TO COMPUTE WINDING RESISTANCE 141

B. CALCULATION OF THE CONSTANTS CHARACTERISING IMPULSE WAVE SHAPES 144

C. THE FORTRAN COMPUTER PROGRAM USED TO COMPUTE INTERTURN CAPACITANCE 149

D. FORTRAN PROGRAM USED TO CALCULATE LAYER-TO-LAYER CAPACITANCE 151

E. FORTRAN COMPUTER PROGRAM FOR CALCULATING SECTION-TO-SECTION CAPACITANCE 154

F. THE FORTRAN COMPUTER PROGRAM FOR CALCULATING SELF-INDUCTANCE USING THE HEXAGONAL REPRESENTATION . 156

G. THE FORTRAN PROGRAM FOR COMPUTING SELF-INDUCTANCE USING THE CIRCULAR REPRESENTATION DEPICTED IN FIG. 3.13 177

H. EMTP COMPANION NETWORK MODELS 180

I. SIMPLIFICATION OF THE EQUIVALENT CIRCUIT OF THE TRANSFORMER 183

J. THE EMTP JOB FORMAT 191

K. PROPERTIES OF RTEmp 193

LIST OF FIGURES

Figure		Page
2.1	Transformer Construction	6
2.2	Equivalent Circuit of a Layer	8
2.3	Model of a Section of the Transformer	9
2.4	Transformer Model	11
3.1	Experimental Set-up for measurement of dc resistance	14
3.2	Triangular Wave	16
3.3	Voltage Distribution in a Layer of n Turns	18
3.4	Coil-to-coil and Coil-to-tank Capacitors	22
3.5		
	(a) The four HV coils	
	(b) Representation of the HV coils	23
3.6	Conductor Configuration formed by Layers in opposite Sections	26
3.7	Conductor Configuration formed by Layers and end Plate	28
3.8	Shape of Winding Turn	30
3.9	Hexagonal Representation of Turns	31
3.10	Turn representation obtained by replacing the curved portions by rectangles of the same area ...	31
3.11	Turn representation; turn enclosed by rectangle	32
3.12	Representation of a turn; the area of the circle is equal to that of the rectangle enclosing the turn ..	33

Figure		Page
3.13	Representation of a turn; the diameter of the circle is equal to the diagonal of the square portion of the turn	33
3.14	Turn representation derived by excluding the curved portions	34
3.15	Two-turn Layer	35
3.16	Current filaments inclined at each other	38
4.1	Experimental Set-up for Impulse voltage Distribution tests	49
4.2	Modified Inter-section connection	50
5.1(a)	Resistive element	
(b)	Circuit Element Model for a Capacitor	
(c)	Circuit Element Model for an Inductor	53
5.2	Impulse voltage distribution along the HV winding; hexagonal turn representation 1/50 μs wave	56
5.3	Impulse voltage distribution along the HV winding; hexagonal turn representation 1/50 μs wave chopped at 1 μs	57
5.4	Impulse voltage distribution along the HV winding; hexagonal turn representation 0.5/2.5 μs wave	58
5.5	Impulse voltage distribution along the HV winding; turn representation as in Fig. 3.13: 1/50 μs wave	59

Figure		Page
5.6	Impulse voltage distribution along the HV winding; turn representation as in Fig. 3.13: 1/50 μs wave chopped at 1 μs	60
5.7	Impulse voltage distribution along the HV winding; turn representation as in Fig. 3.13: 0.5/2.5 μs wave	61
5.8	Impulse voltage distribution along the HV winding; hexagonal turn representation and the representation depicted in Fig. 3.13: 1/50 μs wave	62
5.9	Impulse voltage distribution along the HV winding; hexagonal turn representation and the representation depicted in Fig. 3.13: 1/50 μs wave chopped at 1 μs	63
5.10	Impulse voltage distribution along the HV winding; hexagonal turn representation and the representation depicted in Fig. 3.13: 0.5/2.5 μs wave	64
5.11	Voltage-time plot at 2% of winding from line end computed using original and reduced networks: 1/50 μs wave response ...	69
5.12	Voltage-time plot at 25% of winding from line end computed using original and reduced networks: 1/50 μs wave response ...	70

Figure		Page
5.13	Voltage-time plot at 75% of winding from line end computed using original and reduced networks: 1/50 μs wave response ...	71
6.1	Test Chamber	76
6.2	Experimental Assembly for Breakdown Tests	78
6.3	Experimental Set-up for Investigating the Conduction Characteristics of RTEmp	80
6.4	Current-time plots for RTEmp fluid	81
6.5(a)	Impulse voltage of positive polarity	
(b)	Time-derivative of the Impulse voltage	85
6.6	Time-derivative of an impulse voltage of negative polarity	86
6.7	Computed impulse voltage distribution along the HV winding of mineral oil and RTEmp-filled transformers: 1/50 μs wave	91
6.8	Computed impulse voltage distribution along the HV winding of mineral oil and RTEmp-filled transformers: 1/50 μs wave chopped at 1 μs	92
6.9	Computed impulse voltage distribution along the HV winding of mineral oil and RTEmp-filled transformers: 0.5/2.5 μs wave	93
7.7	Circuit model of the six-section transformer	100
7.8	Computed impulse voltage distribution along the HV windings of the four-section and six-section transformers: 1/50 μs wave	107

Figure		Page
7.9	Computed impulse voltage distribution along the HV windings of the four-section and six-section transformers:1/50 μs wave chopped at 1μs ..	108
7.10	Computed impulse voltage distribution along the HV windings of the four-section and six-section transformers: 0.5/2.5 μs wave	109
7.11	Initial Voltage Distribution Circuit for the Four-section Transformer	111
7.12	Initial Voltage Distribution Circuit for the Six-section Transformer	111
8.1	The four components of the transferred Voltages and their Resultant	114
8.2	Equivalent Circuit of Electrostatic Transference between windings	115
8.3	Equivalent Circuit of the Electromagnetic Transference between windings	116
8.4	Circuit Model for the Low- and High-voltage Windings	118
8.5	Domestic Load connected to the Low-voltage Winding ...	128
8.6	Non-interlaced Low-voltage Winding	131
8.7	Interlaced Low-voltage Winding	131
B1	Curves for deriving constants a and b from the ratio between the time to fall to half of the maximum value and the time to reach the peak (t2/t1)	147

Figure		Page
H1	Capacitive branch	181
H2	Capacitor Model	181
H3	Inductor	182
H4	Inductor Model	182
I1(a)	Two identical series-connected circuit segments	
(b)	Simplified Equivalent Network	183
I2(a)	Electric Network Equivalent of two consecutive Transformer Layers	
(b)	Simplified Equivalent network	
(c)	Further Simplified Equivalent Network	184
I3	Electrical network equivalent of a transformer section; section-to-section and layer-layer capacitance excluded	187
I4	Innermost three and outermost two layers of the transformer section	188
I5	Application of star-delta transformation to innermost and outermost layers in Fig. I4	188
I6	Network obtained by combining the capacitive elements in Fig. I5	189
I7	Reduced network	189
I8	Further reduced network	190

LIST OF TABLES

Table		Page
3.1	Direct-current and impulse resistance	17
3.2	Interturn Capacitance	20
3.3	Layer-to-layer Capacitance	21
3.6	Section-to-section Capacitance	27
3.7	Layer-to-earth Capacitance	29
3.8	Self-inductance values obtained by using different turn representations	41
3.9	Computer Time required to Determine Self-inductance values	41
3.10	Layer-to-layer mutual-inductance	45
4.1	Specifications of the recurrent Surge Generator	48
5.1	Maximum layer-to-layer and section-section voltages ...	65
5.2	Circuit element models for the Integral of voltage method	73
6.1	Breakdown Voltages for the 0.25 cm Spacing	79
6.2	Current Monitor Characteristics	81
6.3	Layer-to-layer Capacitance of RTEmp-filled and mineral oil transformers	88
6.4	Coil-to-coil and coil-to-tank Capacitances of the mineral oil and RTEmp-filled Transformers	88
6.5	Capacitance between the outermost LV and innermost HV Layers of the Mineral oil and RTEmp-filled Transformers	89
6.6	Maximum Layer-to-layer and Section-to-section voltages for Mineral oil and RTEmp-filled Transformers	90

Table		Page
7.1	Interturn capacitance for the three thicknesses of formel	95
7.2	Maximum layer-to-layer and section-to-section voltage stresses for different thicknesses of formel coating	96
7.3	Maximum Layer-to-layer and Section-to-section Voltage Stresses for the Various Clearances of the Coils from the tank	98
7.30	Winding Resistance of the six-section Transformer	101
7.31	Interturn Capacitance of the six-section Transformer ..	101
7.32	Layer-to-layer Capacitance for the six-section transformer	102
7.33	Self-inductance for the Six-section Transformer computed using the turn Representation shown in Fig. 3.9	103
7.34	Layer-to-layer Mutual-inductance for the six-section Transformer	103
7.35	Section-to-section Capacitance for the Six-section Transformer	105
7.36	Layer-to-earth Capacitance for the Six-section transformer	105
7.4	Maximum layer-to-layer and section-to-section Voltages for the six-section and the four-section Transformers	106
8.1	Layer-to-layer Capacitance for the LV Winding of the Four-section Transformer	119

Table		Page
8.2	Self-inductance for the LV Winding of the four-section Transformer	120
8.3	Layer-to-layer Mutual-inductance for the LV winding of the Four-section Transformer	120
8.4	Resistance for the LV of the Four-section Transformer ..	123
8.5	Mutual-inductance between the LV and HV of the four-section transformer	124
8.6	Layer-to-layer Capacitance for the LV of the six-section transformer	125
8.7	Self-inductance of the LV of the six-section Transformer	125
8.8	Mutual-inductance between the LV and HV of the six-section transformer	127
8.9	Surges transferred from the HV to the LV of the Four-section transformer	129
8.10	Surges Transferred from the HV to the LV of the six-section Transformer	130
8.11	Surges transferred from the LV to HV of the four-section transformer	132
8.12	surges transferred from the LV to the HV of the six-section transformer	133
B1	Impulse wave constants	148
K1	Electrical properties of RTEmp	193
K2	Physical and Chemical properties of RTEmp	194
K3	Thermal properties of RTEmp	194

Chapter I

INTRODUCTION

With the growing need for economical design of transformer insulation, it is desirable to be able to predict, at the design stage, the impulse voltage distribution throughout the windings.

Since the fabrication of the first transformer in 1882 ,the problem of insulation breakdown due to uneven distribution of impulse voltages along transformer windings has received considerable attention.

Quantitative analysis of the effect of impulse waves on transformer windings was first reported by Wagner [1] in 1915. He advocated the standing-wave theory according to which oscillations in the windings can be resolved into standing waves, that is, harmonics both in space and time. To simplify the computations, a unit step applied voltage and a transformer having uniformly distributed capacitance and inductance were assumed. In spite of these assumptions, the theory required tedious work to obtain design data. Therefore, it was not readily applicable to insulation design [2].

An exposition of the principles of the travelling-wave theory was later given by Rudenberg [2] for a unit step applied voltage and for windings with uniformly distributed parameters. In the travelling-wave theory analysis, an incident wave is represented by an infinite series of sinusoidal components. According to this

theory, a transformer winding is able to propagate only those oscillations having a frequency below a critical value; higher frequency oscillations establish standing exponential distributions similar to the initial distribution of the standing-wave analysis. This method does not take into account the effect of mutual coupling between winding sections.

Lewis [3] suggested the representation of the transformer winding by a ladder-type network composed of a finite number of uniform sections. He analyzed this network for a unit step voltage and took into account the effect of mutual-inductance by modifying the self-inductance values.

In 1953, Abbeti [4] introduced the use of scale-models in conjunction with a recurrent-surge oscillograph to predict the impulse voltage distribution in larger power transformers. Although this method can be used to obtain results of sufficient accuracy for design purposes, it suffers from a number of disadvantages. In addition to the complexities involved in the calculation of scaling factors, models are expensive to construct and each type of transformer requires a different model. Appreciating these problems, Waldvogel and Rouxel [5], and later Macwhirter, Fahnkopt et al.[6] modified Lewis's method [3]. They investigated the response of transformer windings to surges by using an analog computer based on the equivalent circuit. However, the use of the analog computer dictated the assumption of uniform winding sections; which implies that only transformers with uniformly distributed parameters can be analyzed.

Dent, Hartil et al.[7], further modified Lewis's theory and developed a method readily applicable to the computation of voltage stress distribution along uniform and non-uniform windings for any form of applied voltage wave, including chopped waves. In this method, the simultaneous differential equations which result from circuit relationships are solved by the Runge-Kutta method with the help of a digital computer. However, the computer time and storage required to analyze circuit models make it uneconomical to use this approach as a routine design procedure.

Recent papers on the subject of impulse phenomena [8,9] have indicated that by using new techniques of circuit analysis, for example, the companion-network approach, in conjunction with efficient matrix algorithms, the work involved in setting up the transformer models and the time of computation can be reduced significantly. This makes it economically feasible to incorporate the analysis of impulse voltage distribution into the routine design procedure.

To date, only transformers with disc-type windings have been analyzed for impulse voltage distribution. However, some transformers, notably the distribution type, are of barrel-type construction, that is, they comprise of layers wound one over the other.

In this study, a barrel-type transformer is modelled. The circuit model is analyzed to determine the voltage stress distribution along both the high- and the low-voltage windings for surges emanating from either the low- or the high-voltage side. The ef-

fect of different wave shapes, including chopped waves, is investigated. The model is solved by the Electromagnetics Transients Program (EMTP) [10].

In order to evaluate the accuracy of the EMTP simulation, impulse tests at low voltage were carried out on the actual transformer using a recurrent surge generator.

A systematic determination of the effect of changing various parameters was carried out.

Due to the nature of the modelling employed, the number of elements in the equivalent network for a particular case, could be prohibitively large. A technique of network reduction was developed; its implementation is shown to yield results of good accuracy.

In an attempt to make transformers using nontoxic liquid dielectric-coolants, RTEmp fluid is being considered as an alternative to mineral oil. The modelling of an RTEmp-filled transformer requires the knowledge of the breakdown and conduction characteristics of the fluid. RTEmp is known to conduct at 60 Hz. However, the impulse and power frequency resistances are different. Therefore, tests were carried out to investigate both the breakdown and conduction characteristics of RTEmp at various temperatures for positive and negative polarities of impulse voltage. This enabled the study of impulse voltage distribution in an RTEmp-filled transformer to be carried out.

1.1 FORMAT OF DISSERTATION

In Chapter II, the description of a distribution transformer is given and its electric cicuit model is developed. Chapter III deals with the determination of the transformer winding constants. The experimental determination of impulse voltage distribution along the transformer windings is given in Chapter IV. The method of solution and computation of voltage stress distribution are given in Chapter V. In Chapter VI, the experimental determination of the breakdown and conduction characteristics of RTEmp fluid is given and an RTEmp-filled transformer is modelled. The effects, on impulse voltage distribution, of the variation of design parameters are discussed in Chapter VII. The transference of surge from an impulsed to a nonimpulsed winding is dealt with in Chapter VIII. Finally, the conclusions of this thesis and suggestions for further work are summarized in Chapter IX.

Chapter II

MODELLING OF TRANSFORMER WINDINGS

2.1 TRANSFORMER DESCRIPTION

The electric circuit model is to be developed for a single-phase, core-type transformer with concentric windings and a rating of 75 kVA, 16000/120/240 V.

The transformer comprises of two core limbs of rectangular cross-section. On each limb two low-voltage sections are wound one over the other. Each of the two sections consists of seven layers made out of full-width aluminium strip conductor.

The high-voltage winding on each limb is made up of two sections wound one below the other and over the low-voltage winding; each section consists of eleven layers wound using flattened aluminium wire.

The construction of the transformer is depicted in Fig. 2.1.

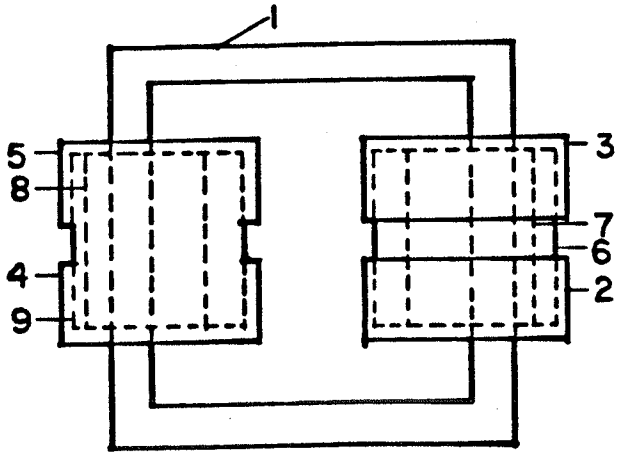

FIG. 2.1: Transformer Construction.

1- Core

2- Bottom High-voltage Section on right Limb

3- Top High-voltage Section on right Limb

4- Bottom High-voltage Section on left Limb

5- Top High-voltage Section on left Limb

6- Outer Low-voltage Section on right Limb

7- Inner Low-voltage Section on right Limb

8- Inner Low-voltage Section on left Limb

9- Outer Low-voltage Section on left Limb

2.2 DETERMINATION OF THE ELECTRICAL CIRCUIT EQUIVALENT OF THE TRANSFORMER

Under surges originating from the high-voltage end, the low-voltage winding can be assumed to be at ground potential [6,13]. Therefore, the development of the equivalent circuit of a transformer for surge conditions arising out of impulses on the high-voltage end, basically involves a determination of the model of the high-voltage winding.

To develop the model, the high-voltage winding was partitioned into individual layers. Each layer was then represented by lumped circuit parameters. This involves modelling the following three physical processes:

1. Electrostatic coupling between the turns of the winding.
2. Magnetic coupling between turns.
3. losses resulting from winding resistance.

In the equivalent circuit of a layer, shown in Fig. 2.2, the inductive element L represents the magnetic coupling between turns, resistor R accounts for the losses due to winding resistance while capacitor C is due to electrostatic coupling between turns.

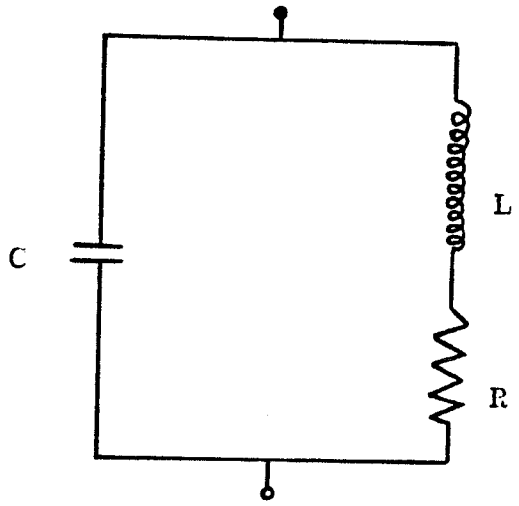

FIG. 2.2: Equivalent Circuit of a Layer.

The representations of the layers were connected as shown in Fig. 2.3 to obtain the section model. The magnetic coupling between layers of the same section is represented by layer-to-layer mutual-inductance. Layer-to-layer capacitance models electrostatic coupling between layers while layer-to-earth capacitance accounts for the capacitive coupling between the windings and earth.

The complete model of the transformer was obtained by joining the four sections together as shown in Fig. 2.4.

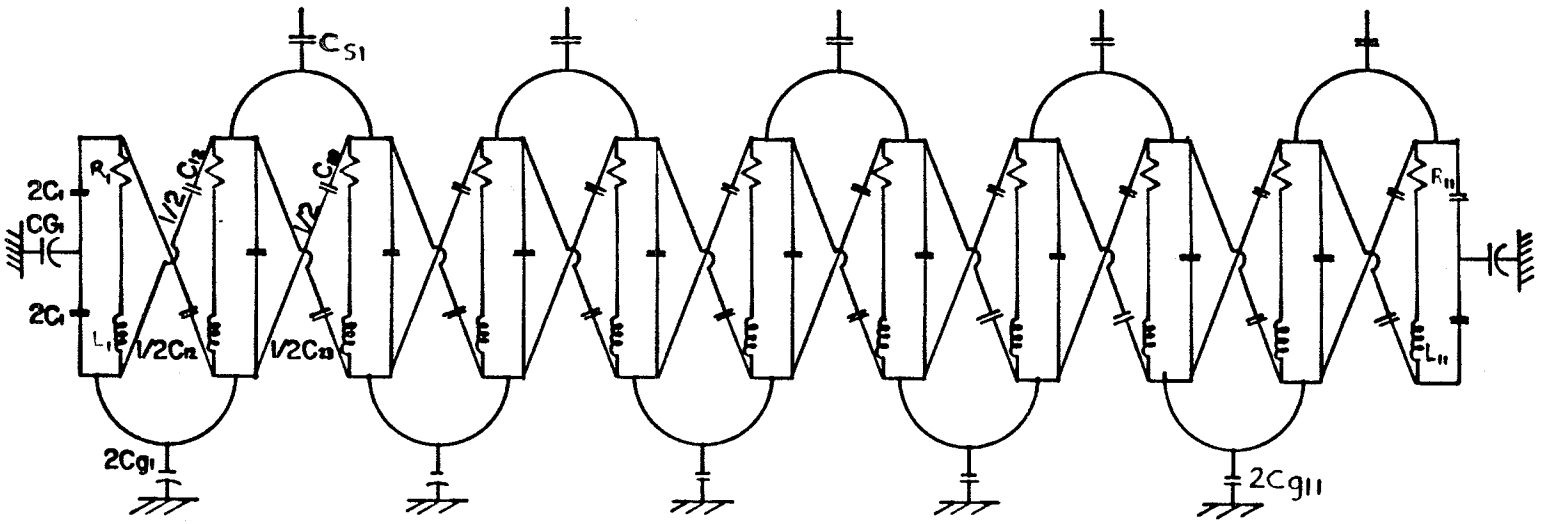

FIG. 2.3: Model of a Section of the Transformer.

L1 - Self-inductance of Layer 1

L2 - Self-inductance of Layer 2

:

:

L11 - Self-inductance of Layer 11

C1 - Turn-to-turn Capacitance of Layer 1

C2 - Turn-to-turn Capacitance of Layer 2

:

:

C11 - Turn-to-turn Capacitance of layer 11

R1 - Winding Resistance of Layer 1

:

:

R11 - Winding Resistance of Layer 11

C12 - Capacitance between Layers 1 and 2

Cg1 - Capacitance of layer 1 to earth

:

:

Cg11 - Capacitance of layer 11 to earth

Cs1 - Section-to-section capacitance

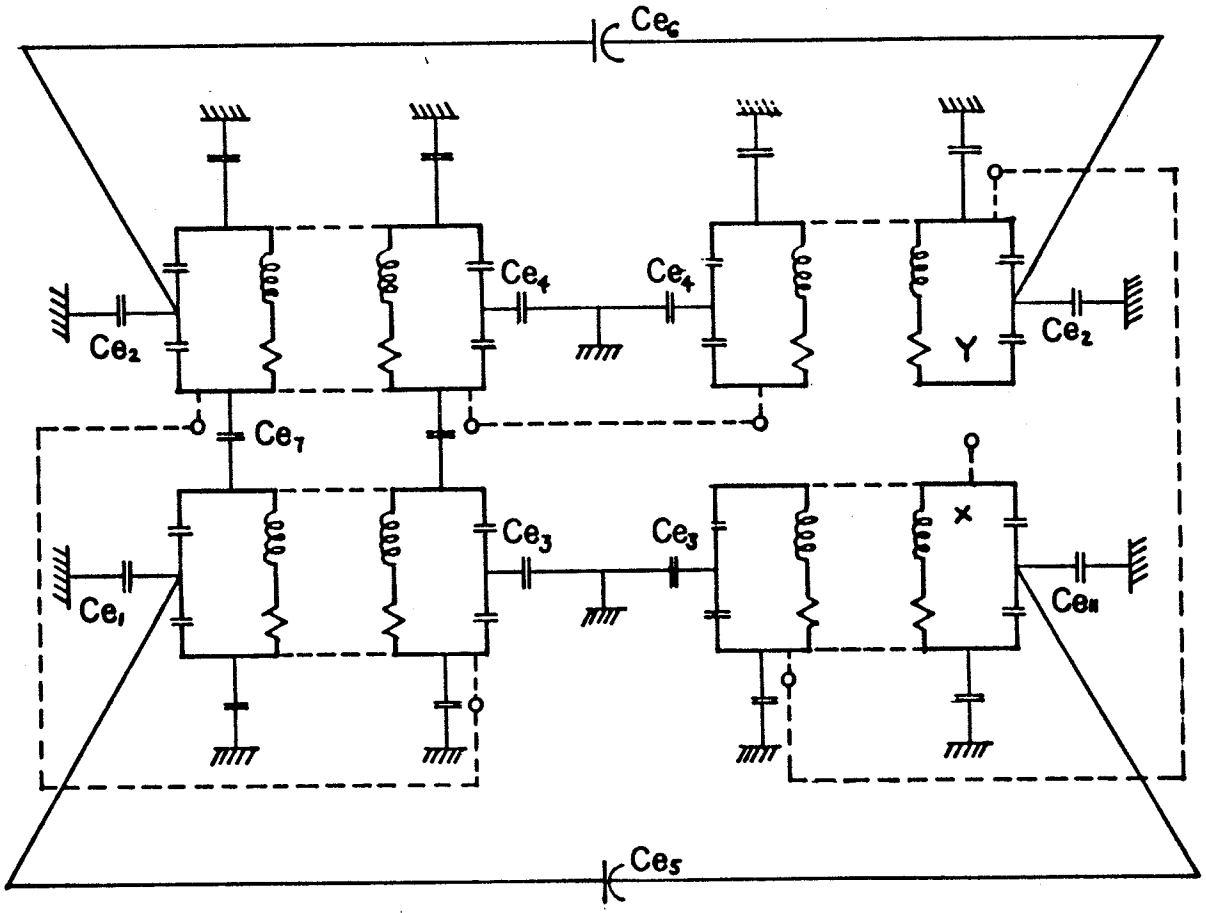

FIG. 2.4: Transformer Model.

Ce1 - Coil-to-ground Capacitance for Bottom Section

Ce2 - Coil-to-ground Capacitance for Top Section

Ce3 - Capacitance between Innermost High-voltage Layer and Outermost Low-voltage Layer

Ce4 = Ce3

Ce5 - Coil-to-coil Capacitance for Bottom Section

Ce6 - Coil-to-coil Capacitance for Top Section

Ce7 - Section-to-section Capacitance

The winding constants which have been identified are:

1. Winding resistance.
2. Turn-to-turn capacitance.
3. Layer-to-layer capacitance.
4. Capacitance between outermost high-voltage layer and tank.
5. Capacitance between innermost high-voltage layer and outermost low-voltage layer.
6. Capacitance between coils on different limbs.
7. Capacitance between sections on the same limb.
8. Layer-to-earth capacitance.
9. Self-inductance of layers.
10. Mutual-inductance between layers.

Chapter III

DETERMINATION OF WINDING CONSTANTS

3.1 WINDING RESISTANCE

Winding resistance is frequency-dependent by virtue of skin-effect. In this study, the direct-current resistance(Rdc) was determined and then modified to obtain impulse resistance (Rac).

3.1.1 Direct-current Resistance

The direct-current resistance was calculated by using the basic relationship, equation 3.1, between resistance (R), conductor length (L), cross-sectional area (A) and resistivity (p).

$$R = \frac{pL}{A} \tag{3.1}$$

In this case, p and A are known. To determine Rdc, all that is required is conductor length for each layer. The details of the computations are given in the computer program in Appendix A.

Using the arrangement shown in Fig. 3.1, a direct-current test was carried out on the transformer so as to check on the accuracy of the resistance values obtained by the above method.

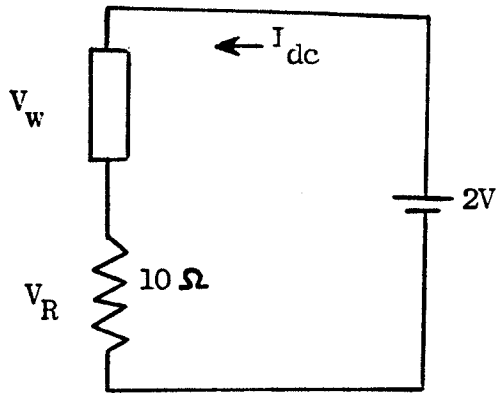

FIG. 3.1: Experimental set-up for measurement of the dc resistance.

A Keith 160B digital multimeter was used to measure voltage Vr across a 10-ohm resistor and voltage Vw across the winding. The results are given below:

Vr = 0.7565 V

Vw = 1.2246 V

Rdc was computed as follows:

Idc = Vr/r = 0.7565/10 = 0.07565 A

Rdc = Vw/Idc = 1.2246/0.07565 = 16.2Ω.

The calculated value of Rdc is 15.9Ω. The results show that there is no significant discrepancy between the experimental and theoretical values of direct-current resistance.

3.1.2 Impulse Resistance

To find impulse resistance, the dominant frequency of the standard impulse wave had to be determined.

A standard lightning impulse is defined in IEEE Standard Number 4 (1978) as an impulse having a virtual front time of 1.2 μs and a half-value time of 50 μs. The tolerances are specified below:

Crest value ±3%

Front time ±30%

Time to half-value ±20%

In this study, a 1/50 μs wave, which is well within the above tolerances, was used because it can accurately be reproduced in the laboratory, since the front and half-value times are integer values.

The analytical expression for the impulse voltage, V, is:

$$V = A(e^{-at} - e^{-bt}) \qquad (3.2)$$

where A, a and b are constants. The evaluation of these constants is given in Appendix B.

The dominant frequency is estimated by assuming that the front of the impulse wave constitutes one quarter of a cycle of a triangular wave as illustrated in Fig. 3.2.

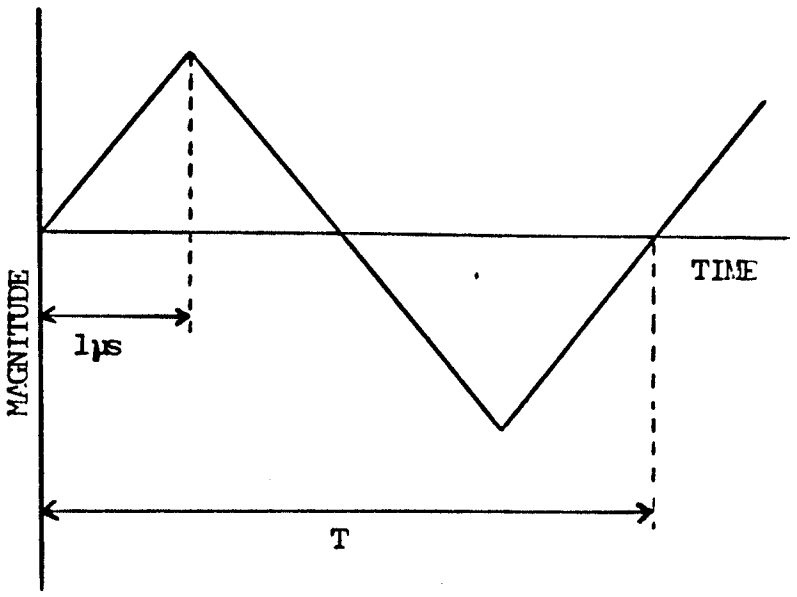

FIG. 3.2: Triangular Wave.

For the wave depicted above, period T=4 μs. The fundamental frequency of the impulse wave is given by:

$$f = \frac{1}{T} = \frac{1}{4\times10^{-6}} = 250000 \text{ Hz}$$

Impulse resistance is given by [24]:

$$Rac = Rdc\{ 1 + 4\pi(r)^3 (s)^2 [w/2p]^{1/2} \} \qquad (3.3)$$

where s = number of turns/cm

p = resistivity of the conductor in Ωcm

w = angular frequency in radians per second

r = radius of the conductor wire in centimetres.

Here,

p = 3.52μΩcm

r = 0.1075125 cm

s = 4.139483 turns/cm

In this case, since the wire is of rectangular cross-section, a wire of circular cross-section with a cross-sectional area equal to that of the rectangular wire was assumed. The details of the computation are given in Appendix A. In Table 3.1, the values of direct-current and impulse resistance are tabulated.

TABLE 3.1: Direct-current and Impulse Resistance

Layer number	D.C. resistance (Ω)	Impulse resistance for a 1/50 μs wave (Ω)	Impulse resistance for a .5/2.5 μs wave (Ω)
1	0.3575	2.890	3.939
2	0.3649	2.950	4.021
3	0.3723	3.010	4.103
4	0.3798	3.070	4.185
5	0.3872	3.130	4.267
6	0.3946	3.190	4.349
7	0.4021	3.251	4.430
8	0.4095	3.311	4.512
9	0.4169	3.371	4.594
10	0.2491	2.014	2.745
11	0.2440	1.973	2.689

The layers are labelled 1 to 11 with the innermost layer assigned the number 1 and the outermost layer the number 11.

3.2 INTERTURN CAPACITANCE

In the following analysis, a formula for calculating interturn capacitance is developed.

A layer consisting of n turns is shown in Fig. 3.3.

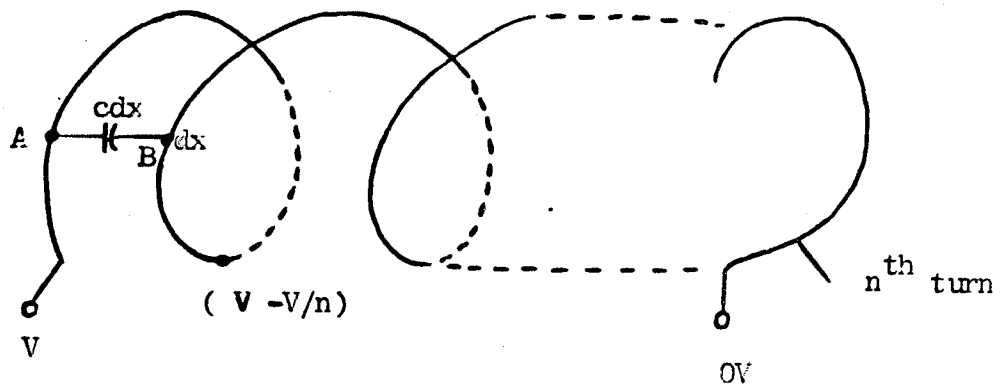

FIG. 3.3: Voltage Distribution in a Layer of n Turns.

C = capacitance per unit length

dx = incremental distance

Assuming a uniform voltage distribution throught the n turns of the layer, the voltage drop across each turn is V/n. Therefore, the voltage difference between two corresponding points of consecutive turns, for example A and B, is V/n. The capacitance across these two points is Cdx.

The energy stored in each elemental capacitance is given by:

$$dE = (1/2)(V/n)^2 Cdx \qquad (3.4)$$

The total energy stored in the capacitance system of two consecutive turns is found by integrating expression (3.4):

$$E = (C/2)(V/n)^2 \int_0^L dx = (C/2)(V/n)^2 L \qquad (3.5)$$

where L = perimeter of a turn.

For n turns, there are (n-1) pairs of consecutive turns. Therefore, the total energy stored in the layer can be expresed as:

$$Et = (n-1)E = \{(n-1)/(2n^2)\}CV^2 L = (1/2)CeqV^2 \qquad (3.6)$$

where Ceq = interturn capacitance of the layer.

From relation (3.6),

$$Ceq = \{C(n-1)L\}/(n^2) \qquad (3.7)$$

But the capacitance per unit length, that is, C, is given by:

$$C = \{(\epsilon_f \epsilon_o w/d\} \text{ F/m}$$

where ϵ_f = constant of permittivity of formel coating on the conductor

ϵ_o = permittivity of free space

w = conductor thickness

d = thickness of formel layer between two consecutive turns.

Substituting for C in relation (3.7) yields:

$$Ceq = \{\epsilon_f \epsilon_o w)/d\}\{(n-1)/n^2\}L \qquad (3.8)$$

The computer program for the computation of interturn capacitance is given in Appendix C. The values of interturn capacitance are tabulated in Table 3.2.

TABLE 3.2: Interturn Capacitance

Layer	Capacitance (pF)
1	6.79
2	7.08
3	7.37
4	7.66
5	7.97
6	8.28
7	8.59
8	8.91
9	9.24
10	16.0
11	17.2

The numbering of layers is as explained earlier.

3.3 LAYER-TO-LAYER CAPACITANCE

In order to calculate the capacitances that account for the electrostatic coupling between consecutive layers, that is, the layer-to-layer capacitances (e.g. C12, Fig. 2.3), each layer was assumed to be an open-ended hollow-conductor of rectangular cross-section. The conductor was subdivided into four parts each consisting of one side. Each side was paired with the corresponding side of the consecutive layer thereby making four pairs of conductors. This constituted an arrangement of four parallel-connected capacitors. The capacitances between conductor pairs were calculated and the total capacitance obtained by summing up the four capacitances. The details of the computation are given in Appendix D.

The layer-to-layer capacitance values are tabulated in Table 3.3.

TABLE 3.3: Layer-to-layer Capacitance

Layers	Capacitance (nF)
1,2	6.68
2,3	6.81
3,4	6.95
4,5	7.09
5,6	7.23
6,7	7.37
7,8	7.51
8,9	7.64
9,10	7.78
10,11	7.58

The numbering of the layers is as explained earlier.

3.4 CAPACITANCE BETWEEN THE INNERMOST HIGH-VOLTAGE LAYER AND THE OUTERMOST LOW-VOLTAGE LAYER

To calculate the capacitance between the innermost high-voltage layer and the outermost low-voltage layer, each layer was again assumed to be an open-ended hollow conductor of rectangular cross-section. The conductors were divided into segments each comprising of one side. The corresponding segments were paired thus obtaining a system of parallel-connected capacitors. The value of the capacitance was found to be 0.36 μF.

3.5 CAPACITANCE BETWEEN THE OUTERMOST HIGH-VOLTAGE LAYER AND TANK AND THE CAPACITANCE BETWEEN SECTIONS ON DIFFERENT LIMBS

The coil-to-coil and coil-to-tank capacitances are depicted in Fig. 3.4.

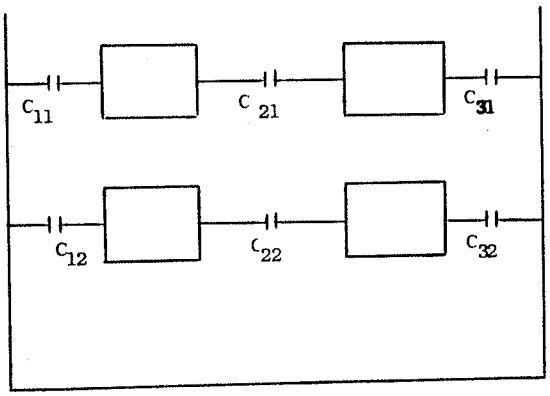

FIG. 3.4: Coil-to-coil and Coil-to-tank Capacitors

C11 = C31 = Capacitance between outermost high-voltage layer of top section and tank

C12 = C32 = Capacitances between tank and outermost high-voltage layer of bottom section

C21 = Capacitance between top sections on different limbs

C22 = Capacitance between bottom sections on different limbs

3.5.1 Coil-to-tank Capacitance

To compute coil-to-tank capacitance, the four coils, shown in Fig. 3.5(a), were replaced by a cylinder depicted in Fig. 3.5(b).

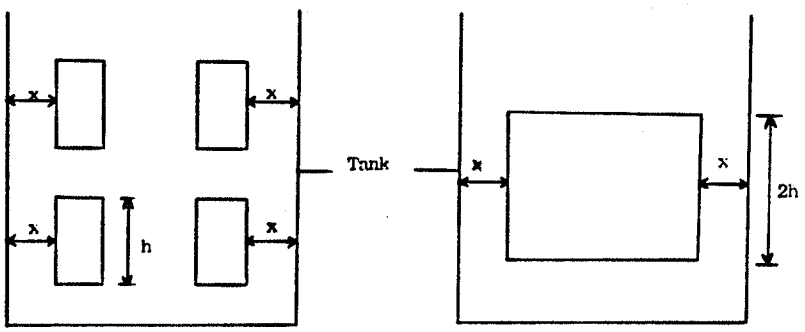

(a) (b)

FIG. 3.5

(a) The four HV coils

(b) Representation of the HV coils

The radius of the inner cylinder (Fig. 3.5(b)) is such that the actual separation between the coils and tank is preserved. The capacitance between the two cylinders was calculated by using the coaxial cable formula [15],

$$C = (2\pi\epsilon_o\epsilon_r)/\{\ln(Rb/Ra)\} \qquad (3.9)$$

here

ϵ_r = dielectric constant of transformer oil

ϵ_o = 8.854 pF/m = free space permittivity

Ra = 0.27305 m = radius of tank

Rb = 0.22905 m = radius of the cylinder representing the coils

It is assumed that both cylinders have height equal to 2h. Substituting these figures into equation (3.9) gives:

$$C = [2x8.854x2.2]/[\ln(0.22905/0.27305)] = 696.51 \text{ pF/m}$$

Multiplying by height yields:

$$Ct = 154.8 \text{ pF.}$$

The capacitance attributed to each of the four coils = 154.8/4

$$=38.7 \text{ pF}$$

Therefore,

$$C11 = C31 = C12 = C32 = 38.7 \text{ pF}$$

3.5.2 Coil-to-coil Capacitance

To estimate the coil-to-coil capacitance, shown as C21 and C22 in Fig. 3.4, the coils were assumed to be of rectangular cross-section. The capacitance between coils on different limbs is basically that between the directly opposite sides of the outermost layers of coils. The sides of the layers were considered as plates. The parallel-plate formula " $C = \epsilon_0 \epsilon_r A/d$ " was used.

In this case,

d = 0.02132 m = separation between outermost layers of coils on either limb

ϵ_r = 2.2 = dilectric constant of transformer oil

ϵ_0 = 8.854 pF/m = free space permittivity

A = (coil width)x(coil height)

width of coil = .210185 m

height of coil = .111125 m

therefore,

$$C = [2.2x8.854x0.210185x0.111125]/0.02132 = 21.3 \text{ pF}$$

hence, C21 = C22 = 21.3 pF.

Many simplifying assumptions were made in the above computations. It was found necessary, therefore, to evaluate the accuracy of the calculations by experimental measurements. Full-scale models of the outermost high-voltage layers were constructed and placed in the tank. Capacitance measurements were then carried out. The results are given below in terms of expressions relating capacitance values.

$$C11 + C31 = 115 \quad (3.8)$$

$$C21 + C31 = 85 \quad (3.9)$$

$$C12 + C32 = 80 \quad (3.10)$$

$$C22 + C32 = 60 \quad (3.11)$$

The element values are in picofarads.

Since C11 = C31, relation (3.8) can be written as

$$2C11 = 115$$

Hence,

$$C11 = C31 = 57.5 \text{ pF}$$

Substituting for C31 into (3.9) yields:

$$C21 + 57.5 = 85$$

Therefore,

$$C21 = 27.5 \text{ pF}.$$

Similary, expressions (3.10) and (3.11) are used to obtain:

$$C22 = 20 \text{ pF}$$

$$C12 = C32 = 40 \text{ pF}$$

It can be noted that the capacitance values yielded by the theoretical and experimental methods are in reasonable agreement.

3.6 SECTION-TO-SECTION CAPACITANCE

Layers in opposite sections form a configuration of conductors shown in Fig. 3.6.

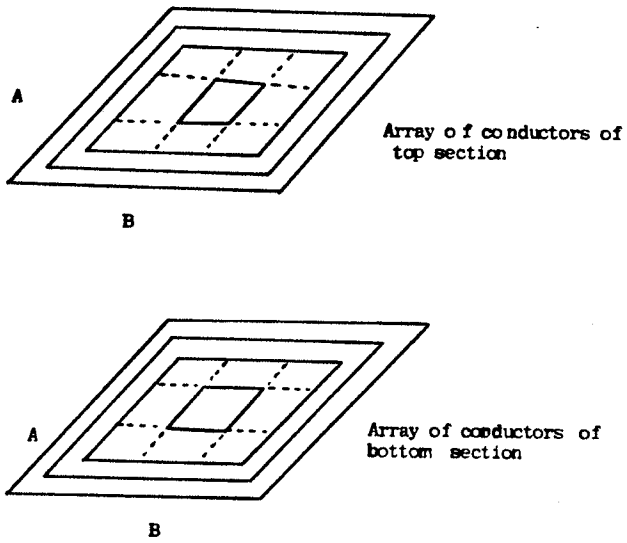

FIG. 3.6: Conductor Configuration formed by Layers in opposite Sections.

The capacitance between two parallel plates of sides A and B separated by a distance equal to the gap between conductors in opposite sections was computed. The value obtained was then multiplied by the ratio of the actual area occupied by the conductors to the plate area. The figure of capacitance so obtained was then divided among the eleven layers in proportion to their dimensions. The details of the computations are given in Appendix E.

The values of section-to-section capacitances are listed in Table 3.6.

TABLE 3.6: Section-to-section Capacitance

Layers	Capacitance (pF)
1	1.84
2	1.88
3	1.92
4	1.96
5	2.00
6	2.03
7	2.07
8	2.11
9	2.15
10	2.19
11	2.23

3.7 LAYER-TO-EARTH CAPACITANCE

The transformer being modelled has rectangular metallic plates at the bottom and top of the windings for mechanical support. The plates and layers can be visualized as forming an arrangement depicted in Fig. 3.7.

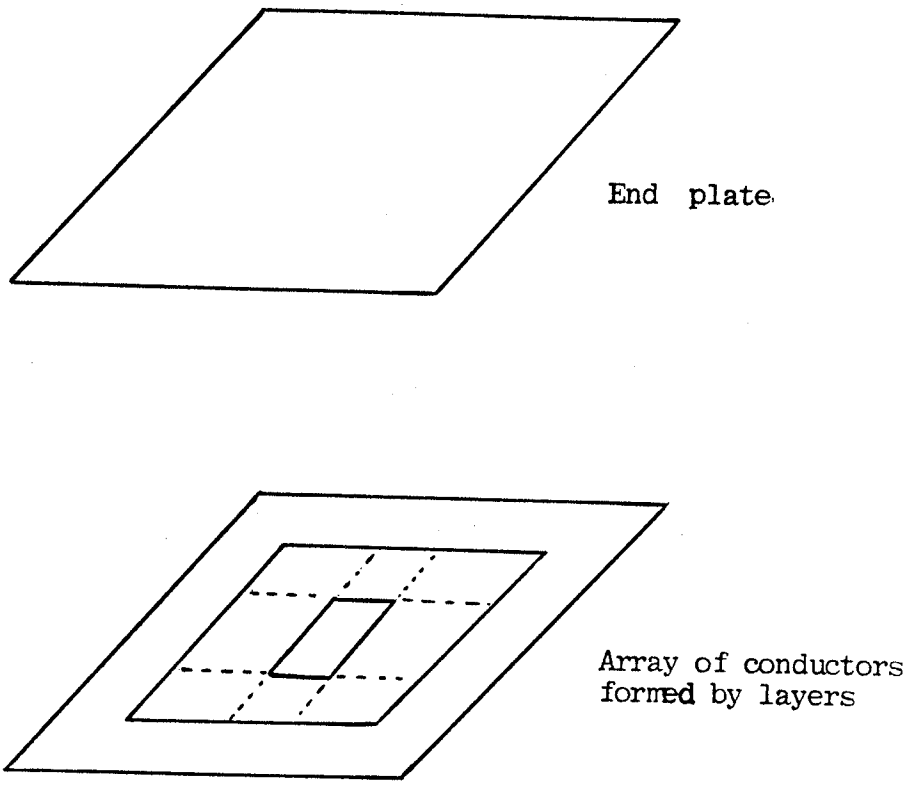

FIG. 3.7: Conductor Configuration formed by Layers and end Plate.

The approach used for finding section-to-section capacitance was applied in this case too. The values of layer-to-earth capacitances are tabulated in Table 3.7.

TABLE 3.7: Layer-to-earth Capacitance

Layer	Capacitance (pF)
1	3.23
2	3.29
3	3.36
4	3.43
5	3.50
6	3.56
7	3.63
8	3.70
9	3.76
10	3.83
11	3.90

3.7.1 Computation of Self-inductance

The shape of the winding turns, Fig. 3.8, is such that neither a single equation nor a combination of relations can be found for calculating the self-inductance values.

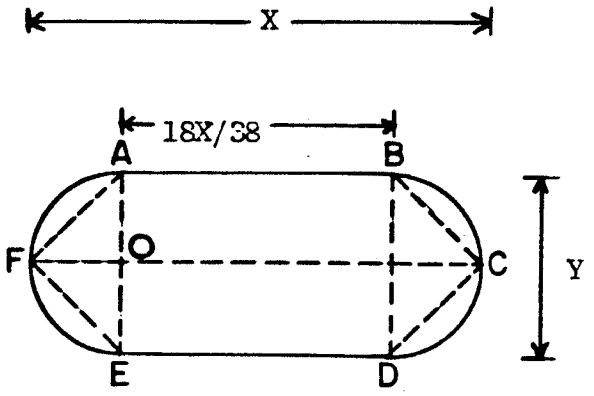

FIG. 3.8: Shape of Winding Turn.

Measurements carried out on the actual transformer revealed that the ratio of the length of the flat portion to the total length, X, indicated in Fig. 3.8, is 18:38 and that the width (y) is nearly equal to the length of the flat portion.

The self-inductance of layers of different shapes, but of the same cross-sectional area and height, do not differ significantly [20]. In order to determine the self-inductance values of the transformer layers, several representations of the turns were considered.

If the curves BC, CD, EF, and FA in Fig. 3.8 are replaced by straight lines, the hexagon ABCDEF, shown in Fig. 3.9, is obtained.

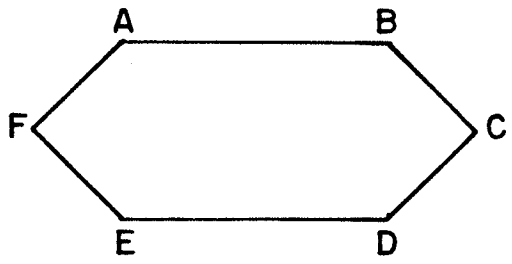

FIG. 3.9: Hexagonal Representation of Turns.

An alternative representation of the transformer turns is derived by assuming that the two curved portions of the turns, shown as AFEA and BCDB in Fig. 3.8, are semicircles of radius AO. Each semicircle is then replaced by a rectangle of the same area; but of width equal to that of the turn. The length (L) of the rectangle is derived as follows:

Area of rectangle = 18XL/38 =

area of semicircle = $(\pi/2)(AO)^2 = (\pi/8)(18X/38)^2$

Therefore,

$$L = 0.186X$$

The derived representation is depicted in Fig. 3.10.

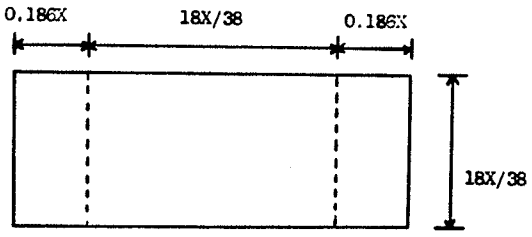

FIG. 3.10: Turn representation obtained by replacing the curved portions by rectangles of the same area.

Observation of the transformer turns revealed that the replacement of the curved portions of the turns by semicircles, as discussed above, results in an underestimation of the area. A rectangle, with dimensions such that it just encloses a turn, can instead be used as a turn representation. This leads to a rectangular representation shown in Fig. 3.11. In this case, the cross-sectional areas of the turns are overestimated.

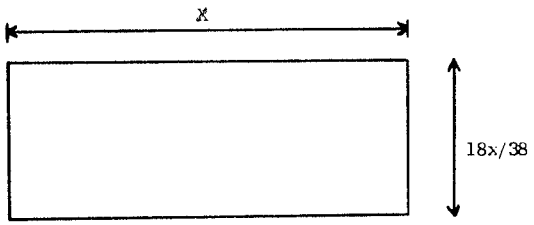

FIG. 3.11: Turn representation; turn enclosed by the rectangle.

The self-inductances of the layers of the cross-sections shown in Figs. 3.9-3.11 can be determined by using a collection of analytical expressions. However, the self-inductance of a layer of circular cross-section can be calculated by a single equation [21].

A circle of cross-sectional area equal to that of the rectangle in Fig. 3.11 was considered as a turn representation. The circle is shown in Fig. 3.12. But, this circle, just like the rectangle from which it was derived, leads to an overestimation of the areas of the turns.

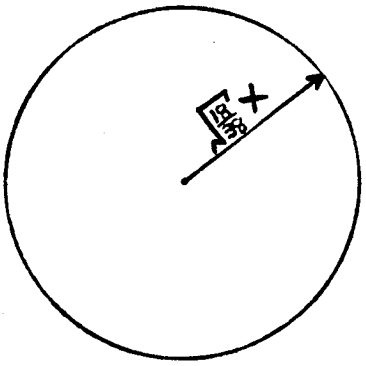

FIG. 3.12: Representation of a turn; the area of the circle is equal to that of the rectangle enclosing the turn.

The area of a turn can also be approximated by that of a circle whose radius is determined as shown below in Fig. 3.13.

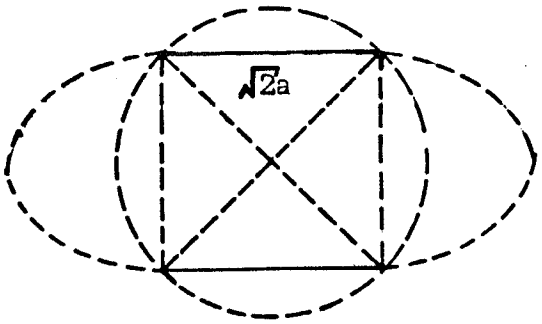

FIG. 3.13: Representation of a turn; the diameter of the circle is equal to the diagonal of the square portion of the turn.

Here a= 9X/38, hence the radius of the circle shown dotted is $\sqrt{2}$a.

The area of the above circle is within 1% of that of the hexagon depicted in Fig. 3.9.

The basic problem encountered in the derivation of the equivalents of the turns is that the areas of the curved portions (AFEA and BCDB, Fig. 3.8) cannot be estimated accurately. The square shown as ABDE in Fig. 3.8 was considered so as to determine the extent to which the curved portions contribute to the self-inductance of a layer. In Fig. 3.14, square ABDE is depicted.

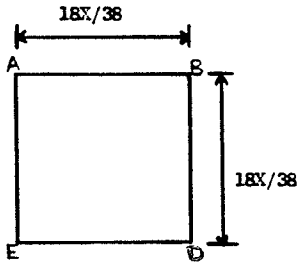

FIG. 3.14: Turn representation derived by excluding the curved portions.

It can be noted that of the above representations (Figs. 3.9-3.14), the one depicted in Fig. 3.9 is closest in area and shape to the actual transformer turns. Therefore, the set of values of self-inductance that was obtained for the hexagonal shape was adopted as a basis for evaluating the accuracy attained by using the other representations.

3.7.1.1 Calculation of Self-inductance using the Hexagonal shape

For illustrative purposes consider a layer, shown in Fig. 3.15, consisting of two turns. The self-inductance of the layer is given by:

$$L = L1 + L2 + M12 \qquad (3.12)$$

where

L1 and L2 are respectively the self-inductances of turns 1 and 2

M12 = mutual-inductance between turns 1 and 2

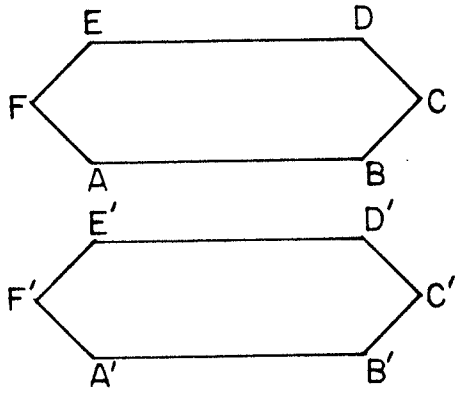

FIG. 3.15: Two-turn Layer.

The value of the self-inductance of the hexagon ABCDEF (Fig. 3.15) is obtained by adding the sum of the self-inductances of the sides and twice the sum of the mutual couplings between all possible side pairs.

Thus,

$$L_1 = L_{AB} + L_{BC} + L_{CD} + L_{DE} + L_{EF} + M_{AB,BC} + M_{AB,CD} + M_{AB,DE} + M_{AB,EF} + M_{AB,FA} + M_{BC,CD} + M_{BC,DE} + M_{BC,EF} + M_{BC,FA} + M_{CD,DE} + M_{CD,EF} + M_{CD,FA} + M_{DE,EF} + M_{DE,FA} + M_{EF,FA} \quad \ldots\ldots\ldots\ldots\ldots\ldots\ldots\ldots (3.13)$$

where the subscripted L's denote self-inductances and the subscripted M's represent mutual-inductances between side pairs.

The mutual-inductance between the two turns is calculated by adding up the mutual inductances between all possible combinations of conductor segments, taken two at a time. Therefore,

$$M_{12} = M_{AB,A'B'} + M_{AB,B'C'} + M_{AB,C'D'} + M_{AB,D'E'} + M_{AB,E'F'} + M_{AB,F'A'} + M_{BC,A'B'} + M_{BC,B'C'} + M_{BC,C'D'} + M_{BC,D'E'} + M_{BC,E'F'} + M_{BC,F'A'} + M_{CD,A'B'} + M_{CD,B'C'} + M_{CD,C'D'} + M_{CD,D'E'} + M_{CD,E'F'} + M_{CD,F'A'} + M_{DE,A'B'} + M_{DE,B'C'} + M_{DE,C'D'} + M_{DE,D'E'} + M_{DE,E'F'} + M_{DE,F'A'} + M_{EF,A'B'} + M_{EF,B'C'} + M_{EF,C'D'} + M_{EF,D'E'} + M_{EF,E'F'} + M_{EF,F'A'} + M_{FA,A'B'} + M_{FA,B'C'} + M_{FA,C'D'} + M_{FA,D'E'} + M_{FA,E'F'} + M_{FA,F'A'} \quad \ldots\ldots (3.14)$$

3.7.2 Computation of Self-inductance of a Straight Conductor Segment

Since the winding conductor is of rectangular cross-section, the formula for calculating self-inductance of a straight conductor of rectangular cross-section [21] was used.

Self-inductance is given by:

$$L = 0.0021[\ln\{2l/(B + C)\} + (1/2) - \ln(e)\} \ \mu H \qquad (3.15)$$

where

l = length of conductor

b and c are the sides of the cross-section of the conductor.

All the dimensions are in centimetres.

The term ln(e) is a function of b/c and is obtainable from Table 3 of the given reference.

Calculation of Mutual-inductance between conductor segments

In order to compute the mutual-inductance between straight conductor segments, each conductor is replaced by a current filament through its centre [21]. In Fig. 3.16, two filaments AB and ab are shown.

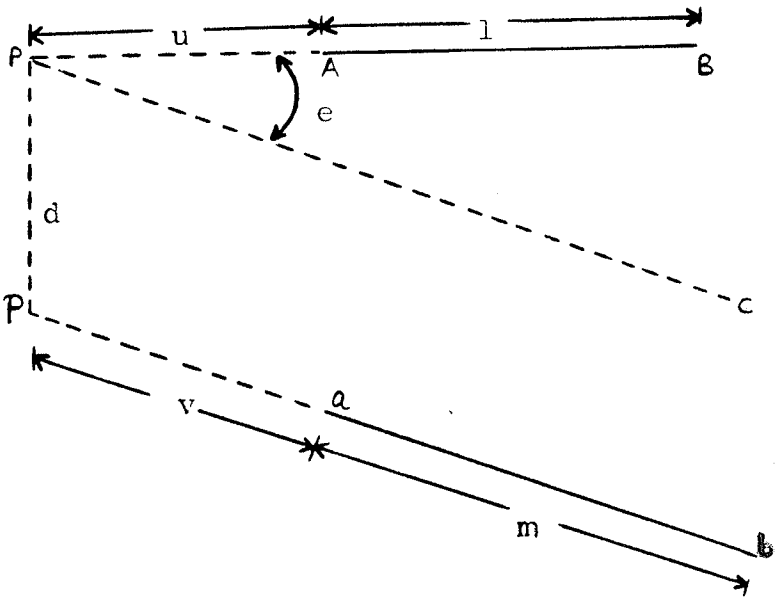

FIG. 3.16: Current Filaments inclined at each other

Line pc, in Fig. 3.16, represents the line of intersection of the planes passing through the filaments in such a manner as to intersect at right angles. Pp is a common perpendicular to the filaments. Let the four distances between the ends of the filaments be designated as follows:

Bb = R1, Ba = R2, Aa = R3, Ab = R4.

The mutual-inductance of filaments AB and ab is given by [21]:

$$M/0.002\cos e = (u+l)\tanh^{-1}\{m/(R1+R2)\} + (v+m)\tanh^{-1}\{l/(R1+R4)\} - u\tanh^{-1}\{m/(R3+R4)\} - v\tanh^{-1}\{l/(R2+R3)\} - \Omega(1/2)d/\sin e \quad (3.16)$$

In which

$$\Omega = \tan^{-1}[\{d^2\cos e + (u+1)(v+m)\sin^2 e\}/d(R1)\sin e] -$$

$$\tan^{-1}[\{d^2\cos e + (u+1)v\sin^2 e\}/d(R2)\sin e]$$

$$\tan^{-1}[\{d^2\cos e + uv\sin^2 e\}/d(R3)\sin e] -$$

$$\tan^{-1}[\{d^2\cos e + u(v+m)\sin^2 e\}/d(R4)\sin e]$$

where

$$\cos e = a^2/2lm$$

$$a^2 = R4^2 - R3^2 + R2^2 - R1^2$$

The above analysis can be extended to compute self-inductance of multiturn layers. For a layer of n turns,

$$L = nL1 + 2(n-1)M12 + 2(n-3)M13 + \ldots\ldots\ldots + M1n \qquad (3.17)$$

where

Mij = mutual-inductance of any two turns separated by (j-i-1) turns.

The details of the computation are given in Appendix F.

The calculation of self-inductance was also carried out using the turn representations shown in Figs. 3.10, 3.11 and 3.14. The approach was similar to that used in the case of the hexagonal shape except that, in the new cases, there were no inclined filaments.

For the circular cross-section, The relation for finding self-inductance of a layer of circular cross-section [21] was used. Self-inductance is expressed as:

$$L = 0.004bk(\pi an)^2 \qquad (3.18)$$

in which

a = mean radius of turns

b = axial dimension of cross-section

n = number of turns

k = correction factor to take into account the effect of ends; it is obtainable, as a fuction of b/a, from Table 36 of the given reference.

The details of the computations are given in Appendix G. The values of self-inductance obtained by using each of the above methods are tabulated in Table 3.8.

TABLE 3.8: Self-inductance values obtained by using different representations of transformer turns.

Layer	Turn representation as in:					
	Fig.3.11	Fig.3.10	Fig.3.14	Fig.3.9	Fig.3.13	Fig.3.12
1	0.5054	0.4382	0.2731	0.3763	0.3446	0.4766
2	0.5227	0.4535	0.2832	0.3897	0.3532	0.4948
3	0.5401	0.4688	0.2934	0.4032	0.3619	0.5114
4	0.5576	0.4843	0.3037	0.4167	0.3706	0.5269
5	0.5752	0.4998	0.3140	0.4304	0.3796	0.5438
6	0.5930	0.5155	0.3245	0.4442	0.3878	0.5609
7	0.6109	0.5313	0.3350	0.4581	0.3989	0.5781
8	0.6288	0.5472	0.3457	0.4621	0.4071	0.5954
9	0.6469	0.5632	0.3564	0.4861	0.415	0.6128
10	0.2959	0.2591	0.1685	0.2215	0.1913	0.2775
11	0.2860	0.2507	0.1636	0.2142	0.1840	0.2682

The values of inductance are in millihenries.

TABLE 3.9: Computer Time required to Determine Self-inductance values

Turn representation as in:	Time (s)
Fig. 3.9	5.62
Fig. 3.10	0.2
Fig. 3.11	0.2
Fig. 3.12	0.02
Fig. 3.13	0.02
Fig. 3.14	0.2

The results tabulated in Table 3.8 reveal that the self-inductance values calculated by using the representation shown in Fig. 3.13 are closest to those computed by assuming the hexagonal shape (Fig. 3.9). The time required to compute the self-inductance of layers of circular cross-section is much less than that required in each of the other cases (Table 3.9).

The transformer model was analyzed using the self-inductance values of the hexagonal representation and those of the circular shape (Fig. 3.13). The two sets of results were compared.

3.7.3 Determination of Layer-to-layer Mutual-inductance

Considering winding sections i and j, the mutual-inductance between them is given by:

$$Mij = Kij(LiLj)^{1/2} \tag{3.19}$$

where

Mij = mutual-inductance

kij = coupling coefficient between sections i and j

Li and Lj are self-inductances

Okuyama [16] has proposed the following formula for determining the coupling coefficient:

$$Kij = e^{\{-xij(Ri+Rj)\}/(RiRj)} \tag{3.20}$$

where

xij = distance between sections i and j

Ri = radius of section i

Rj = radius of section j

The derivation of relation (3.20) was not given. However, since the equation is given in terms of radii of sections, it can be inferred that it is meant for coils of circular cross-section. Since the coils of the transformer being analyzed are not of circular cross-section, Okuyama's expression cannot readily be applied.

According to Dent et al. [7], the lines of magnetic flux are analogous to electrostatic potentials arising out of the initial voltage distribution of impulse voltage along transformer windings. Therefore, the fraction of the flux from section i linking section j, that is, the coupling coefficient Kij, is given by the ratio of the initial voltages in the two sections. The ratio is given by [19]:

$$(Vi/Vj) = Kij = e^{-aXij/l} \qquad (3.21)$$

where

$$a = [Cg/Cs]^{1/2}$$

Cg = total distributed capacitance to earth of windings

Cs = total distributed capacitance between winding sections

l = transverse length of the winding

xij = distance between i and j sections.

Relation (3.19) was used to determine the mutual coupling between layers. The mutual-inductance values are tabulated in Table 3.10.

3.7.4 Section-to-section Mutual-inductance

The dominant frequency of the standard impulse wave (1/50 μs) is 250 kHz (subsection 3.1.2). The impulse wave basically consists of components whose frequencies are close to the dominant one.

At high frequencies, like the one mentioned above, the capacitive reactance of the transformer is much less than the inductive reactance. Therefore, currents flow through the capacitances in preference to the inductances. In the case of the transformer being analyzed, the section-to-section capacitances (Table 3.6) are small compared to the other capacitances (Tables 3.1, 3.2 and 3.7). Consequently, the flux linkages are concentrated in individual sections. Hence section-to-section inductive coupling is negligible under the impulse conditions considered in this study.

TABLE 3.10: Layer-to-layer mutual-inductance

Layers	Mutual coupling for the turn representation shown in Fig. 3.13 (mH)	mutual coupling for the turn representation depicted in Fig. 9 (mH)
1,2	0.3347	0.3673
1,3	0.3250	0.3584
1,4	0.3154	0.3495
1,5	0.3062	0.3407
1,6	0.2969	0.3321
1,7	0.2889	0.3245
1,8	0.2799	0.3235
1,9	0.2711	0.3066
1,10	0.1766	0.1985
1,11	0.1661	0.1873
2,3	0.3430	0.3802
2,4	0.3329	0.3708
2,5	0.3232	0.3615
2,6	0.3134	0.3523
2,7	0.3049	0.3432
2,8	0.2954	0.3342
2,9	0.2861	0.3253
2,10	0.1864	0.2106
2,11	0.1753	0.1987
3,4	0.3513	0.3932

TABLE 3.10 continued

Layers	Mutual coupling for the turn representation shown in Fig. 3.13 (mH)	mutual coupling for the turn representation depicted in Fig. 9 (mH)
3,5	0.3411	0.3833
3,6	0.3307	0.3735
3,7	0.3217	0.3639
3,8	0.3118	0.3544
3,9	0.3019	0.3449
3,10	0.1966	0.2233
3,11	0.1850	0.2107
4,5	0.3598	0.4062
4,6	0.3488	0.3959
4,7	0.3394	0.3856
4,8	0.3289	0.3755
4,9	0.3185	0.3655
4,10	0.2074	0.2367
4,11	0.1952	0.2232
5,6	0.3680	0.4194
5,7	0.3581	0.4085
5,8	0.3470	0.3979
5,9	0.3361	0.3873
5,10	0.2188	0.2508

TABLE 3.10 continued

Layers	Mutual coupling for the turn representation shown in Fig. 3.13 (mH)	mutual coupling for the turn representation depicted in Fig. 9 (mH)
5,11	0.2059	0.2366
6,7	0.3773	0.4327
6,8	0.3656	0.4214
6,9	0.3541	0.4102
6,10	0.2306	0.2656
6,11	0.2170	0.2505
7,8	0.3866	0.4461
7,9	0.3744	0.4342
7,10	0.2438	0.2812
7,11	0.2294	0.2652
8,9	0.3943	0.4595
8,10	0.2568	0.2976
8,11	0.2416	0.2807
9,10	0.2703	0.3148
9,11	0.2543	0.2969
10,11	0.1800	0.2089

Chapter IV

EXPERIMENTAL DETERMINATION OF IMPULSE VOLTAGE DISTRIBUTION

Impulse tests were carried out on the actual transformer to evaluate the accuracy of the simulation by electric circuit models.

Tests carried out by other researchers [12,18] have revealed that the magnitude of impulse voltage is not a significant factor in the determination of impulse voltage distribution. Therefore, it is sufficient to impulse the transformer with low voltages using a recurrent surge generator.

A laboratory-built recurrent surge generator of the specifications given in Table 4.1 was available.

TABLE 4.1: Specifications of the Recurrent Surge Generator

Peak voltage (V)	Output capacitance (μF)	Chop time (μs)	Fastest front (μs)	Longest tail (μs)
600	.001 to .1	0.1	0.5	500

Test Assembly

The schematic diagram of the testing circuit is shown in Fig. 4.1. The voltage was fed to a Tektronix type 549 fast-storage oscilloscope.

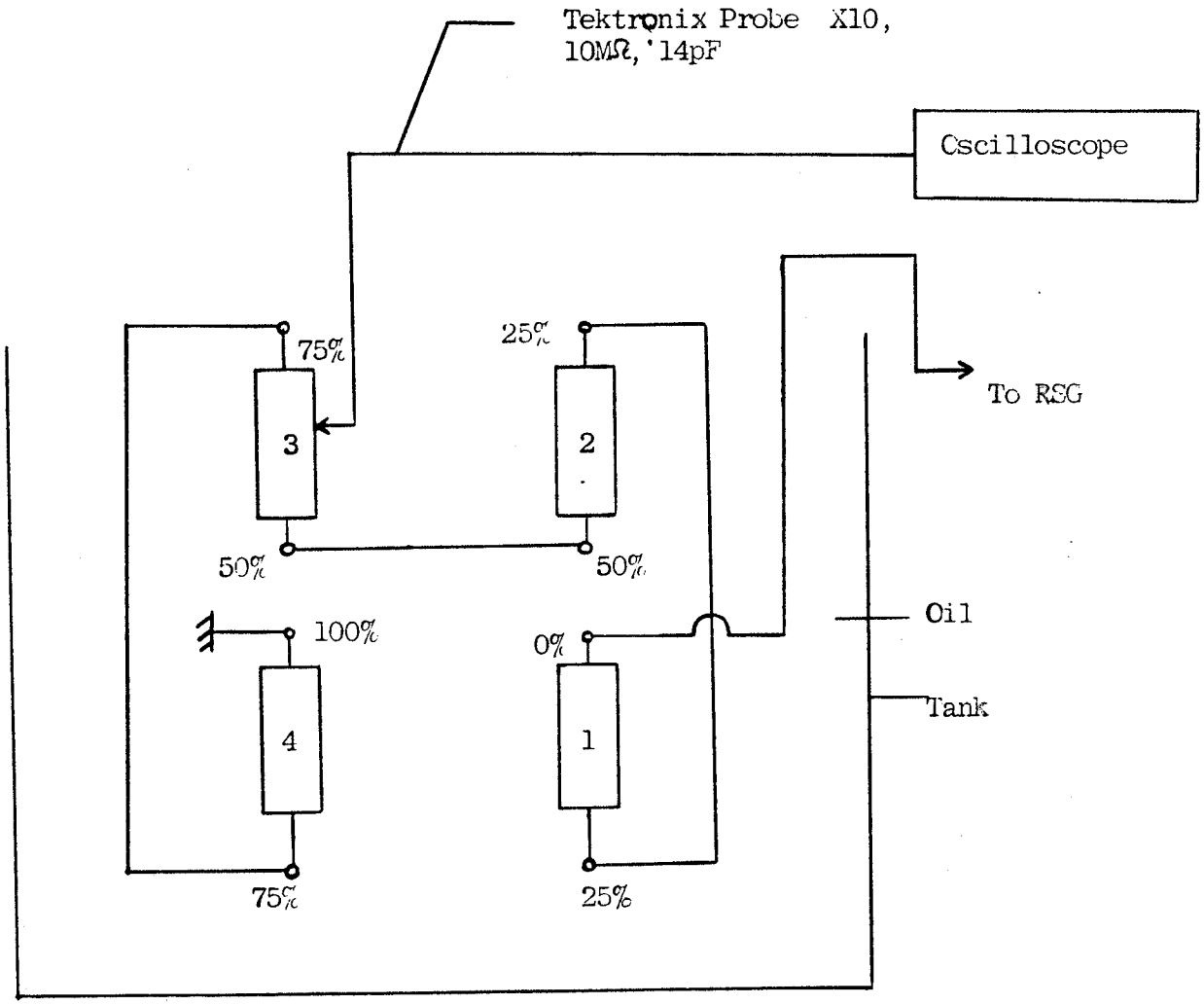

FIG. 4.1: Experimental Set-up for Impulse voltage Distribution tests

Here

1,2,3,4 are winding sections

Test Procedure

With the low-voltage winding earthed and grounded, the recurrent surge generator was adjusted to give a 1/50 μs impulse waveform of peak value 400 V at the input terminals of the high-voltage winding. By using a probe, voltage waveforms at different winding positions were monitored on the oscilloscope and photographed by a polaroid Schackman 7000 camera.

The bottom part of the winding could not be accessed (Fig. 4.1). Each winding section constitutes approximately 25% of the whole winding. Therefore, by probing only the top sections, the portion of the winding accessed is between 25% and 75% of the total winding measured from the line end. The impulse voltage distribution in the rest of the winding can be estimated by exploiting the symmetry of the transformer. The inter-section connections are changed to those shown in Fig. 4.2.

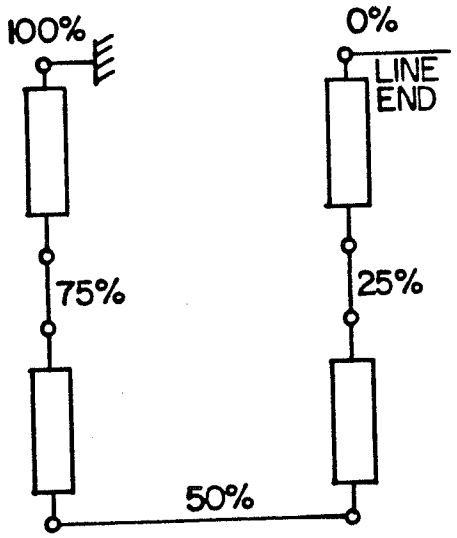

FIG. 4.2: Modified Inter-section connection.

With the sections connected as shown in Fig. 4.2, 0 to 25% and 75% to 100% of the winding measured from the impulsed end is accessible.

The above procedure was repeated for the standard wave chopped at peak(1 μs) and for the 0.5/2.5 μs wave. The results are shown in Figs. 5.2-5.4.

Chapter V

METHOD OF SOLUTION AND COMPUTATION OF IMPULSE VOLTAGE DISTRIBUTION

The voltage stress distribution along the transformer windings was computed using the Electromagnetics Transients Program (EMTP). Compared to other solution techniques, the EMTP offers a number of important advantages; it is accurate, numerically stable and requires less computer time and storage. Furthermore, problems of large size can be handled. For example, the electrical network representation of the transformer being studied consists of forty-four resistors, sixty capacitors, forty-four self-inductance branches and incorporates two-hundred and twenty mutual couplings.

5.1 THE ELECTROMAGNETIC TRANSIENTS PROGRAM

The EMTP is a solution technique used in the analysis of electrical networks. It was developed at the Bonneville Power Administration (BPA) by H.W.Dommel [10].

In the EMTP, a problem is formulated through a companion-network approach. To obtain a companion network, each nonresistive circuit element of the original network is modelled as a resistor in parallel with a current source. The circuit element model is derived by expressing branch current in terms of node voltages as illustrated in Appendix H.

The models are shown in Fig. 5.1 for a time step of dt.

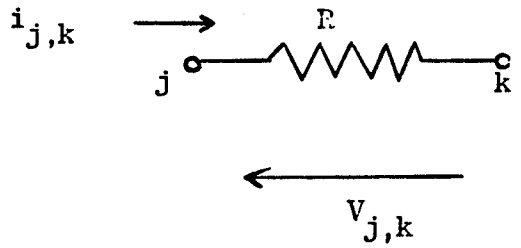

FIG. 5.1(a): Resistive Element.

$$I_c(t) = (2C/\Delta t)V_{j,k}(t-\Delta t) + i_{j,k}(t-\Delta t)$$

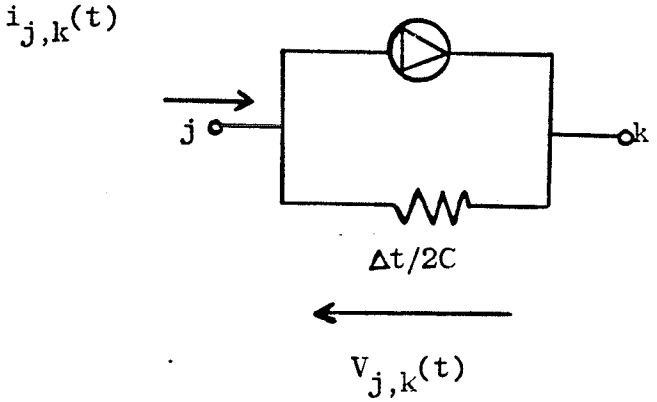

FIG. 5.1(b): Circuit Element Model for a Capacitor, C.

$$I_L(t) = (\Delta t/2L)V_{j,k}(t-\Delta t) - i_{j,k}(t-\Delta t)$$

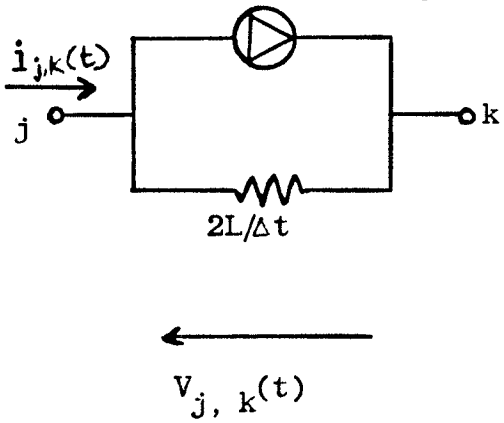

FIG. 5.1(c): Circuit Element Model for an Inductor, L.

In the derivation of the equations describing the component elements, trapezoidal-rule integration is used. The network equations take the form:

$$[Y]\{V(t)\} = \{i(t)\} + \{Ic(t)\} + \{Il(t)\} \qquad (5.1)$$

where

[Y] = nodal admittance matrix

{V(t)} = vector containing nodal voltages at time t

{i(t)} = vector containing specified nodal current sources

{Ic(t)} = vector containing nodal injected current sources which simulate the past history of the capacitive elements

{Il(t)} = vector containing nodal injected current sources which simulate the past history of the inductive elements.

A step-by-step picture of the network state is given by the solution of (5.1) at each time step. In Appendix J , the format of an EMTP job is given.

5.2 COMPUTATION OF IMPULSE VOLTAGE DISTRIBUTION

Several models of the transformer were analyzed in order to assess the significance of the various factors involved in the representation of the winding by the equivalent circuit shown in Fig 2.4. The factors considered were:

1. Mutual coupling between layers.
2. Modification of d.c resistance by skin-effect at high frequencies.

In the first model, the mutual coupling between layers was not taken into account and dc resistance values were used. The second model was obtained by changing the resistances in the first model to impulse resistances. By considering mutual-inductance and using dc resistance values, the third model was obtained. The fourth model was similar to the third except that the impulse resistance values were used.

The above four models were analyzed for impulse voltage distribution using an AMDAHL 470/V7 computer under an OS/MVS2 JES 2.2 operating system. The impulse waveforms used were:

1. The 1/50 μs wave.
2. The 1/50 μs wave chopped at the peak (1 μs).
3. The 0.5/2.5 μs wave.

The results are given in Figs. 5.2-5.10 and Table 5.1.

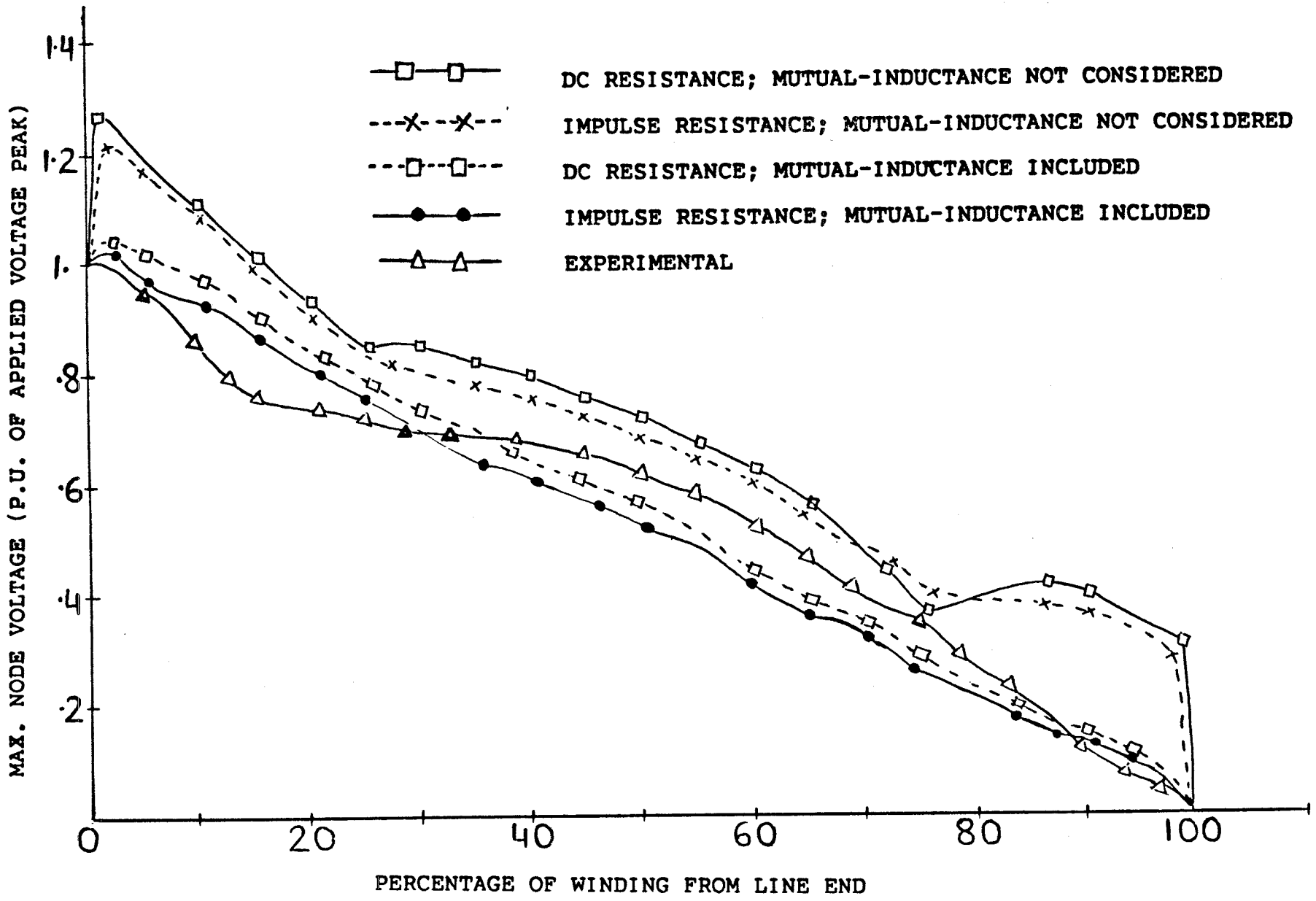

FIG. 5.2 Impulse voltage distribution along the HV winding; hexagonal turn representation: 1/50 μs wave.

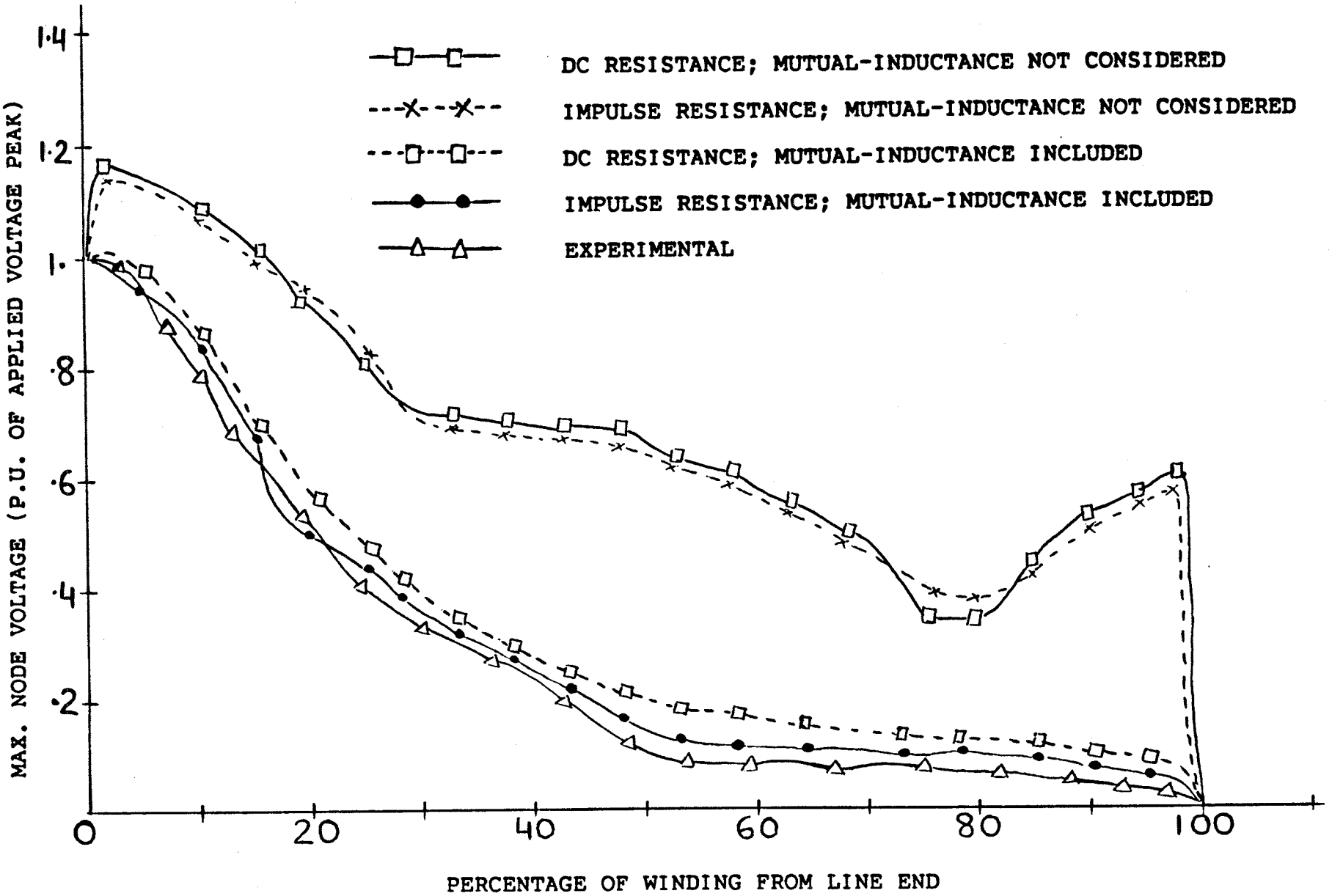

FIG. 5.3 Impulse voltage distribution along the HV winding; hexagonal turn representation: 1/50 μs wave chopped at peak.

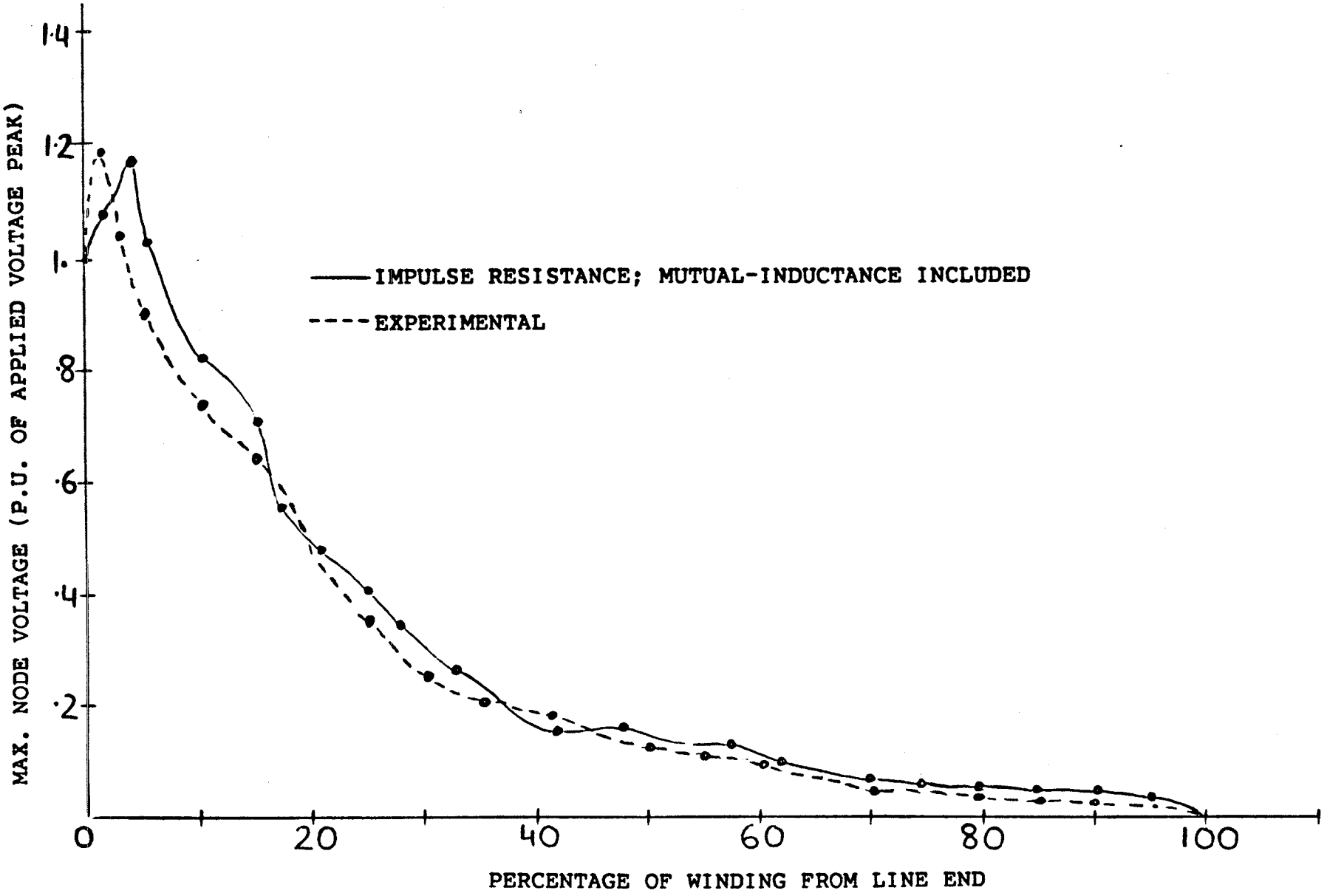

FIG. 5.4 Impulse voltage distribution along the HV winding; hexagonal turn representation: 0.5/2.5 μs wave.

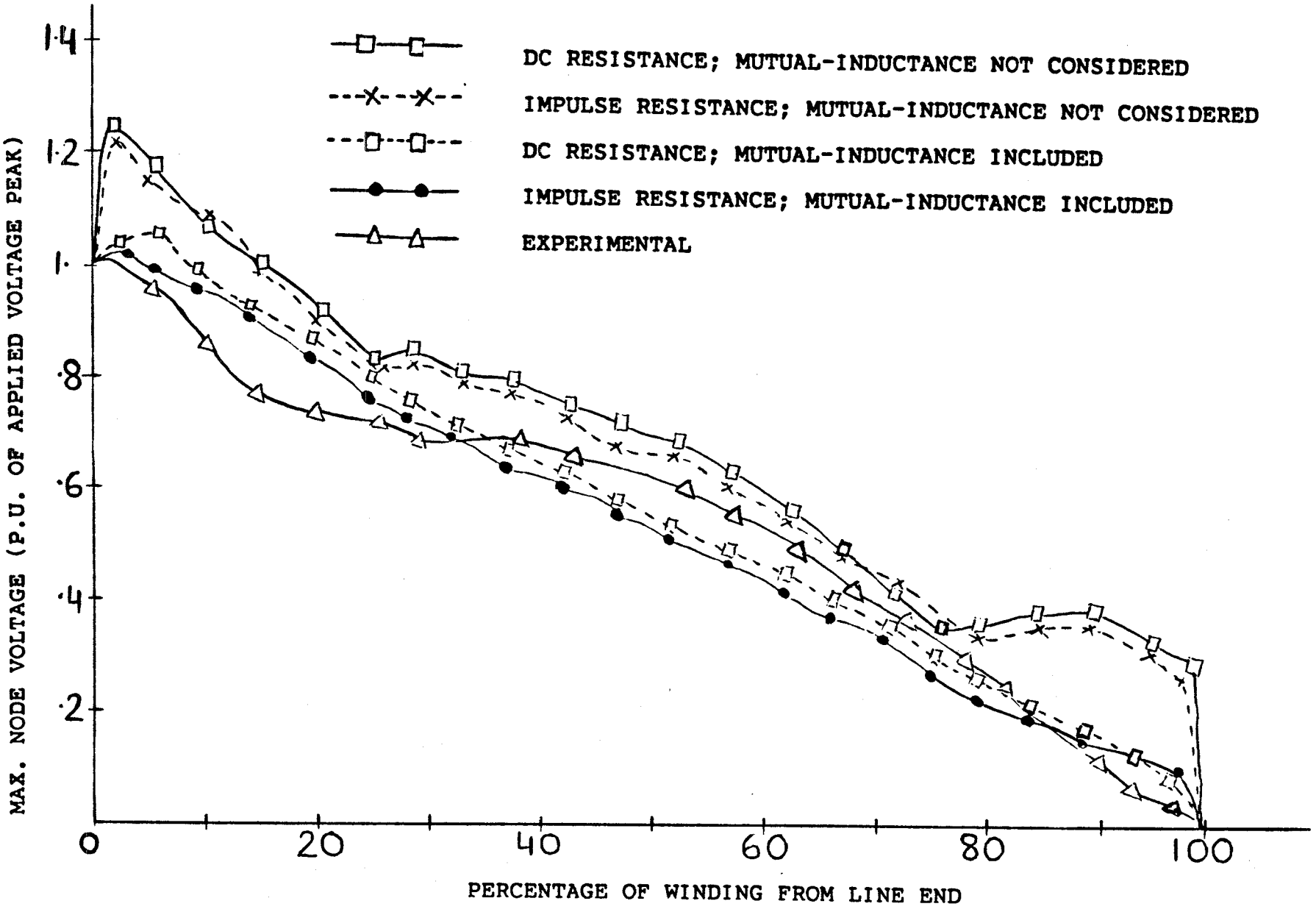

FIG. 5.5 Impulse voltage distribution along the HV winding; turn representation as in Fig. 3.13: 1/50 μs wave.

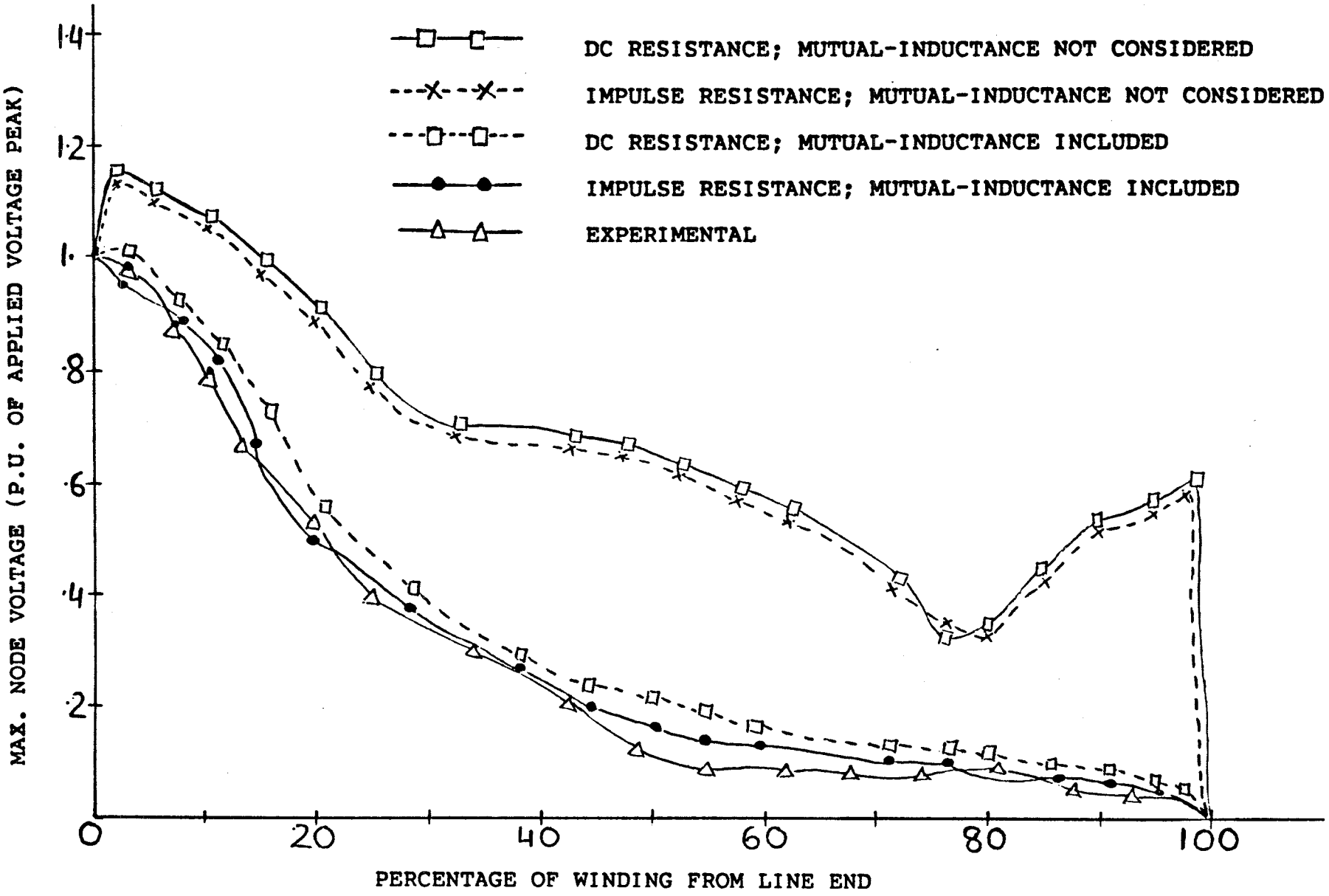

FIG. 5.6 Impulse voltage distribution along the HV winding; turn representation as in Fig. 3.13: 1/50 μs wave chopped at 1 μs.

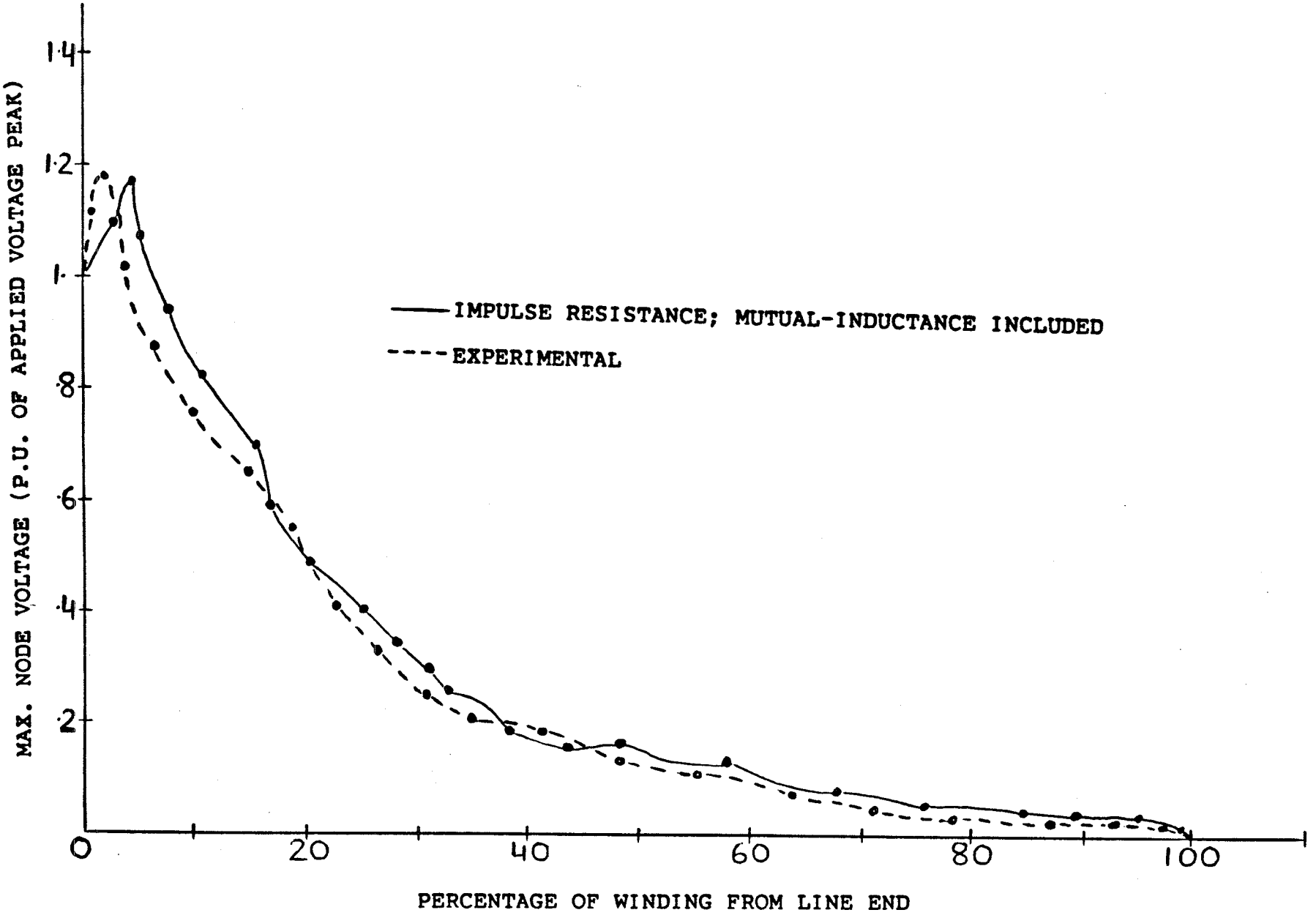

FIG. 5.7 Impulse voltage distribution along the HV winding; turn representation as in Fig. 3.13: 0.5/2.5 μs wave.

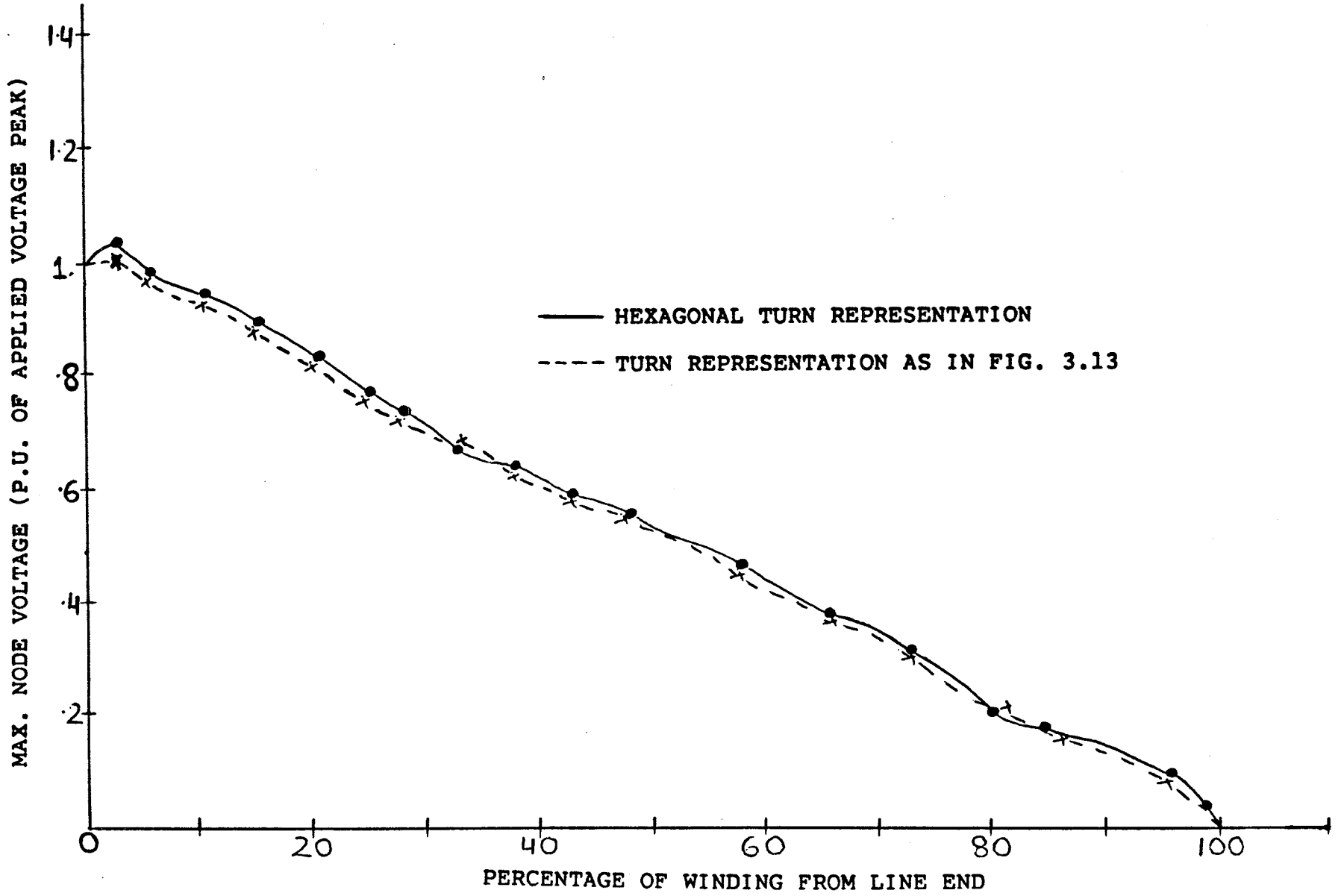

FIG. 5.8 Impulse voltage distribution along the HV winding; hexagonal turn representation and the representation depicted in Fig. 3.13: 1/50 μs wave.

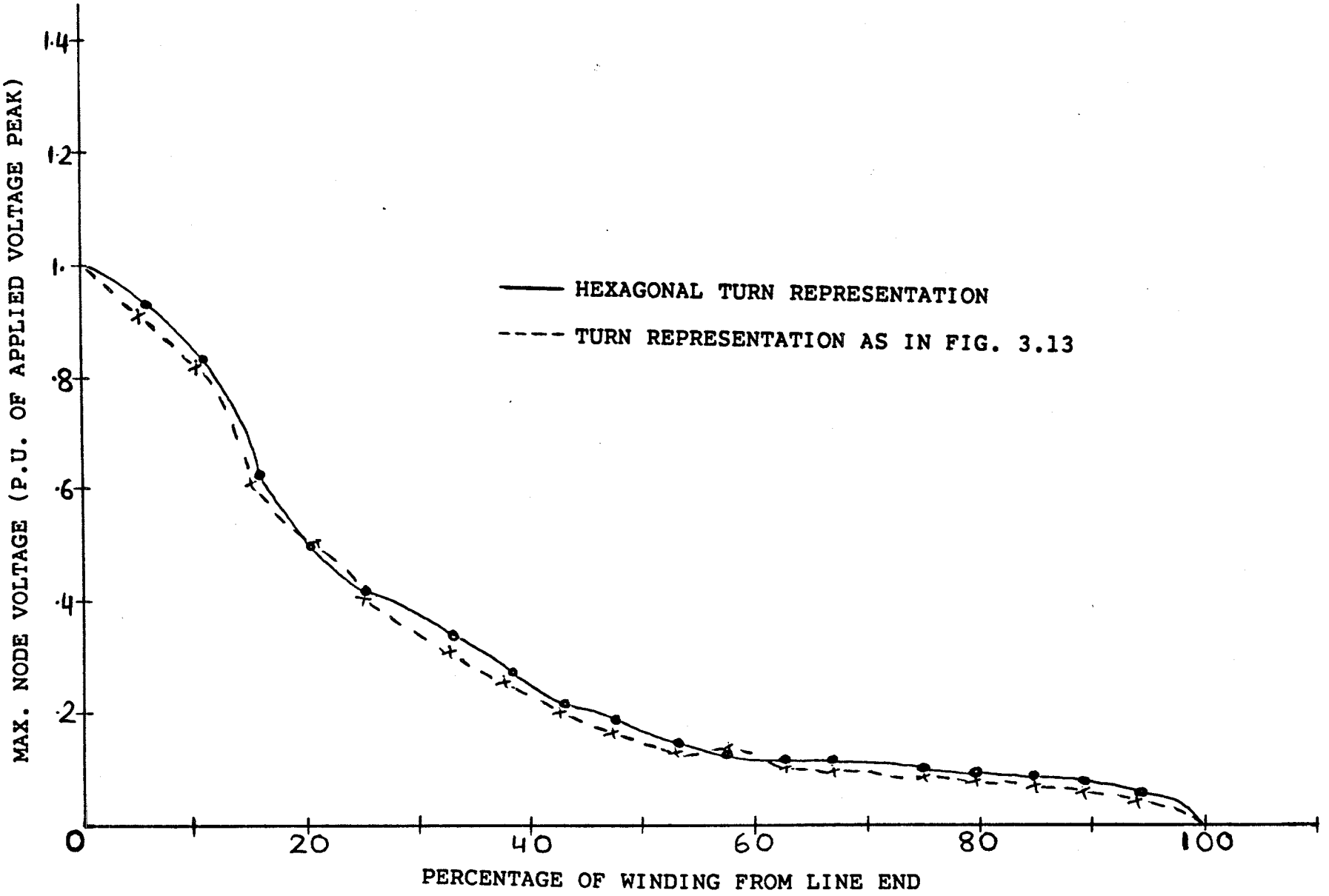

FIG. 5.9 Impulse voltage distribution along the HV winding; hexagonal turn representation and the representation depicted in Fig. 3.13: 1/50 μs wave chopped at 1 μs.

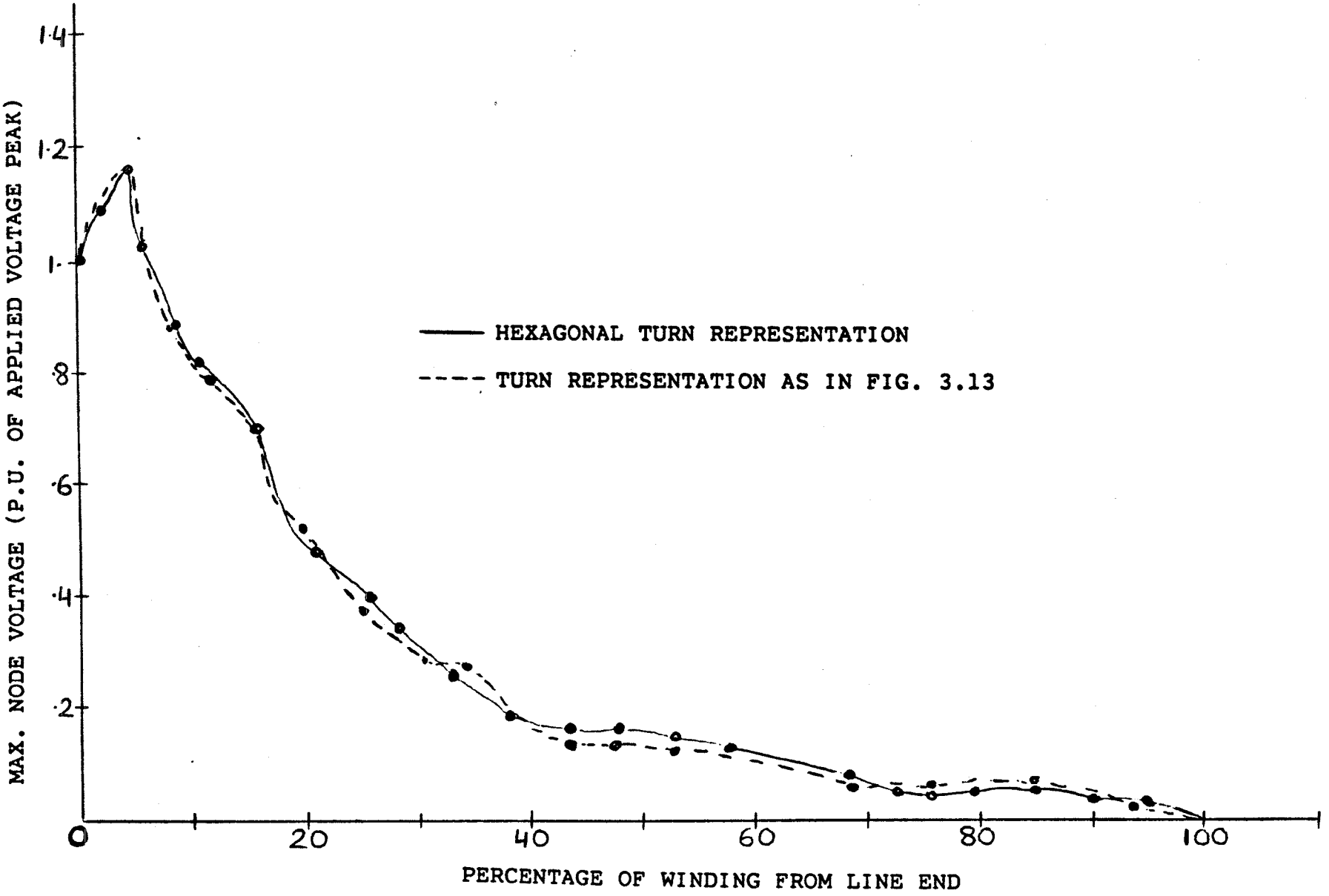

FIG. 5.10 Impulse voltage distribution along the HV winding; hexagonal turn representation and the representation depicted in Fig. 3.13: 0.5/2.5 μs wave.

TABLE 5.1: Maximum Layer-to-layer and Section-to-section Voltages

Applied waveform	Max. layer-to-layer voltage in p.u.*	Max. section-to-section voltage in p.u.*
1/50 μs	0.14	0.61
1/50 μs chopped at 1 μs	0.14	0.61
0.5/2.5 μs	0.15	0.57

* The voltages are given in p.u. of peak of impulse voltage.

The above table is for both the hexagonal representation (Fig. 3.9) and that depicted in Fig. 3.13.

Figures 5.8-5.10 show that there is no significant difference in the voltage stress distribution predicted by using the hexagonal configuration and that obtained with the circular representation shown in Fig. 3.13. This is not unexpected because the two sets of inductance values do not differ by more than 15% .

It is seen that the use of the impulse resistance instead of the dc resistance does not result in appreciable difference in the impulse voltage distribution.

The figures show that the inclusion of the mutual effects not only results in lower response magnitudes throughout the winding, but also in better agreement between the computed and experimental values. This is especially striking in the case of the chopped wave response, Fig. 5.3 and 5.6; in this case the results agree remarkedly well. This is possibly because the accuracy of the

method of taking the mutuals into account (eqn. 3.21) improves with increasing frequency.

The figures also show that the chopped wave results in more severe stressing than the full standard wave; the 0.5/2.5 μs wave gives the worst distribution of the three waveforms.

In all the cases, the maximum layer-to-layer stress occurred between the first and second layers from the line end. The maximum section-to-section stress occurred between the outermost layers of the line end coil and the coil immediately below it; these layers are shown as X and Y in Fig. 2.4.

Computer Time and Storage

On the average, the analysis of each model required 36 seconds of execution time and a memory allocation of 1214k.

5.3 SIMPLIFICATION OF THE TRANSFORMER MODELS AND AN ALTERNATIVE TO THE EMTP SOLUTION TECHNIQUE

Although the EMTP is less costly than other methods of circuit analysis, using it to analyze the transformer models requires a lot of computer time and storage.

In order to derive its model, the transformer was segmented into layers. Therefore, the size of the equivalent network is determined by the number of layers.

A transformer could be made up of such a large number of layers that it becomes too costly to analyze its model by a computer. In some cases, computer memory may not be sufficient for the storage of all the circuit elements. The particular setup of the EMTP im-

poses limitations, not only on the number of mutually coupled branches, but also on the overall size of the network. Furthermore, results of sufficient accuracy may be obtained even if the transformer is represented by a small number of circuit elements.

5.3.1 Simplification of Transformer Models

Earlier researchers partitioned transformer windings into an arbitrary number of segments depending on the storage capacity of the computers available and on the accuracy sought. This kind of segmentation can give reasonably accurate results in the case of uniform windings [4,5].

In subdividing a winding, a uniform distribution of circuit parameters is assumed in each segment. But in practice, there is a continuous variation of parameters along the winding; the variation being generally more pronounced in the barrel-type than in the disc-type of winding. Simplification of the model of the barrel-type transformer, such as that shown in Fig. 2.4, can be done, not by partitioning the transformer into fewer divisions, but through reducing the original network equivalent by combining circuit segments. The procedure followed is given in Appendix I.

In order to evaluate the effectiveness of the proposed method of circuit reduction, the model of the original transformer, shown in Fig. 2.4, consisting of eleven layers per section, was simplified in two stages; first to seven layers and then to five layers per section. The two derived models were analyzed. The results are compared with those of the original model in Figs. 5.11-5.13.

Figures 5.11-5.13 show that the results yielded by using the simplified models are in good agreement with those obtained by using the detailed circuit.

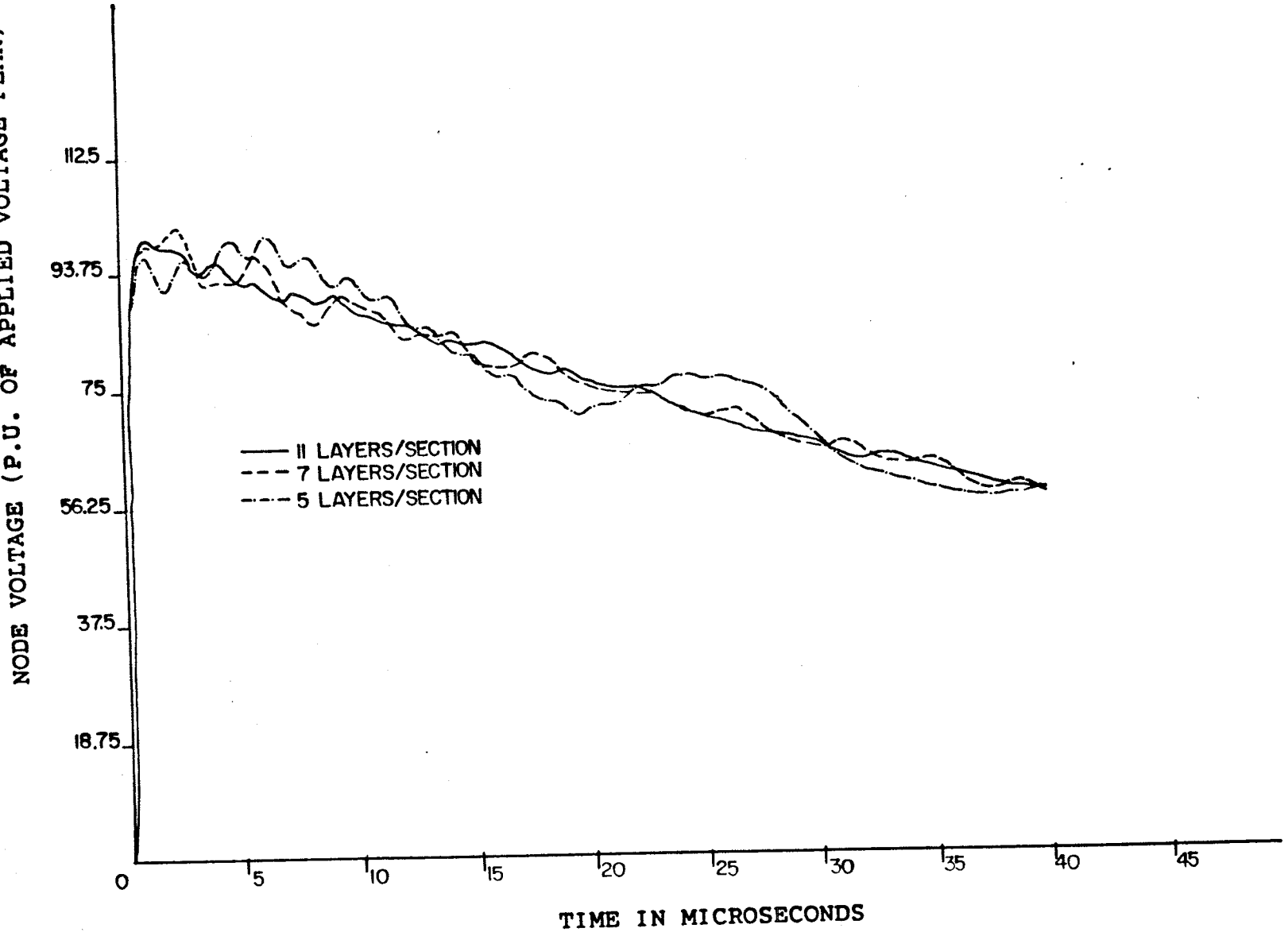

FIG. 5.11 Voltage-time plot at 2 % of winding from line end computed using original and reduced networks: 1/50 μs wave response.

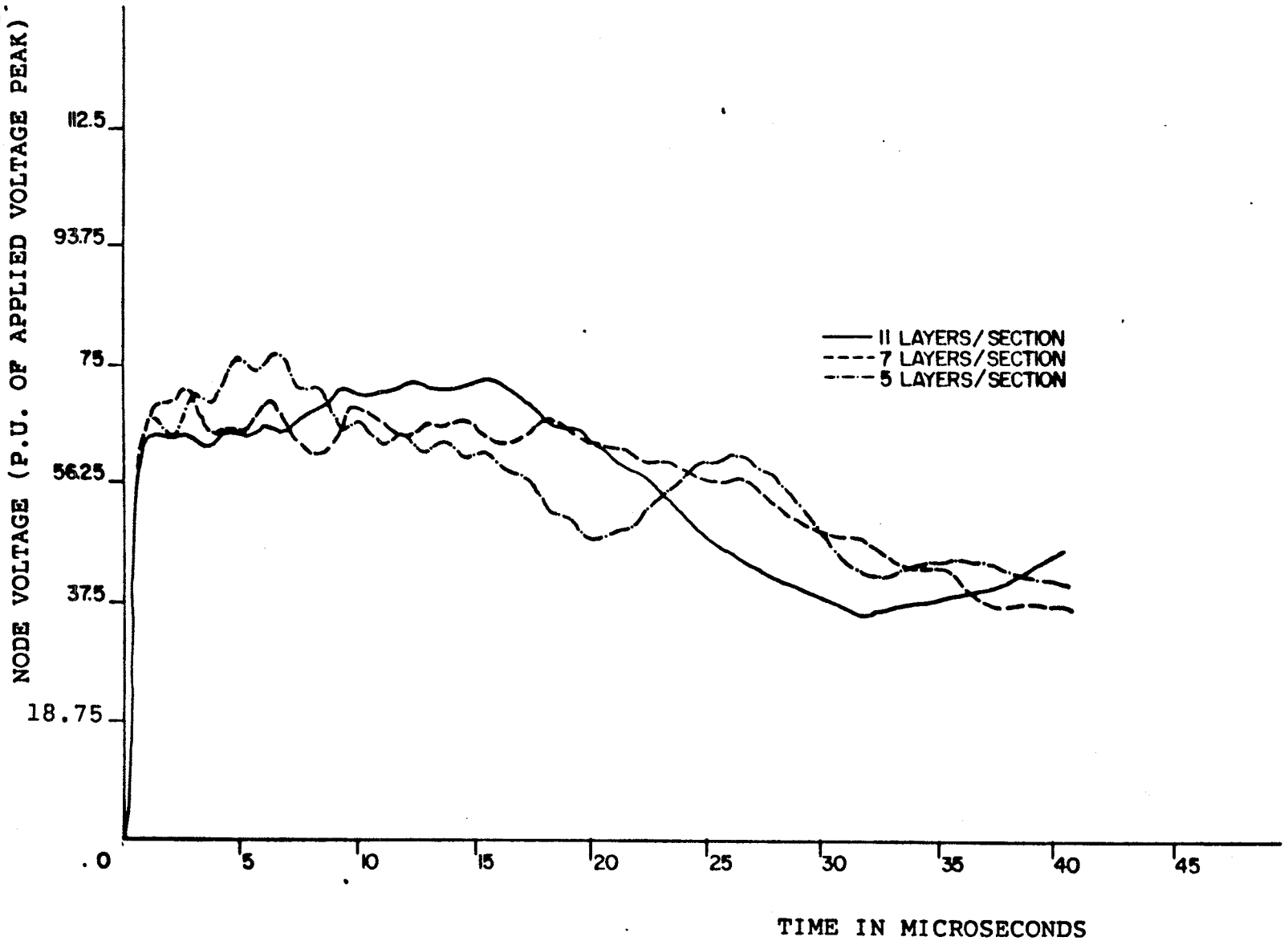

FIG. 5.12 Voltage-time plot at 25 % of winding from line end computed using original and reduced networks: 1/50 μs wave response.

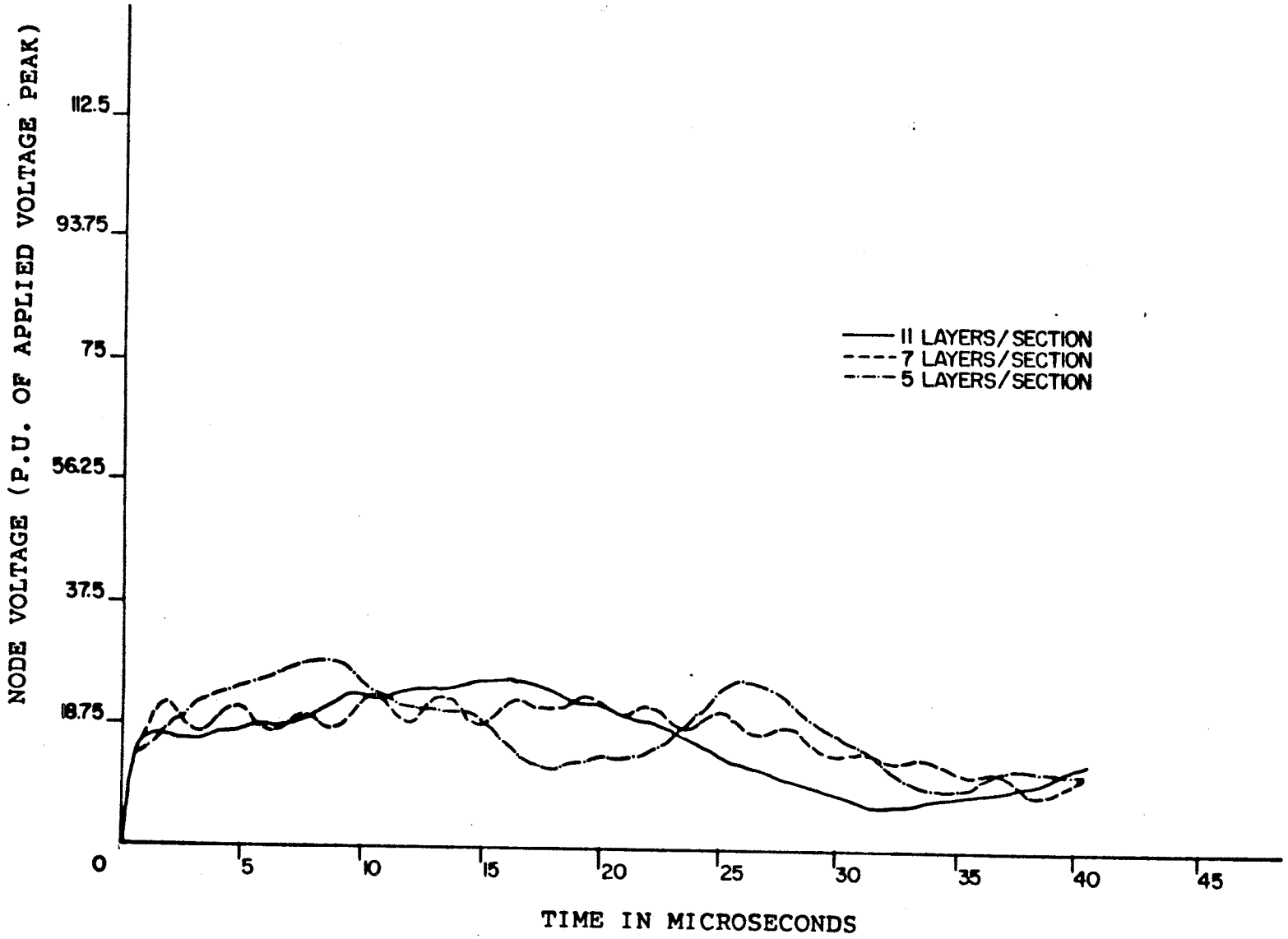

FIG. 5.13 Voltage-time plot at 75 % of winding from line end computed using original and reduced networks: 1/50 μs wave response.

5.3.2 An Alternative to the EMTP Solution Technique

In the EMTP solution technique (section 5.1), the network equations take the form:

$$[Y]\{V(t)\} = \{i(t)\} + \{Ic(t)\} + \{Il(t)\} \tag{5.1}$$

Relation (5.1) can be written as:

$$[Y]\{V(t)\} = \{i(t)\} - \{I(t)\} \tag{5.2}$$

where

$$\{I(t)\} = - \{Ic(t)\} - \{Il(t)\} \tag{5.3}$$

In equation (5.3), $\{I(t)\}$ is the past history current vector, that is, the vector which contains nodal injected current sources which simulate the network history.

The time taken in building up the past history current vector significantly contributes to the overall time required to analyze a network by the EMTP [9].

The analysis of transformer models revealed that the resistive elements are not of paramount importance; it is the inductive and capacitive elements that are most important. Therefore, results of sufficient accuracy for design purposes, can still be obtained even after eliminating some or all the resistances.

The circuit elements can be modelled as inductors or capacitors in parallel with current sources [22]. For illustrative purposes, the modelling of circuit elements as inductors paralleled by current sources will be considered. For this solution technique, known as the Integral of Voltage Method, the solution variable is the integral of voltage while in the EMTP it is the voltage [9].

The circuit element models for the integral of voltage method are given in Table 5.2.

TABLE 5.2: Circuit Element Models for the Integral of Voltage Method

Circuit element	Describing equations	Integral of voltage method model
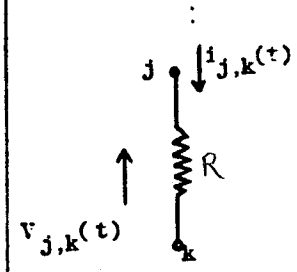	$i_{j,k}(t)=\frac{1}{R}\frac{df_{j,k}(t)}{dt}$ $=\frac{2}{R\Delta t}f_{j,k}(t)-I_R(t)$ $I_R(t)=\frac{2}{R\Delta t}f_{j,k}(t-\Delta t)+i_{j,k}(t-\Delta t)$	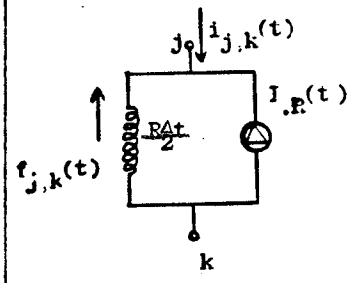
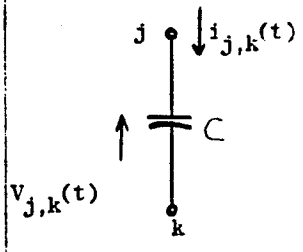	$i_{j,k}(t)=C\frac{d^2f_{j,k}(t)}{dt^2}$ $=\frac{4C}{\Delta t^2}f_{j,k}(t)-I_C(t)$ $I_C(t)=\frac{4C}{\Delta t^2}f_{j,k}(t-\Delta t)+$ $2v_{j,k}(t-\Delta t)+i_{j,k}(t-\Delta t)$	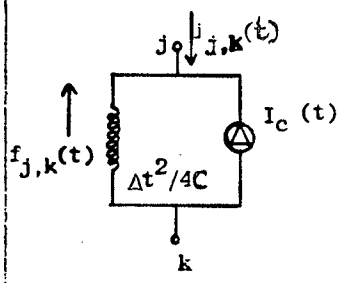
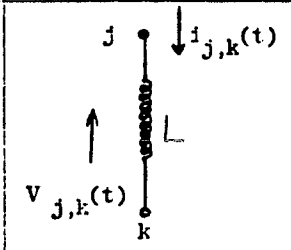	$i_{j,k}(t)=\frac{1}{L}f_{j,k}(t)$	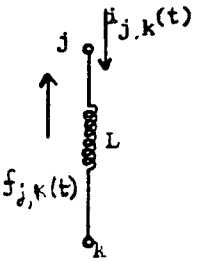

$$f_{j,k}(t)=\int V_{j,k}\,dt$$

The past history current vector for the integral of voltage method takes the form [9]:

$$\{I(t)\} = - \{Ic(t)\} - \{Ir(t)\} \tag{5.4}$$

where

$\{Ic(t)\}$ = vector containing nodal injected current sources which simulate the past history of the capacitive elements

$\{Ir(t)\}$ = vector containing nodal injected current sources which simulate the past history of the resistive elements.

If the resistive elements are excluded from the model, expression (5.4) becomes

$$\{I(t)\} = - \{Ic(t)\} \tag{5.5}$$

Comparison of relations (5.3) and (5.5) reveals that building the past history current vector in the Integral of Voltage Method involves less work than the construction of the corresponding vector in the EMTP. Therefore, computer time and storage can be saved by using the suggested alternative to the EMTP for analyzing the impulse voltage distribution along the transformer windings.

Chapter VI
STUDY OF THE BREAKDOWN AND CONDUCTION CHARACTERISTICS OF RTEmp AND THE SIMULATION OF AN RTEmp-FILLED TRANSFORMER

In order to design an RTEmp-filled transformer, knowledge of the following characteristics of RTEmp and RTEmp-impregnated paper is required:

1. Impulse resistance
2. dielectric strength

Tests were conducted to determine these properties at various temperatures.

6.1 TEST CHAMBER AND ELECTRODES

The test chamber consisted of a cylindrical glass vessel of outer diameter 15.24 cm, inner diameter 13.65 cm and 17.78 cm height. The cylinder has a brass base supported by steel legs. Strap heaters were mounted on the bottom of the brass plate. Polished brass electrodes of plane shape were arranged inside the cylinder. The low-voltage electrode with a grounded guard electrode were fixed rigidly to a teflon base mounted on a brass rod. The high-voltage electrode was suspended from a threaded brass rod inside a threaded sleeve. The vertical position of this supporting rod could be adjusted to set the electrode spacing. The test chamber is shown in Fig. 6.1.

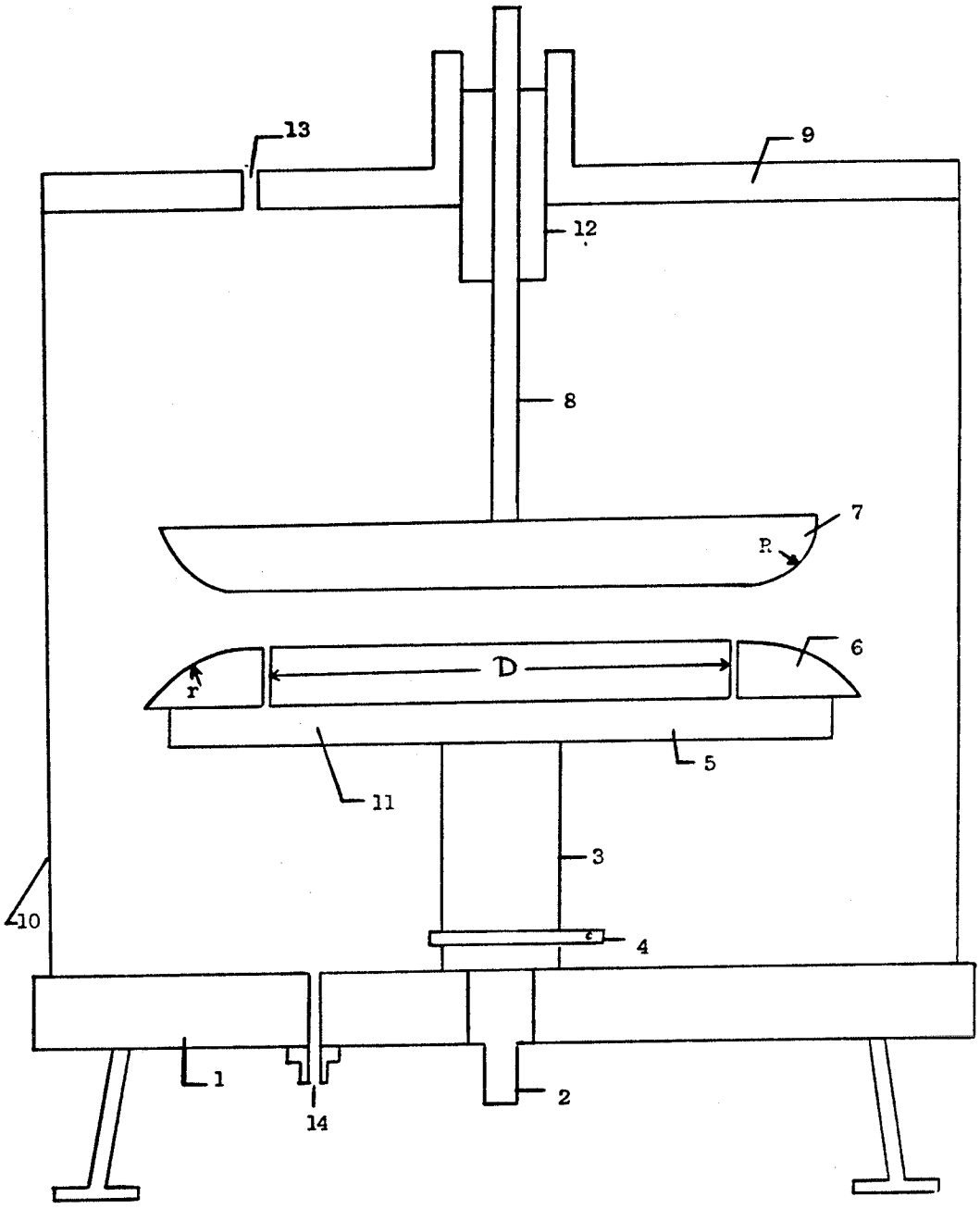

FIG. 6.1: Test Chamber.

1 - Brass base

2 - Exhaust pipe

3 - Brass rod

4 - Conductor for earthing guard electrode

5 - Teflon base

6 - Guard electrode , r = 5.72 cm

7 - HV electrode , R = 0.397 cm

8 - Threaded rod

9 - Acrylic cover

10 - Glass vessel

11 - LV electrode , D = 6.1 cm

12 - Threaded sleeve

13 - Thermocouple

14 - Conductor path

6.2 BREAKDOWN TESTS

The experimental setup used to study the breakdown characteristics of RTEmp fluid is shown in Fig. 6.2.

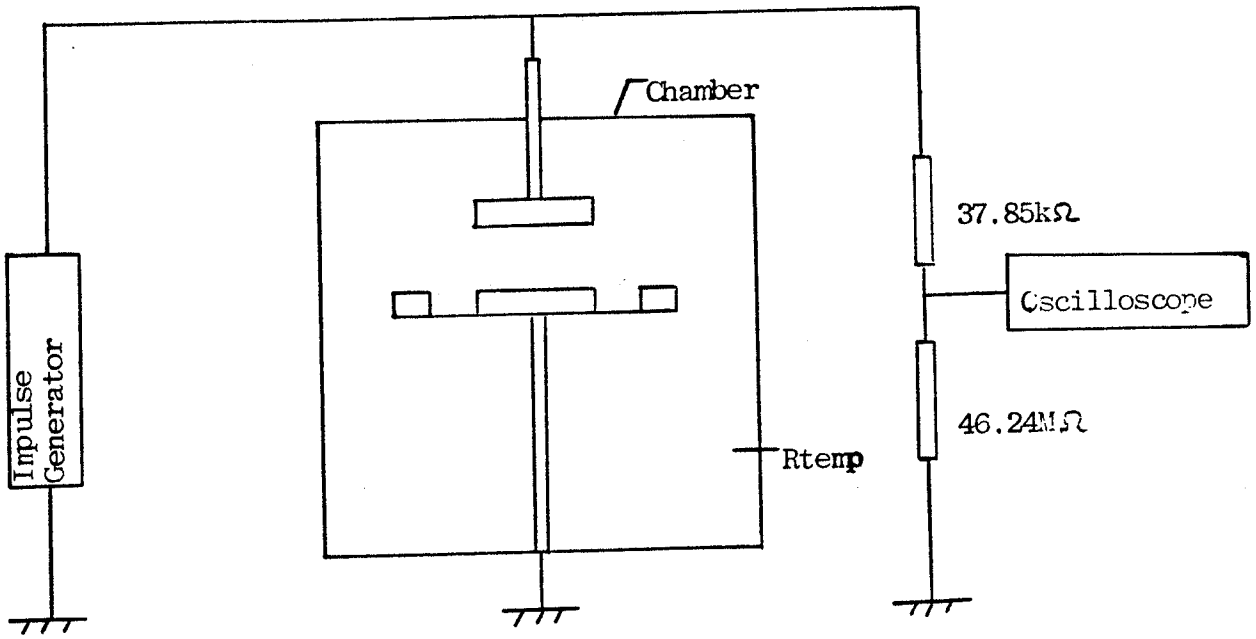

FIG. 6.2: Experimental Assembly for Breakdown Tests.

The tests were conducted for both positive and negative polarity of impulse voltages of standard waveshape at the following temperatures: ambient(25°C), 100°C, 125°C and 150°C. The temperatures were determined by introducing a thermocouple into the gap. The results are listed in Table 6.1.

TABLE 6.1: Breakdown Voltages for 0.25 cm Gap Spacing

Temperature (°C)	Polarity of impulse	Breakdown voltage (kV)
25	-ve	96
25	+ve	108
100	-ve	92
100	+ve	104
125	-ve	91
125	+ve	99
150	-ve	86
150	+ve	97

6.3 DETERMINATION OF CONDUCTION CHARACTERISTICS OF RTEmp

The experimental assembly depicted in Fig. 6.3 was used in determining the conduction characteristics of RTEmp.

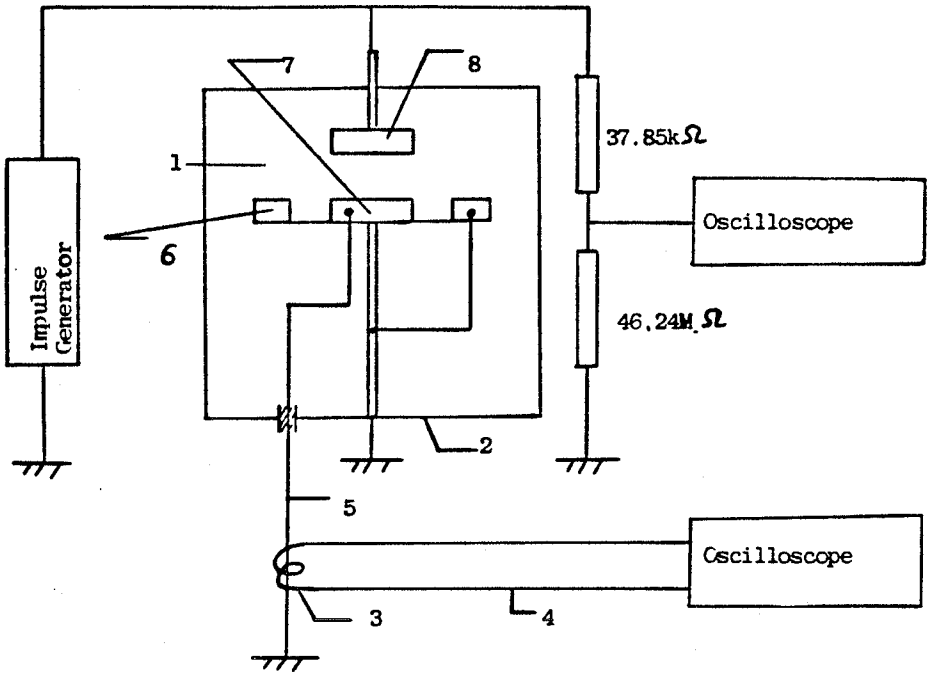

FIG. 6.3: Experimental Set-up for Investigating the Conduction Characteristics of RTEmp.

1 - RTEmp fluid

2 - Test Chamber

3 - Rogowski Coil

4 - Standard 50-ohm Termination

5 - Conductor

6 - Guard Electrode

7 - Low-voltage Electrode

8 - High-voltage Electrode

Test Procedure

The output of the impulse generator was initially set to 50 kV. RTEmp fluid at ambient temperature was subjected to the impulse voltage. The resulting current was monitored by an Ion Physics

Co. current monitor type CM-100-S of the specifications listed in Table 6.2. The magnitude of the voltage was progressively increased until breakdown occured. At each step the current was monitored. The tests were repeated for 100°C, 125°C and 150°C.

TABLE 6.2: Current Monitor Electrical Characteristics

Output sensitivity	Maximum peak current	Pulse Droop % per	Width limit $\int idt$	Maximum allowable ratio= RMS current / frequency	Low frequency
V/A	kA	μs	As*		-3dB Hz
1.0	0.5	1.0	0.002	0.004	1400

* As represents ampere seconds.

The results are shown in Fig. 6.4.

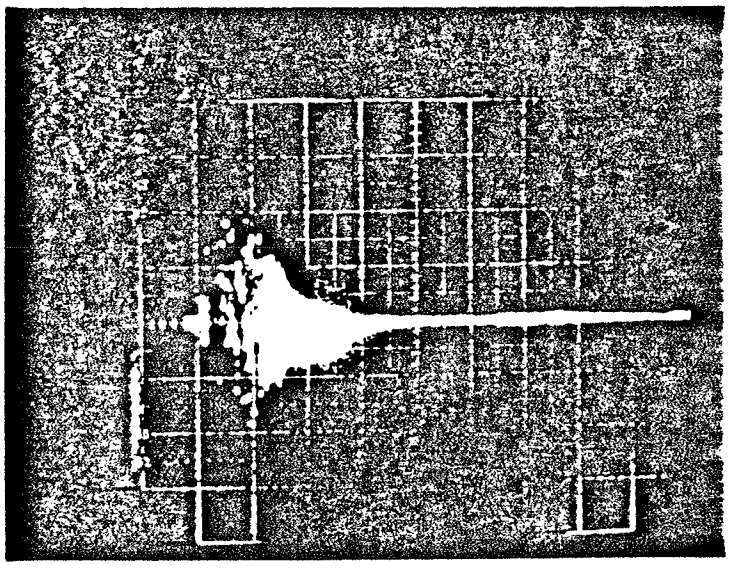

VERTICAL SCALE:
1 AMPERE/DIVISION
HORIZONTAL SCALE:
5 μs/DIVISION

FIG. 6.4(a)

Current-time plot; 25°C, peak voltage 85 kV, negative polarity

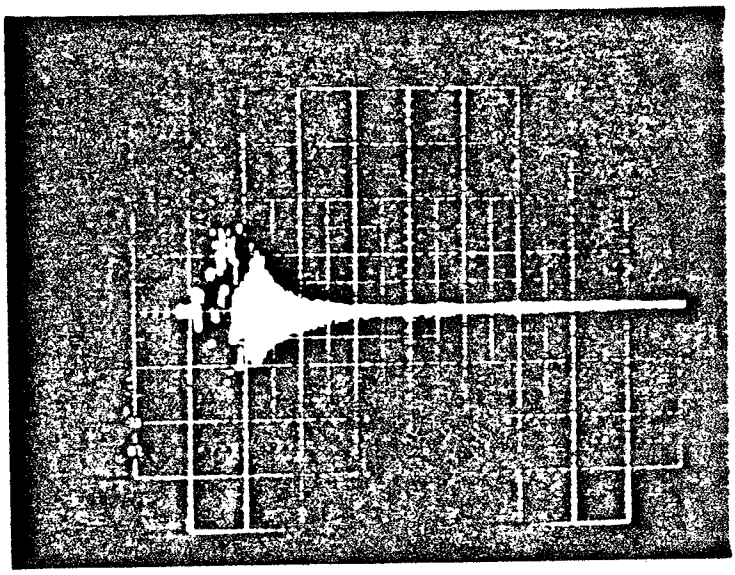

FIG. 6.4(b)

Current-time plot; 25°C, peak voltage 86 kV, positive polarity

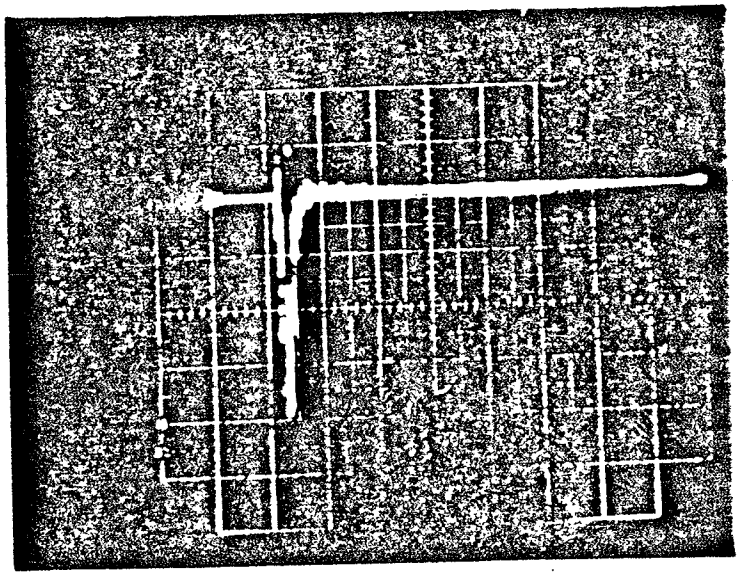

FIG. 6.4(c)

Current-time plot; 100°C, peak voltage 80 kV, negative polarity

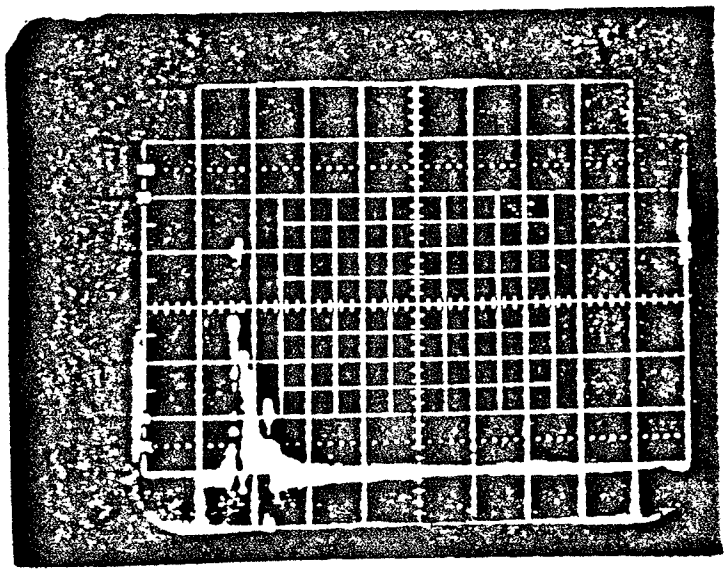

FIG. 6.4(d)

Current-time plot; 100°C, peak voltage 80 kV, positive polarity

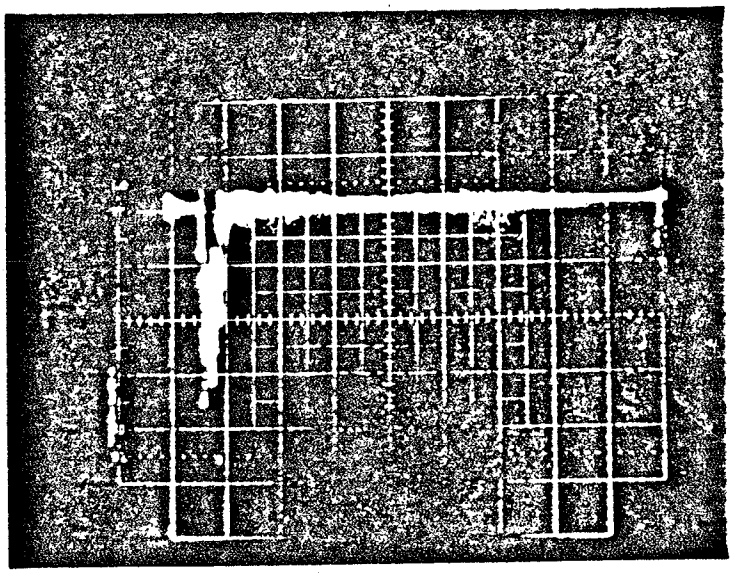

FIG. 6.4(e)

Current-time plot; 125°C, peak voltage 80 kV, negative polarity

Interpretation of Results

The current waveshape of the fluid that exhibits resistive conduction under impulse voltage is derived below:

The impulse voltage, V, can be expressed as:

$$V = A(e^{-at} - e^{-bt}) \qquad (6.1)$$

(The constants A, a and b are as defined in subsection 3.1.2)

Denoting the current by I and impulse resistance by R, the following relation can be obtained:

$$IR = V = A(e^{-at} - e^{-bt})$$

Therefore,

$$I = (A/R)(e^{-at} - e^{-bt}) \qquad (6.2)$$

From relation (6.2) it can be inferred that the conduction current has the same waveshape as the impulse voltage. But the current waveforms which were registered do not have the same shape as the applied voltage (Fig. 6.4). It can therefore be concluded that RTEmp fluid does not exhibit resistive conduction. The currents that were registered are attributed to capacitive conduction. This argument is supported by the following analysis:

Capacitor current is given by:

$$Ic = Cdv/dt \qquad (6.3)$$

In this case C is the capacitance between the high- and low-voltage electrodes with RTEmp as the dielectric (Fig. 6.2). From this equation, it follows that the plot of Ic versus time should have the same shape as the derivative of the impulse voltage, dv/dt. The impulse voltage of positive polarity and its derivative are depicted in Fig. 6.5.

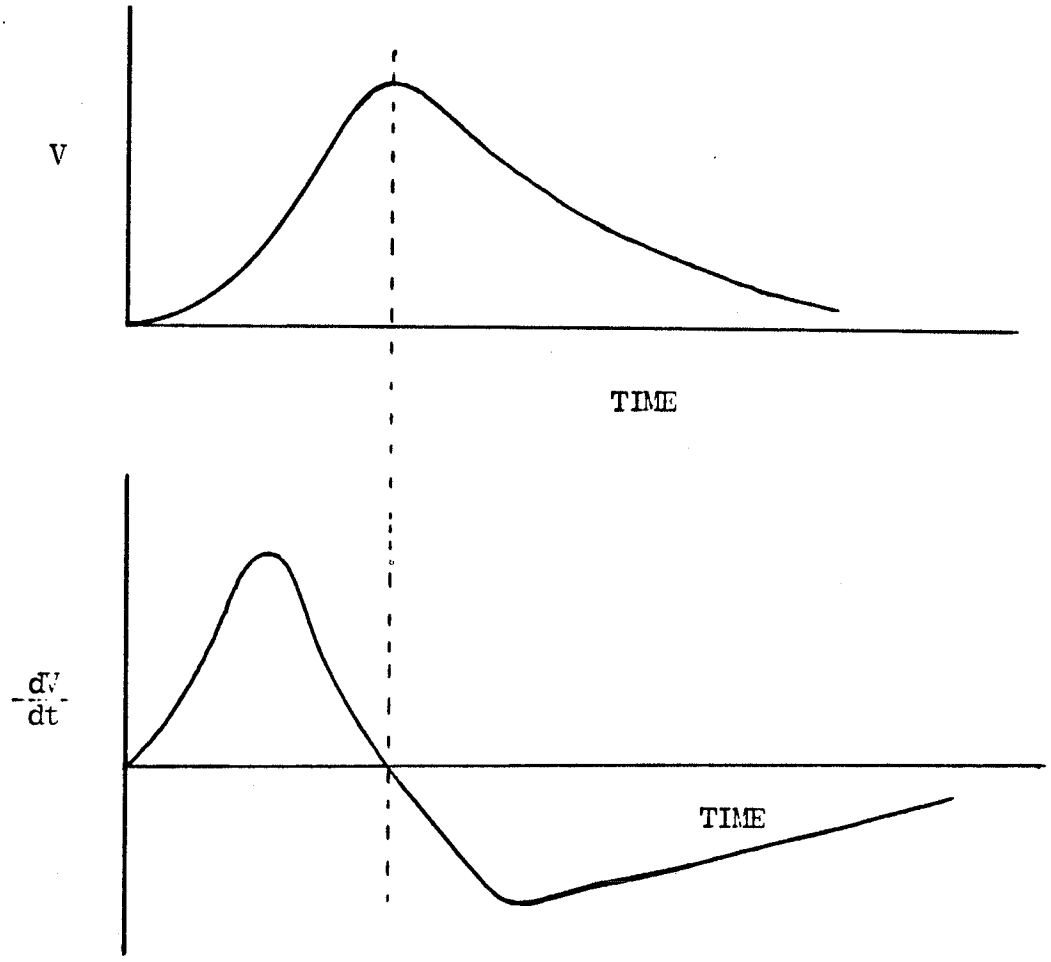

FIG.6.5:

(a)- Impulse voltage of positive polarity

(b)- Time-derivative of the impulse voltage.

The time-derivative of impulse voltage bears a close resemblance to the current oscillograms of temperatures around 100°C and above (Fig. 6.4).

The time-derivative of an impulse wave of negative polarity is shown in Fig. 6.6.

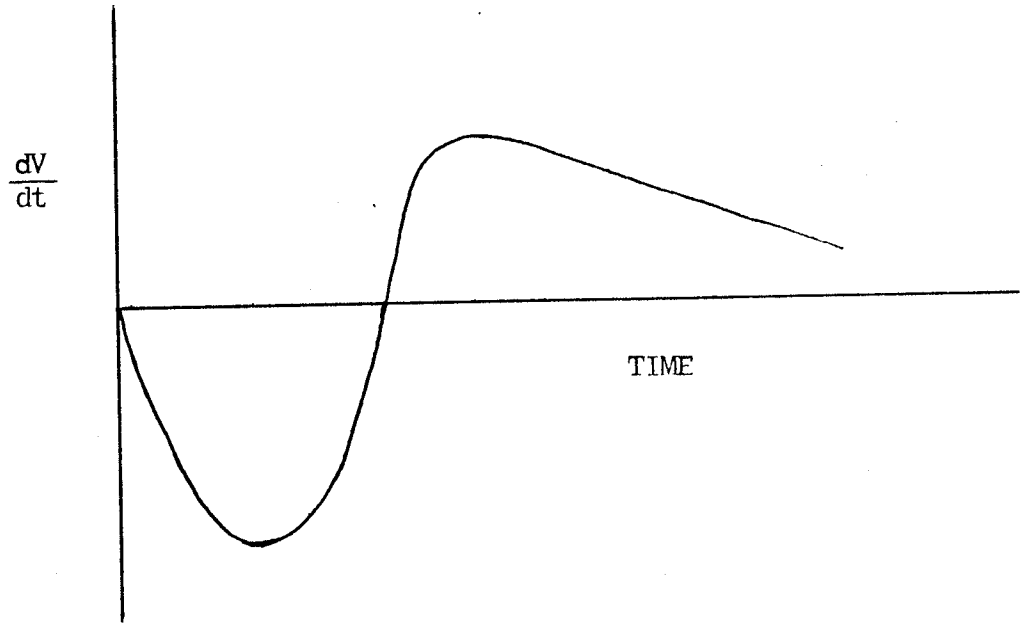

FIG. 6.6: Time-derivative of an impulse wave of negative polarity

The wave depicted above is similar in shape to the current oscillograms for negative polarity of impulses and temperatures of around 100°C and above (Fig. 6.4).

Some known properties of RTEmp are given in Appendix K.

6.4 COMPUTATION OF IMPULSE VOLTAGE DISTRIBUTION ALONG THE WINDINGS OF AN RTEmp-FILLED TRANSFORMER

Since RTEmp does not exhibit resistive conduction under impulse voltages, it can be concluded that the modelling of an RTEmp-filled transformer for computation of voltage stress distribution is the same as that for the mineral oil transformer. Therefore, an RTEmp-filled transformer can also be represented by the electric circuit model depicted in Fig. 2.4.

The difference between the RTEmp case and that of the mineral oil is that the values of the following circuit parameters are different:

1. Layer-to-layer capacitance.
2. Coil-to-tank capacitance.
3. Capacitance between the outermost low-voltage and the innermost high-voltage layers.

Non-impregnable nomex dielectric has been suggested to isolate layers in RTEmp-filled transformers while in mineral oil transformers impregnable paper is used. The dielectric constant of nomex (ϵ_n=3.2) is different from that of paper impregnated with mineral oil (ϵ_p=4.25). Therefore, the layer-to-layer capacitances of an RTEmp-filled transformer are different from those of the mineral oil transformer. For the same reason, the values of the capacitances between the outermost low-voltage and the innermost high-voltage layers are different.

The coil-to-coil capacitance values differ because the dielectric constant of RTEmp (ϵ_t=2.38) is different from that of mineral oil (ϵ_r=2.35).

In Tables 6.3-6.5, the three circuit parameters discussed above are tabulated for mineral oil and RTEmp-filled transformers.

TABLE 6.3: Layer-to-layer Capacitance of RTEmp-filled and mineral oil transformers

Layers	Layer-to-layer capacitance for the mineral oil transformer (nF)	Layer-to-layer capacitance for RTEmp-filled transformer (nF)
1,2	6.68	7.31
2,3	6.81	7.45
3,4	6.95	7.59
4,5	7.09	7.74
5,6	7.23	7.88
6,7	7.37	8.02
7,8	7.51	8.16
8,9	7.64	8.31
9,10	7.78	8.45
10,11	7.58	8.22

TABLE 6.4: Coil-to-coil and Coil-to-tank Capacitances of the mineral oil and RTEmp-filled Transformers

Transformer fluid	Capacitance between top coils (pF)	Capacitance between bottom coils (pF)	Capacitance between each top coil and tank (pF)	Capacitance between each bottom coil and tank (pF)
mineral oil	27.5	20	57.5	40
RTEmp	29.1	21.2	60.9	42.4

TABLE 6.5: Capacitance between the Outermost LV and the Innermost HV Layers of the Mineral Oil and RTEmp-filled Transformers

Fluid used in transformer	Capacitance (μF)
mineral oil	0.36
RTEmp	0.38

The EMTP was again used to analyze the model of the RTEmp-filled transformer. The results obtained were compared with those of the mineral oil transformer as shown in Figs. 6.7-6.9 and Table 6.6.

It can be observed that there is no significant difference between the voltage stress distributions of the mineral oil and RTEmp-filled transformers.

TABLE 6.6: Maximum Layer-to-layer and Section-to-section Voltages for Mineral oil and RTEmp-filled Transformers

for Mineral oil and RTEmp-filled Transformers

Type of fluid used in transformer	Applied waveform	Maximum layer-to-layer voltage given * in p.u.	Maximum section-to-section voltage given * in p.u.
mineral oil	1/50 μs	0.14	0.61
	1/50 μs chopped at 1 μs	0.14	0.61
	0.5/2.5 μs	0.15	0.57
RTEmp	1/50 μs	0.13	0.6
	1/50 μs chopped at 1 μs	0.13	0.6
	0.5/2.5 μs	0.13	0.6

* The voltages are given in p.u. of peak of impulse voltage.

The maximum layer-to-layer voltage was found to occur between the first and second layers from the line end in all the above cases. The maximum section-to-section voltage difference was found to occur between the layers marked X and Y in Fig. 2.4, that is, the first layers of the top and bottom sections on the first limb.

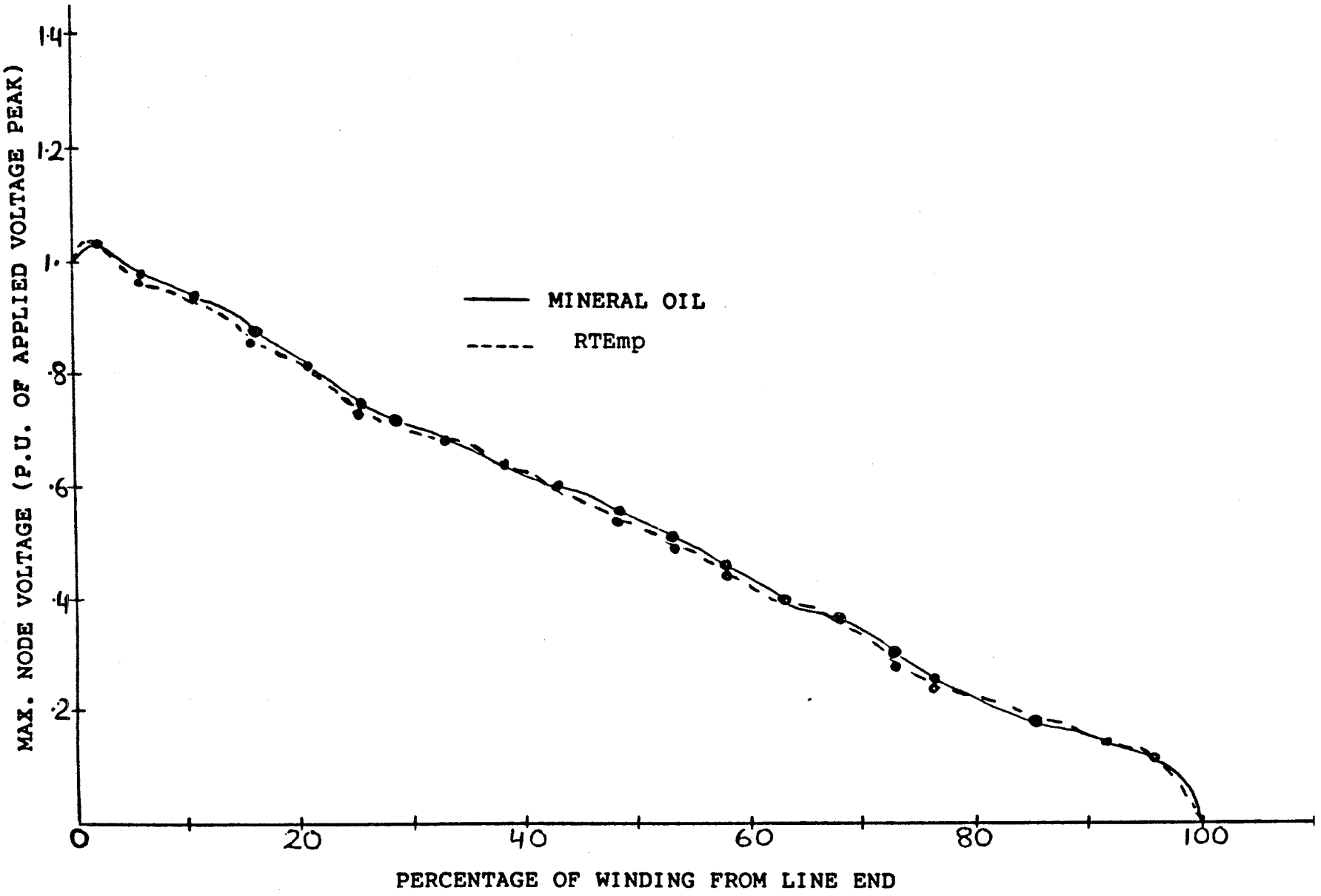

FIG. 6.7 Computed impulse voltage distribution along the HV windings of mineral oil and RTEmp-filled transformers: 1/50 μs wave.

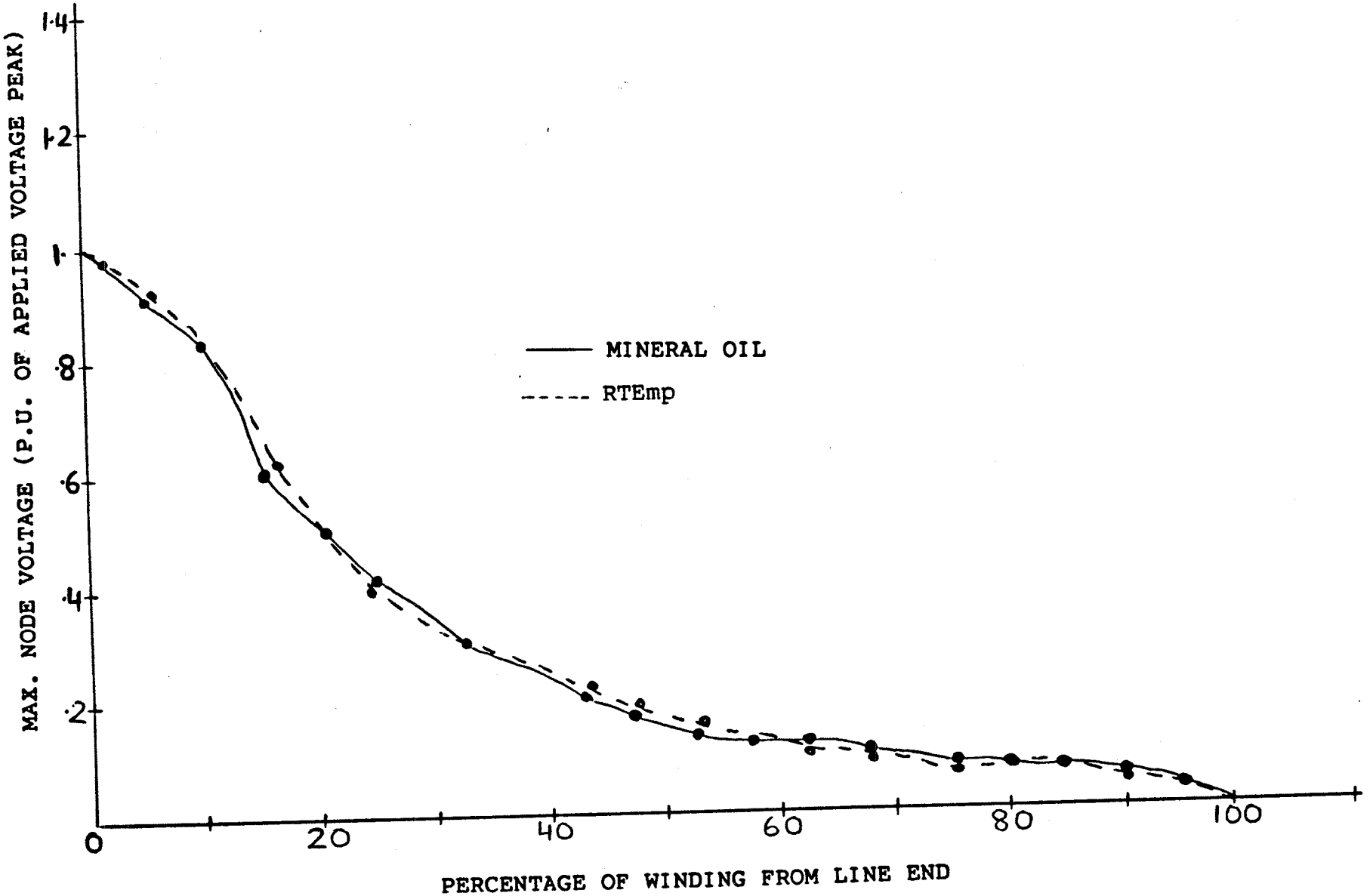

FIG. 6.8 Computed impulse voltage distribution along the HV windings of mineral oil and RTEmp-filled transformers: 1/50 μs wave chopped at 1 μs.

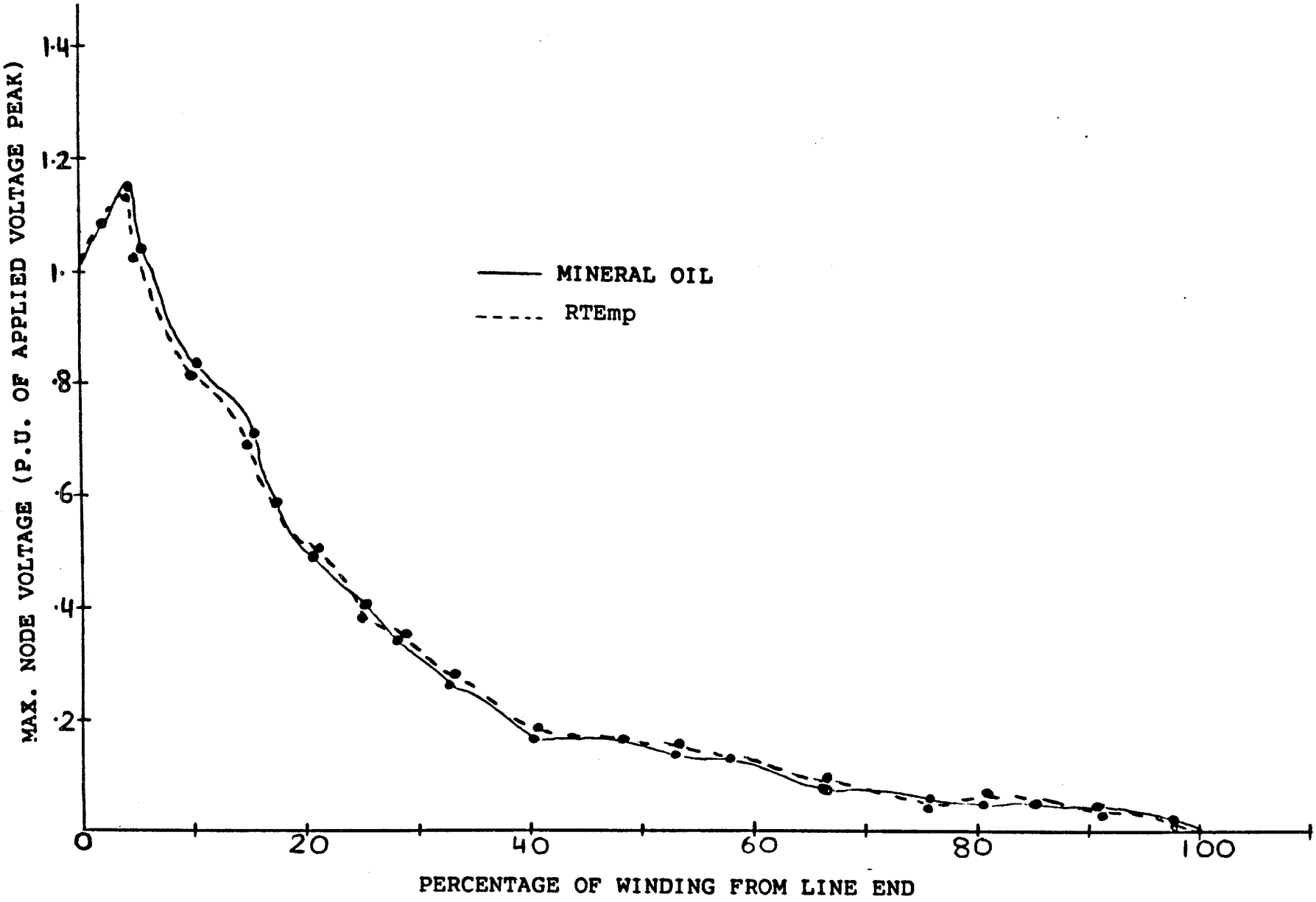

FIG. 6.9 Computed impulse voltage distribution along the HV windings of mineral oil and RTEmp-filled transformers: 0.5/2.5 μs wave.

Chapter VII

VARIATION OF DESIGN PARAMETERS

The effects, on impulse voltage distribution, of the variation of the following three design parameters were investigated:

4. Thickness of insulator coating (formel) on the winding conductor.
5. Clearance of coils from the tank wall.
6. Number of sections constituting each high-voltage coil.

7.1 THICKNESS OF FORMEL COATING

The thickness of formel coating on the high-voltage conductors of the actual transformer is 0.0034". Formel thicknesses of 0.0025" and 0.005" were also used in the model.

Interturn capacitance changes with the variation of formel thickness. The values of interturn capacitance for the three thicknesses of formel are listed in Table 7.1.

TABLE 7.1: Interturn capacitance for the three thicknesses of formel

Layer	Formel thickness		
	0.0034"	0.0025"	0.005"
	(pF)	(pF)	(pF)
1	6.79	9.23	4.56
2	7.08	9.63	4.81
3	7.37	10.02	5.01
4	7.66	10.4	5.21
5	7.97	10.8	5.42
6	8.28	11.3	5.63
7	8.59	11.7	5.84
8	8.91	12.1	6.06
9	9.24	12.6	6.28
10	11.60	15.8	7.89
11	11.72	15.9	7.97

The two new models were analyzed for different impulse shapes. The results are shown compared with those of the original transformer model in Table 7.2. The results revealed that the impulse voltage distributions obtained for the different thicknesses of formel are virtually identical.

TABLE 7.2: Maximum Layer-to-layer and Section-to-section Voltage Stresses for Different Thicknesses of Formel Coating

Thickness of formel coating (inches)	Applied waveform	Maximum layer-to-layer voltage given in p.u.*	Maximum section-to-section voltage given in p.u.*
0.0025	1/50 μs	0.12	0.6
	1/50 μs chopped at 1 μs	0.12	0.6
	0.5/2.5 μs	0.13	0.6
0.0034	1/50 μs	0.14	0.61
	1/50 μs chopped at 1 μs	0.14	0.61
	0.5/2.5 μs	0.14	0.57
0.005	1/50 μs	0.12	0.6
	1/50 μs chopped at 1 μs	0.12	0.6
	0.5/2.5 μs	0.13	0.55

* The voltages are given in p.u. of peak of impulse.

In all the above nine cases, the maximum layer-to-layer voltage was found to be between the first and second layers from the line end while the maximum section-to-section voltage difference was

found to occur between layers marked X and Y in Fig. 2.4, that is, the first layers of the top and bottom sections on the first limb.

7.2 CLEARANCE OF COILS FROM THE TANK WALL

In the tranformer model, alteration of coil-to-tank capacitance values simulates variation in the clearance of the coils from the tank wall.

A 25% increase in coil-to-tank capacitances yields a model corresponding to a 25% decrease in the separation of the coils from the tank. Similarly, an increase in the clearance of the coils from the tank of 25% was simulated by a corresponding reduction of the coil-to-tank capacitance values. The two new models were analyzed for different impulse shapes. The results are shown compared with those of the original transformer model in Table 7.3.

The results revealed that the variation of clearances of the coils from the tank wall does not significantly affect the distribution of impulse voltage distribution along the windings.

TABLE 7.3 Maximum layer-to-layer and Section-to-section Voltage Stresses for Various Clearances of the Coils from the Tank Wall

Clearance of coils from tank wall	Applied waveform	Maximum layer-to-layer voltage given in p.u.*	Maximum section-to-section voltage given in p.u.*
As in actual transformer (0.044 m)	1/50 μs	0.14	0.61
	1/50 μs chopped at 1 μs	0.14	0.61
	0.5/2.5 μs	0.15	0.57
25% reduction in clearance	1/50 μs	0.14	0.61
	1/50 μs chopped at 1 μs	0.14	0.61
	0.5/2.5 μs	0.15	0.57
25% increase in clearance	1/50 μs	0.14	0.61
	1/50 μs chopped at 1 μs	0.14	0.61
	0.5/2.5 μs	0.15	0.57

* The voltages are given in p.u. of peak of impulse.

In all the above nine cases, the maximum layer-to-layer voltage occurred between the first and second layers from the line end. The maximum section-to-section voltage occurred between the first layers of the top and bottom sections of the line end coil; these layers are labelled X and Y in Fig. 2.4.

7.3 NUMBER OF SECTIONS PER HIGH-VOLTAGE COIL

All ealier EMTP simulation studies have been carried out for four-section transformers, that is, transformers for which the high-voltage winding consists of four sections as shown in Fig. 2.1.

An alternative transformer, of the same rating and construction as the original one, but consisting of three sections per high-voltage coil, that is, a total of six sections, was studied.

The electric circuit equivalent of the new model is shown in Fig. 7.7.

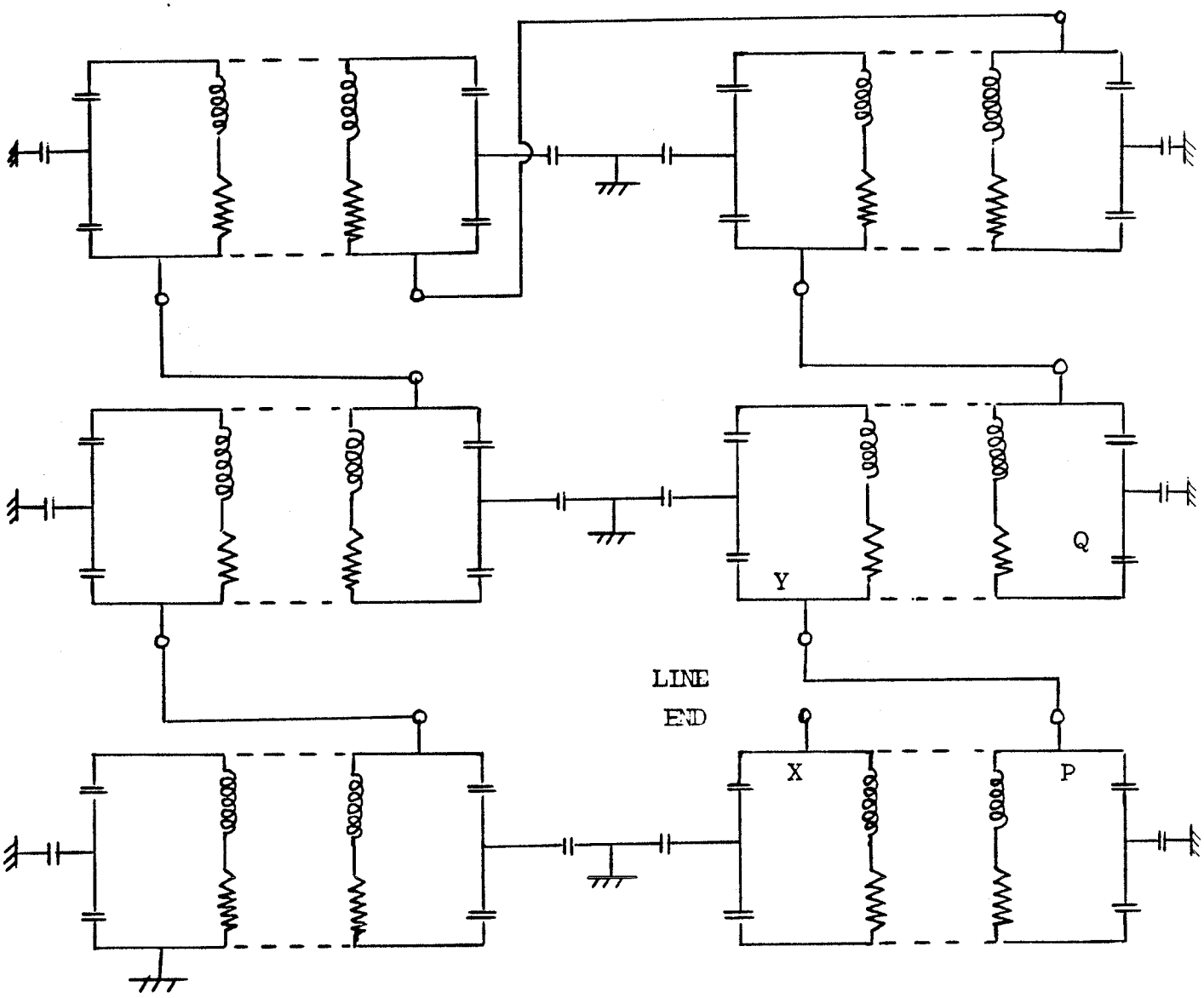

FIG. 7.7: Circuit Model of the six-section Transformer.

The winding constants are tabulated in Tables 7.30-7.36. The model was solved for voltage stress distribution by the EMTP. The results obtained are compared with those of the original transformer in Table 7.4 and Figs. 7.8-7.10.

TABLE 7.30: Winding Resistance of the Six-section Transformer

Layer number	D.C. resistance (Ω)	Impulse resistance for a 1/50 μs wave (Ω)
1	0.2610	2.110
2	0.2654	2.146
3	0.2698	2.181
4	0.2742	2.217
5	0.2786	2.252
6	0.2830	2.288
7	0.2874	2.324
8	0.2918	2.359
9	0.2962	2.395
10	0.3006	2.430
11	0.2209	1.786

TABLE 7.31: Interturn Capacitance of the Six-section Transformer

Layer	Capacitance (pF)
1	14.7
2	15.2
3	15.7
4	16.2
5	16.7
6	17.2

TABLE 7.31 continued

Layer	Capacitance (pF)
7	17.7
8	18.3
9	18.8
10	19.4
11	27.2

TABLE 7.32: Layer-to-layer Capacitance for the Six-section Transformer

Layers	Capacitance (nF)
1,2	6.78
2,3	6.90
3,4	7.01
4,5	7.12
5,6	7.23
6,7	7.35
7,8	7.46
8,9	7.57
9,10	7.68
10,11	6.72

TABLE 7.33: Self-inductance for the Six-section Transformer computed using the Turn Representation shown in Fig. 3.9

Layer	Inductance (mH)
1	0.2064
2	0.2104
3	0.2145
4	0.2185
5	0.2225
6	0.2266
7	0.2307
8	0.2348
9	0.2389
10	0.2431
11	0.1490

TABLE 7.34: Layer-to-layer Mutual-inductance for the Six-section Transformer

Layers	Inductance (mH)	Layers	Inductance (mH)
1,2	0.1972	3,9	0.1628
1,3	0.1885	3,10	0.1554
1,4	0.1800	3,11	0.1152
1,5	0.1720	4,5	0.2086
1,6	0.1643	4,6	0.1993
1,7	0.1569	4,7	0.1903
1,8	0.1498	4,8	0.1817
1,9	0.1430	4,9	0.1735

TABLE 7.34 continued

Layers	Inductance (mH)	Layers	Inductance (mH)
1,10	0.1366	4,10	0.1657
1,11	0.1012	4,11	0.1228
2,3	0.2011	5,6	0.2125
2,4	0.1920	5,7	0.2030
2,5	0.1835	5,8	0.1938
2,6	0.1752	5,9	0.1850
2,7	0.1674	5,10	0.1767
2,8	0.1598	5,11	0.1309
2,9	0.1526	6,7	0.2164
2,10	0.1457	6,8	0.2066
2,11	0.1080	6,9	0.1973
3,4	0.2049	6,10	0.1884
3,5	0.1957	6,11	0.1340
3,6	0.1869	7,8	0.2203
3,7	0.1785	7,9	0.2103
3,8	0.1705	7,10	0.2008
7,11	0.1488	9,10	0.2281
8,9	0.2242	9,11	0.1690
8,10	0.2140	10,11	0.1801
8,11	0.1586		

TABLE 7.35: Section-to-section Capacitance for the Six-section Transformer

Layers	Capacitance (pF)
1	2.16
2	2.20
3	2.24
4	2.27
5	2.31
6	2.34
7	2.38
8	2.42
9	2.45
10	2.49
11	2.52

TABLE 7.36: Layer-to-earth Capacitance for the Six-section Transformer

Layers	Capacitance (pF)
1	4.12
2	4.19
3	4.26
4	4.33
5	4.40
6	4.47
7	4.54

TABLE 7.36 continued

Layers	Capacitance (pF)
8	4.60
9	4.67
10	4.74
11	4.81

TABLE 7.4: Maximum layer-to-layer and Section-to-section Voltages for the Six-section and the Four-section Transformers

Type of transformer	Applied waveform	Maximum layer-to-layer voltage in p.u.*	Maximum section-to-section voltage in p.u.*
four-section	1/50 μs	0.14	0.61
	1/50 μs chopped at 1 μs	0.14	0.61
	0.5/2.5 μs	0.15	0.61
Six-section	1/50 μs	0.061	0.23
	1/50 μs chopped at 1 μs	0.061	0.26
	0.5/2.5 μs	0.066	0.23

* The voltages are given in p.u. of peak of impulse voltage.

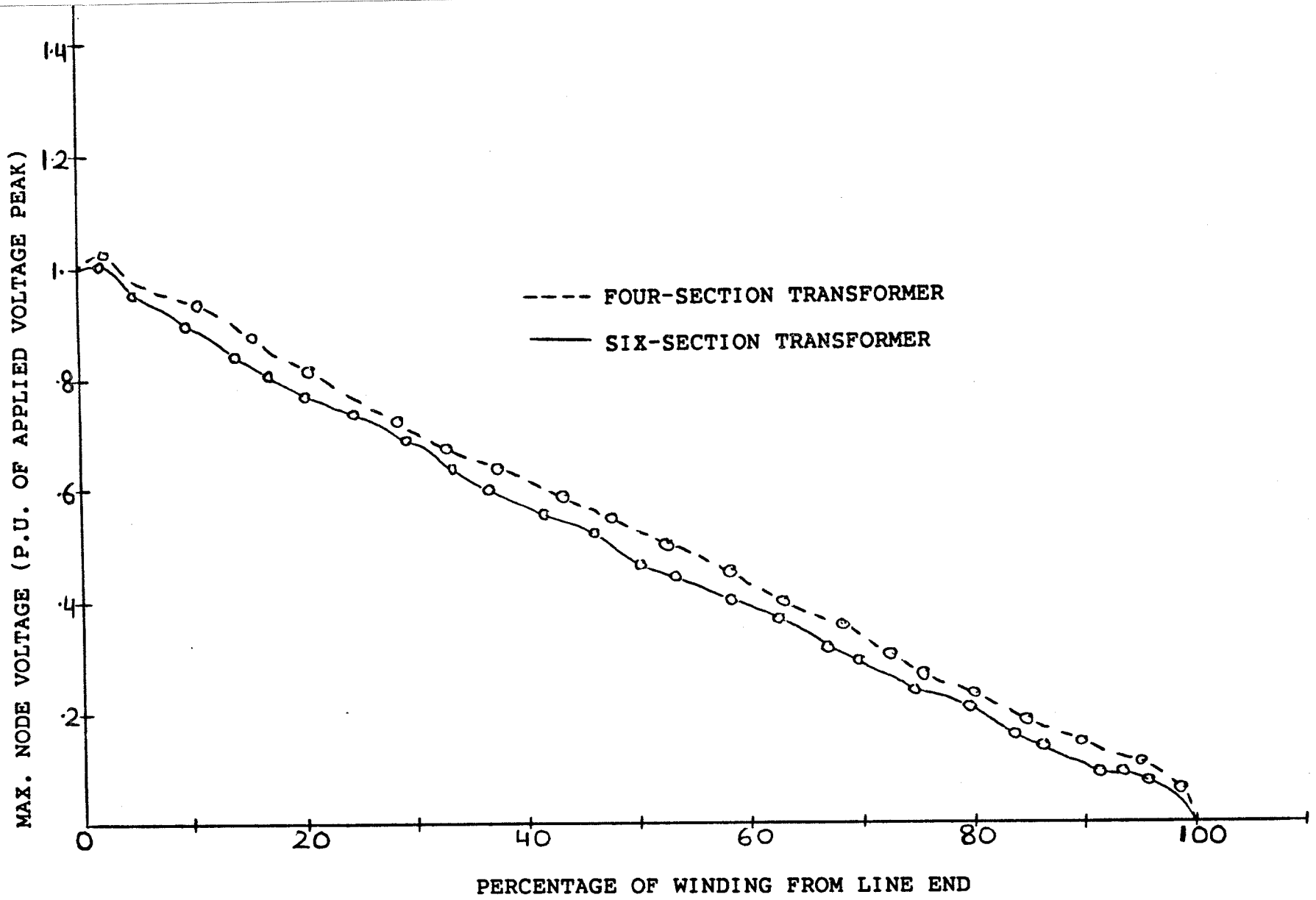

FIG. 7.8 Computed impulse voltage distribution along the HV windings of the four-section and six-section transformers: 1/50 μs wave.

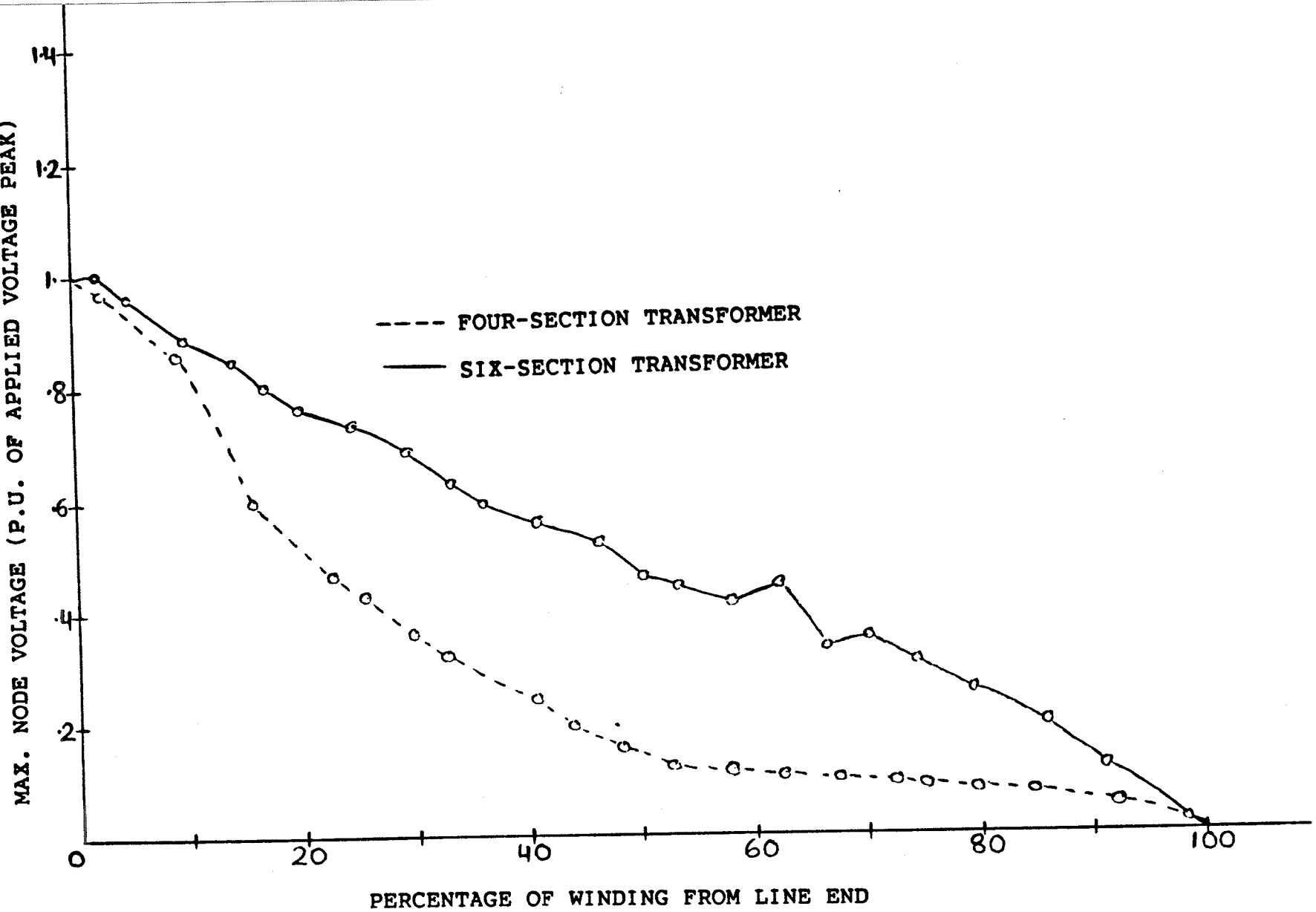

FIG. 7.9 Computed impulse voltage distribution along the HV windings of the four-section and six-section transformers: 1/50 μs wave chopped at 1 μs.

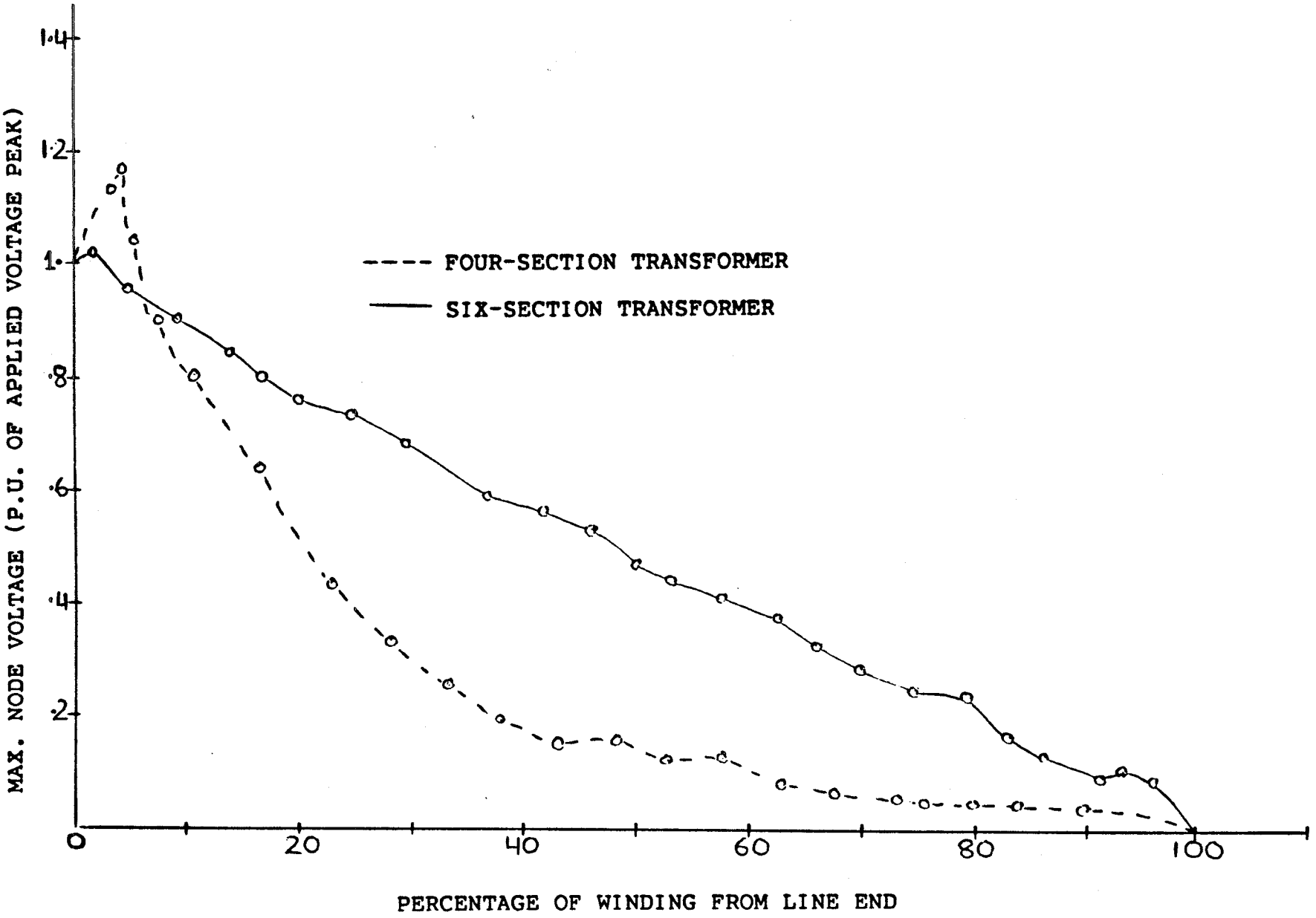

FIG. 7.10 Computed impulse voltage distribution along the HV windings of the four-section and six-section transformers: 0.5/2.5 μs wave.

In all the above six cases, the maximum layer-to-layer stress occurred between the first and second layers from the line end. For the four-section transformer, the maximum section-to-section stress occurred between the outermost layers of the top and bottom sections of the coil to which the impulse is directly applied. In the case of the six-section transformer, for the standard and the 0.5/2.5 μs waves, the maximum section-to-section stress occurred between the innermost layers of the first and second sections from the line end (layers X and Y, Fig. 7.7). With the chopped wave, the maximum section-to-section stress occurred between the outermost layers of the first and second sections from the line end (layers P and Q, Fig. 7.7).

The results indicate that the voltage stresses in the Six-section transformer are less severe than those in the four-section transformer.

Explanation for the Differences in Impulse Response of the Four- and Six-section Transformers

When a voltage surge impinges on the terminals of the transformer, for the first few microseconds [19], the winding can be represented by a purely capacitive network called the initial voltage distribution model. Consider two such networks; one for the four-section transformer (Fig. 7.11) and another for the six-section transformer (Fig. 7.12).

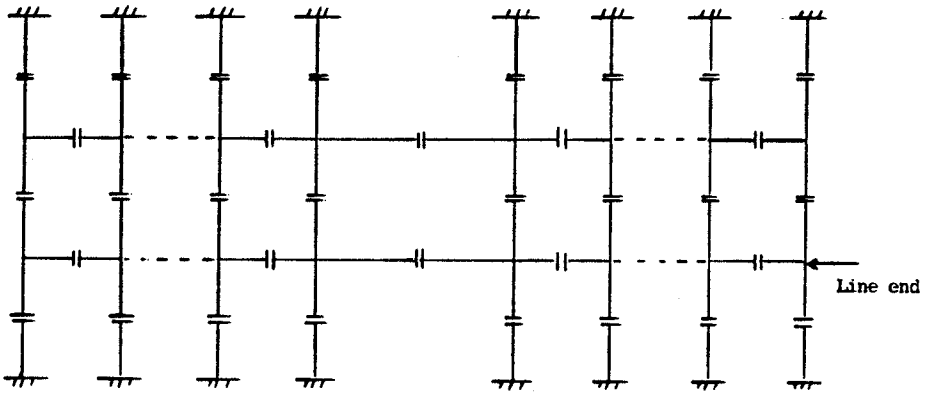

FIG. 7.11: Initial Voltage Distribution Circuit for the Four-section Transformer.

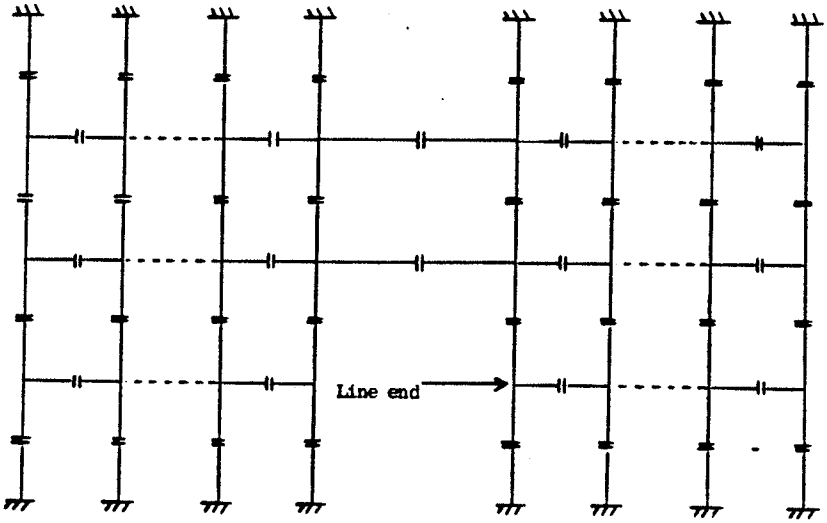

FIG. 7.12: Initial Voltage Distribution Circuit for the Six-section Transformer.

Figures 7.11 and 7.12 show that the six-section transformer possesses more paths for displacement current flow from one section to another than the four-section transformer; charge flow across sections contributes to the establishment of a uniform initial voltage distribution.

Chapter VIII

SURGE TRANSFERENCE FROM AN IMPULSED TO A NONIMPULSED WINDING

When an impulse wave impinges on the terminals of a transformer, transient voltages are produced , not only in the surged winding, but also in the nonimpulsed winding; transferred voltages have been reported to be responsible for insulation failure in the latter winding [11,12,14,23]. Therefore, the design of transformer insulation requires a reasonably accurate estimate of the magnitudes and distributions of surges that are likely to be transferred to the nonimpulsed windings.

The transient voltages transferred from one winding to another consist of four components [12]. These components, shown in Fig. 8.1, are listed below:

1. The electromagnetic component.
2. The electrostatic component.
3. The free oscillations of the nonimpulsed winding.
4. The forced oscillations of the nonimpulsed winding, induced by the free oscillations of the surged winding.

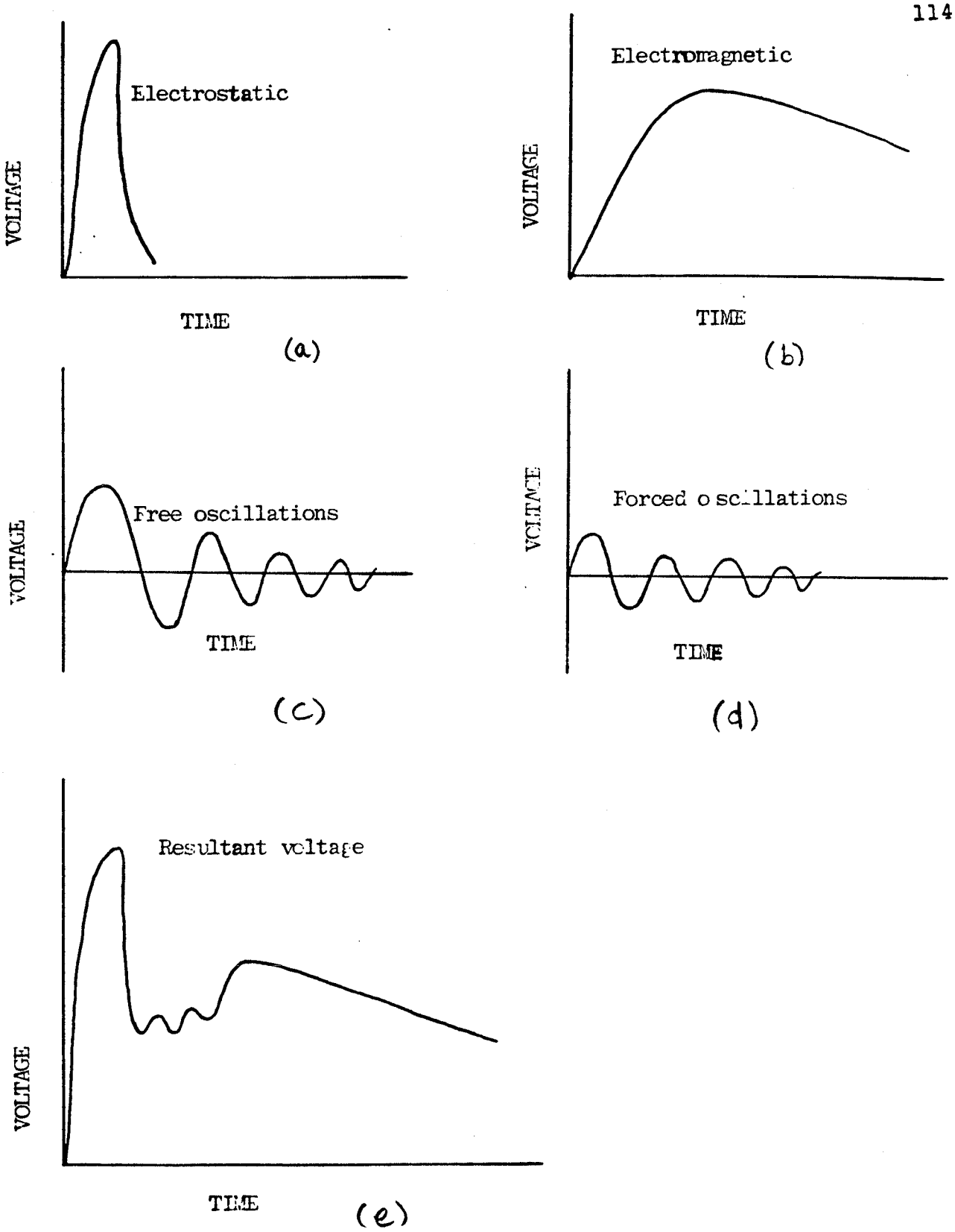

Fig. 8.1: The Four Components of the Transferred Voltages and their Resultant [12].

It is only the first and second components (Figs. 8.1(a) and 8.1(b)) which are of practical importance [12].

The Electrostatic Component

In order to evaluate the electrostatic transference between windings, the transformer can be represented, in an approximate manner, by the circuit shown in Fig. 8.2.

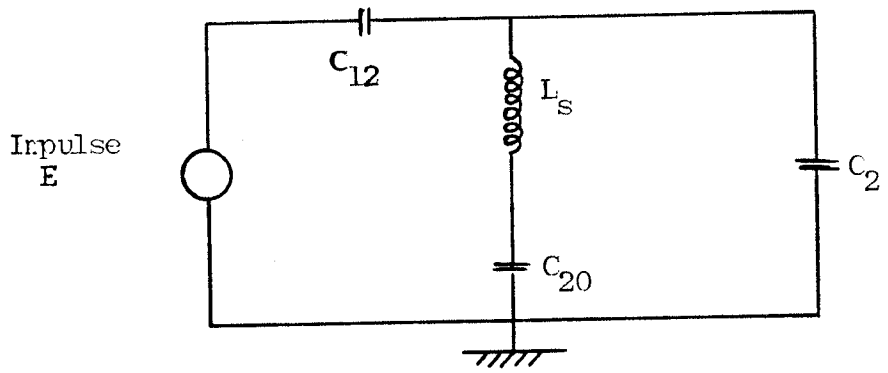

FIG. 8.2: Equivalent Circuit of Electrostatic Transference between windings.

Ls = self-inductance of the nonimpulsed winding

C12 = capacitance between windings

C2 = equivalent capacitance between the line end of the non-impulsed winding and earth

C20 = Capacitance between the neutral end of the nonimpulsed winding and earth

(for a transformer with an earthed neutral, C20=0)

If an impulse wave impinges on one terminal of a two-winding transformer, the nonimpulsed winding gets charged over the capacitance C12 between the two windings and discharges over the leakage inductance Ls and capacitances C2 and C20 to earth.

The Electromagnetic Component

An impulse applied to one winding of a transformer sets up oscillations in that winding. These oscillations are transferred to the nonimpulsed winding by magnetic induction. The nonimpulsed winding then undergoes forced oscillations. The two windings under the conditions of magnetic transference can be represented by the circuit shown in Fig. 8.3.

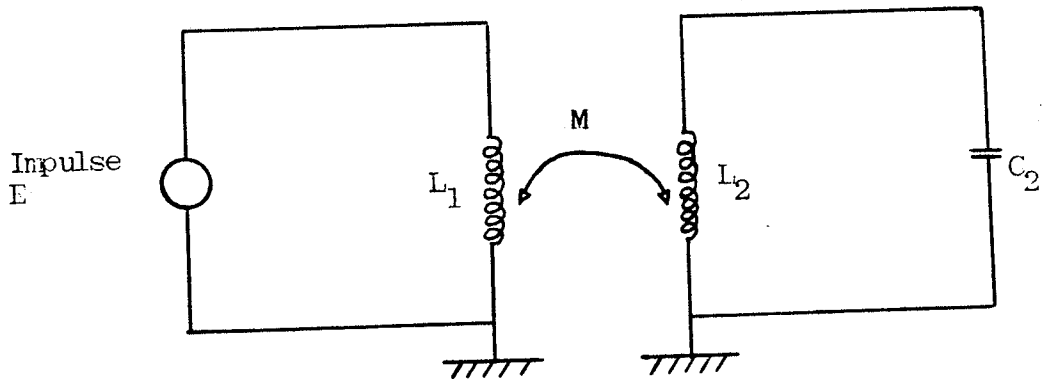

FIG. 8.3: Equivalent Circuit of the Electromagnetic Transference between windings.

L1 = self-inductance of the impulsed winding

L2 = self-inductance of the nonimpulsed winding

M = mutual-inductance between the two windings.

Based on the equivalent circuits depicted in Figs. 8.2 and 8.3, analytical expressions have been derived for determining the mag-

nitudes of transferred surges [24]. However, due to the very approximate nature of the equivalent circuits, the derived equations cannot be used to predict the voltage stress distribution in the nonimpulsed winding; they can only give the transferred voltage across the whole of the winding.

In an attempt to estimate the effects of the transferred surges to sufficient accuracy for design purposes, the two windings were represented by the model depicted in Fig. 8.4; this circuit is for the four-section transformer. The network for the six-section transformer is similar to that in Fig. 8.4.

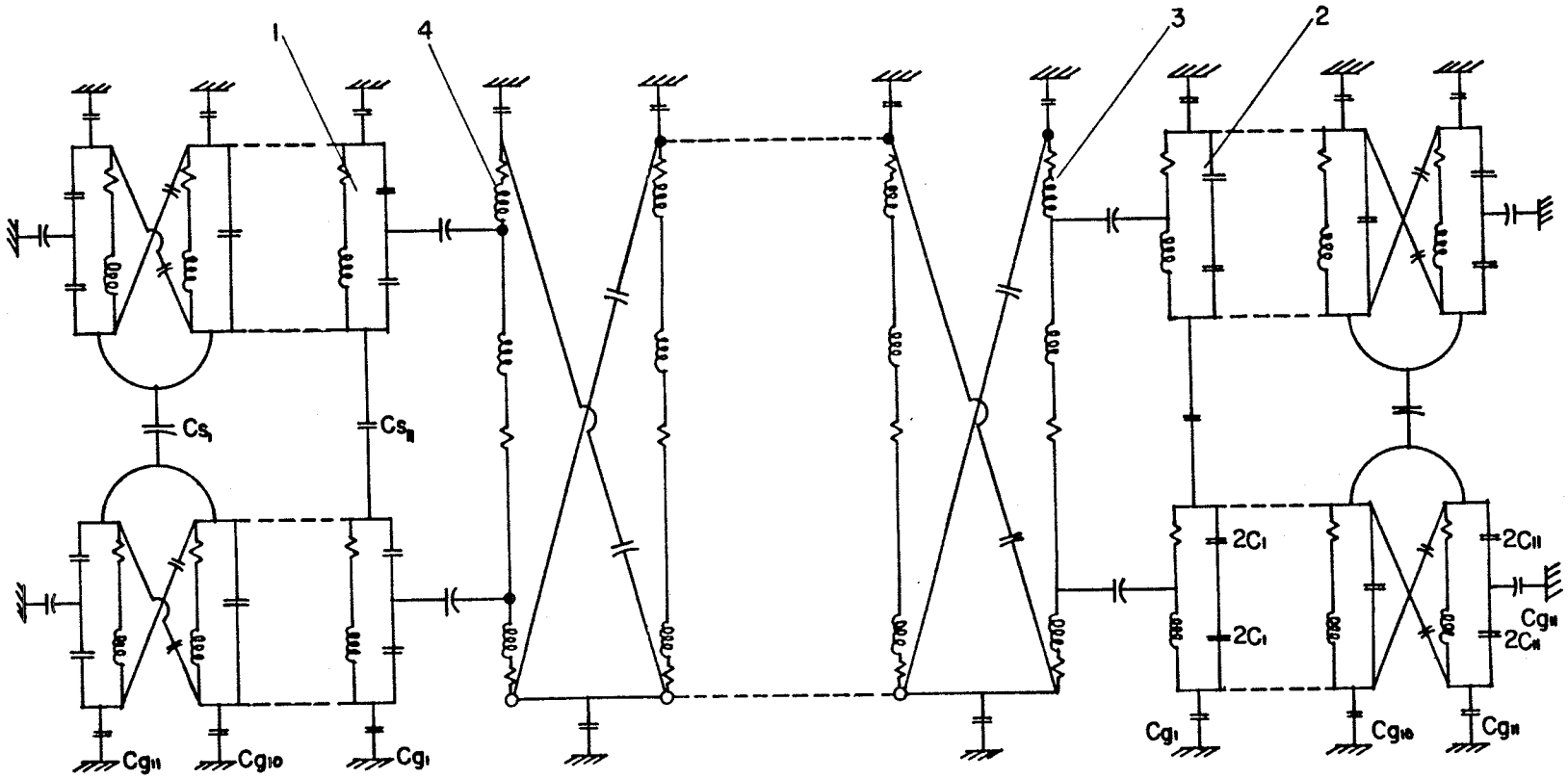

FIG. 8.4: Circuit Model for the Low- and High-voltage Windings.

1,2 - Innermost HV layers

3,4 - Outermost LV layers

To find the circuit parameters of the low-voltage winding, the methods used in Chapter III to determine the element values of the high-voltage winding were adopted.

In Tables 8.1-8.4 the winding constants of the low-voltage winding are listed.

TABLE 8.1: Layer-to-layer Capacitance for the LV Winding of the Four-section Transformer

Layers	Capacitance (nF)
1,2	33.8
2,3	24.6
3,4	36.0
4,5	36.6
5,6	37.2
6,7	37.8
7,8	12.8
8,9	39.0
9,10	39.6
10,11	28.1
11,12	41.9
12,13	42.5
13,14	43.1

TABLE 8.2: Self-inductance for the LV Winding of the Four-section Transformer

Layer	Inductance (μH)
1	0.1904
2	0.1952
3	0.2062
4	0.2100
5	0.2149
6	0.2200
7	0.2238
8	0.2302
9	0.2355
10	0.2394
11	0.2509
12	0.2563
13	0.2618
14	0.2673

TABLE 8.3: Layer-to-layer Mutual-inductance for the LV Winding of the Four-section Transformer

Layers	Inductance (mH)	Layers	Inductance (mH)
1,2	0.1779	2,12	0.1022
1,3	0.1688	2,13	0.09578
1,4	0.1574	2,14	0.08974
1,5	0.1472	3,4	0.1921
1,6	0.1376	3,5	0.1794
1,7	0.1284	3,6	0.1677
1,8	0.1205	3,7	0.1563

TABLE 8.3 continued

Layers	Inductance (mH)	Layers	Inductance (mH)
1,9	0.1128	3,8	0.1465
1,10	0.1053	3,9	0.1371
1,11	0.09992	3,10	0.1279
1,12	0.0936	3,11	0.1212
1,13	0.08772	3,12	0.1134
1,14	0.08222	3,13	0.1062
2,3	0.1852	3,14	0.09947
2,4	0.1725	4,5	0.1961
2,5	0.1613	4,6	0.1832
2,6	0.1507	4,7	0.1706
2,7	0.1406	4,8	0.1599
2,8	0.1319	4,9	0.1496
2,9	0.1234	4,10	0.1395
2,10	0.1152	4,11	0.1321
2,11	0.1092	4,12	0.1236
4,13	0.1157	7,11	0.1724
4,14	0.1083	7,12	0.1611
5,6	0.2007	7,13	0.1506
5,7	0.1869	7,14	0.1408
5,8	0.1751	8,9	0.2149
5,9	0.1637	8,10	0.2000
5,10	0.1526	8,11	0.1892

TABLE 8.3 contined

Layers	Inductance (mH)	Layers	Inductance (mH)
5,11	0.1445	8,12	0.1767
5,12	0.1351	8,13	0.1650
5,13	0.1264	8,14	0.1543
5,14	0.1183	9,10	0.2191
6,7	0.2048	9,11	0.2071
6,8	0.1918	9,12	0.1934
6,9	0.1792	9,13	0.1806
6,10	0.1669	9,14	0.1687
6,11	0.1580	10,11	0.2262
6,12	0.1477	10,12	0.2111
6,13	0.1381	10,13	0.1971
6,14	0.1292	10,14	0.2038
7,8	0.2095	11,12	0.2340
7,9	0.1956	11,13	0.2184
7,10	0.1822	11,14	0.2038
12,13	0.2391		
12,14	0.2230		
13,14	0.2441		

TABLE 8.4 Resistance for the LV Winding of The Four-section Transformer

Layer	Resistance ($\mu\Omega$)
1	56.2
2	57.6
3	60.3
4	61.4
5	62.4
6	63.4
7	64.5
8	65.8
9	66.8
10	67.9
11	70.6
12	71.7
13	72.7
14	73.4

TABLE 8.5: Mutual-inductance between the LV and HV Windings of the Four-section Transformer

LV Layers \ HV layers	1	2	3	4	5	6	7	8	9	10	11
1	.096	.092	.089	.086	.082	.079	.076	.073	.070	.067	.065
2	.101	.097	.094	.090	.087	.083	.079	.073	.073	.070	.068
3	.108	.104	.101	.101	.092	.089	.085	.081	.078	.075	.072
4	.113	.109	.106	.106	.097	.093	.089	.0845	.082	.078	.076
5	.119	.114	.111	.106	.102	.098	.093	.090	.086	.082	.080
6	.125	.120	.117	.112	.107	.102	.098	.094	.090	.086	.084
7	.131	.126	.122	.117	.112	.107	.103	.099	.094	.090	.088
8	.138	.132	.129	.123	.118	.113	.108	.104	.099	.095	.092
9	.145	.139	.135	.129	.124	.119	.113	.109	.104	.100	.097
10	.132	.146	.142	.135	.130	.124	.119	.114	.109	.104	.101
11	.161	.155	.151	.144	.138	.132	.126	.121	.116	.111	.108
12	.170	.155	.151	.151	.145	.139	.132	.127	.122	.116	.113
13	.178	.171	.166	.159	.152	.146	.139	.134	.128	.122	.119
14	.187	.179	.174	.167	.160	.153	.146	.140	.134	.128	.124

The mutual-inductance values are in (μh)

TABLE 8.6: Layer-to-layer Capacitance for the LV Winding of the six-section Transformer

Layers	Capacitance (nF)
1,2	34.4
2,3	35.0
3,4	35.6
4,5	36.2
5,6	36.9
6,7	37.5
7,8	30.8
8,9	38.7
9,10	39.3
10,11	39.9
11,12	40.5
12,13	41.1
13,14	41.7

TABLE 8.7: Self-inductance of the LV winding of the Six-section Transformer

Layer	Inductance (μH)
1	0.1903
2	0.1952
3	0.2002
4	0.2040
5	0.2091
6	0.2143
7	0.2182

TABLE 8.7 continued

Layer	Inductance (μH)
8	0.2381
9	0.2434
10	0.2489
11	0.2529
12	0.2584
13	0.2640
14	0.2680

TABLE 8.8: Mutual-inductance between the LV and the HV Windings for the Six-section Transformer

LV Layers \ HV layers	1	2	3	4	5	6	7	8	9	10	11
1	.045	.044	.044	.043	.043	.043	.042	.043	.043	.042	.042
2	.046	.046	.045	.045	.044	.044	.043	.044	.044	.044	.043
3	.047	.047	.046	.046	.047	.046	.046	.046	.045	.045	.044
4	.048	.048	.048	.047	.047	.046	.046	.047	.046	.046	.045
5	.050	.049	.049	.048	.048	.048	.047	.048	.048	.047	.047
6	.051	.051	.050	.050	.049	.049	.048	.050	.049	.049	.048
7	.052	.052	.052	.051	.051	.050	.050	.051	.050	.050	.049
8	.056	.055	.055	.054	.054	.053	.053	.054	.053	.053	.052
9	.057	.057	.056	.055	.055	.055	.054	.055	.054	.054	.054
10	.059	.058	.058	.057	.057	.056	.055	.057	.056	.056	.055
11	.060	.059	.059	.058	.058	.057	.057	.058	.057	.061	.056
12	.061	.061	.061	.060	.059	.059	.058	.060	.059	.058	.058
13	.063	.063	.062	.061	.061	.060	.060	.061	.061	.060	.059
14	.065	.064	.064	.063	.062	.062	.061	.063	.062	.061	.061

The mutual-inductance values are in (μh)

The circuit model shown in Fig. 8.4 was solved for surge transfer from the high- to the low-voltage winding and vice versa.

Surge Transfer from the High- to the Low-voltage Winding

In the evaluation of surge transfer from the high- to the low-voltage winding, the latter winding was considered connected to a typical domestic load [14] as shown in Fig. 8.5.

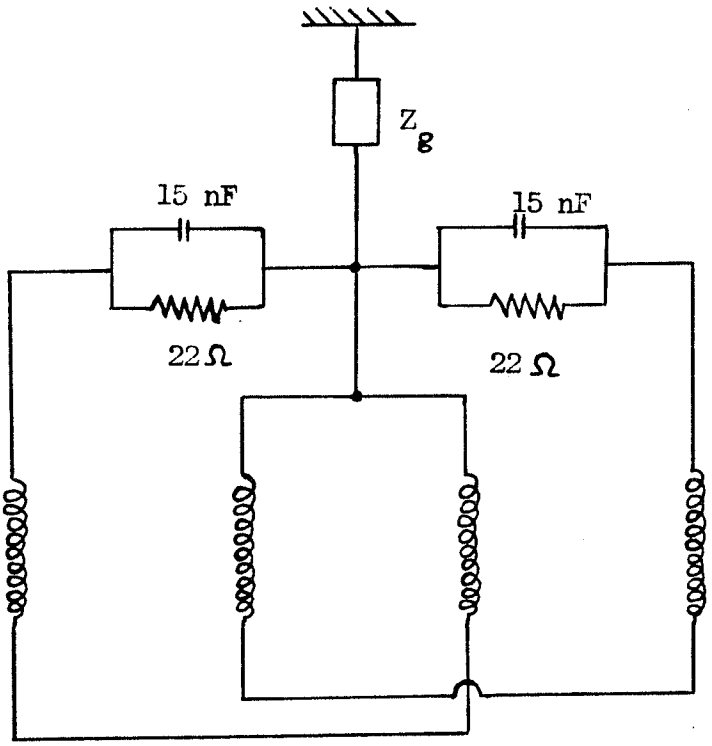

FIG. 8.5: Domestic Load connected to the Low-voltage Winding.

The impulse voltage distribution along the low-voltage winding was computed for different impulse shapes originating from the high-voltage side, with ground resistance, Zg, as parameter. The values of ground resistance used were: 47Ω, 15Ω, 5Ω, 1Ω. The results are shown in Tables 8.9 and 8.10.

TABLE 8.9: Surges Transferred from the HV to the LV winding of the Four-section transformer

Applied waveform	Ground impedance	Maximum LV node voltage in p.u.*	layer-to-layer voltage in p.u.*
1/50 μs	1	0.023	0.047
	5	0.031	0.069
	15	0.050	0.082
	47	0.075	0.093
1/50 μs chopped at 1 μs	47	0.15	0.22

* The voltages are given in p.u. of peak of impulse voltage.

In all the above cases, the maximum node voltage was found to occur in the outermost low-voltage layer, that is, the layer closest to the high-voltage winding. The worst layer-to-layer stress was found to occur between the two outermost low-voltage layers.

TABLE 8.10: Surges Transferred from the HV to the LV Winding of the Six-section Transformer

Applied waveform	Ground impedance	Maximum LV node voltage in p.u.*	Maximum LV layer-to-layer voltage in p.u.*
1/50 μs	1	0.014	0.034
	5	0.019	0.047
	15	0.026	0.059
	47	0.041	0.068
1/50 μs chopped at 1 μs	47	0.087	0.092

* The voltages are in p.u. of peak of impulse voltage.

The positions at which the maximum stresses occurred are the same as those for the four-section transformer.

Transference of Surge from the Low-voltage to the High-voltage side

Examination of the transformers that have failed in practice indicates that distribution transformers are susceptible to failure caused by lightning current surges entering the transformer by the way of the usually unprotected low-voltage terminals [11]. It has also been found that shell-type designs utilizing non-interlaced low-voltage windings are most susceptible to failure; core-type and shell-type designs with interlaced low-voltage windings

are less susceptible [14]. non-interlaced and interlaced low-voltage windings are depicted in Figs. 8.6 and 8.7 respectively.

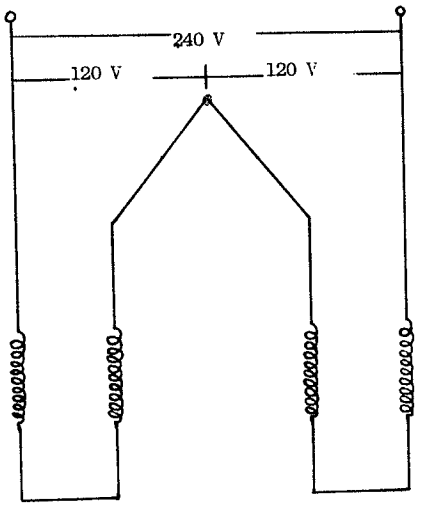

FIG .8.6: Non-interlaced Low-voltage Winding.

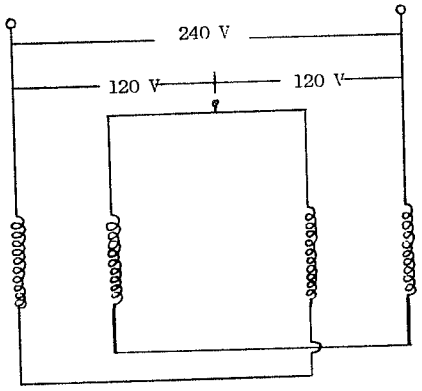

FIG .8.7: Interlaced Low-voltage Winding.

The model shown in Fig. 8.4 and the corresponding model for the six-section transformer were analyzed to determine the voltages induced in the high-voltage winding when currents are injected into the low-voltage terminals. Impulse currents of 7/70 μs waveform and magnitude of 1 kA were used in the EMTP simulation ; currents of that magnitude and waveshape have been reported to strike the low-voltage terminals of distribution transformers [14].

The results of the study are given in Tables 8.11 and 8.12.

TABLE 8.11: Surges transferred from the LV to the HV windings of the Four-section Transformer when Currents are Injected into Both LV Terminals

Ground impedance	Maximum node voltage	Maximum section-to-section voltage	Maximum layer-to-layer voltage
(Ω)	(kV)	(kV)	(kV)
0	2.8	1.7	0.86
1	4.7	3.6	1.15
5	12.5	11.4	3.27
15	32.2	31.1	4.61
47	48.9	47.8	9.54
47*	95.4*	94.6*	14.3*

* These values were obtained with current injection into one node.

TABLE 8.12: Surges transferred from the LV to the HV winding of the six-section transformer when Currents are injected into both LV terminals

Ground resistance	Maximum node voltage	Maximum section-to-section stress	Maximum layer-to-layer stress
(Ω)	(kV)	(kV)	(kV)
0	1.2	0.45	0.33
1	1.8	1.6	0.68
5	5.3	4.4	1.4
15	9.8	11.5	2.7
47	17.4	23.7	4.1
47*	51.6*	49.3*	6.7*

* These values were obtained with current injection into one node.

The following conclusions can be drawn from the results of the above analysis:

1. The surges transferred from the high-voltage side to the low-voltage side are innocuous.
2. The impulses transferred from the low- to the high-voltage winding can be damaging to the insulation in the latter winding.
3. Injection of unbalanced currents into the low-voltage terminals results into transference of higher magnitudes of voltage than the injection of balanced currents.

4. Effective grounding of the transformer is essential in limiting the amplitudes of transferred surges.

Chapter IX

CONCLUSIONS AND FUTURE RESEARCH

The objectives of this study were twofold:

1. To develop an electric circuit model for computing impulse voltage distribution along the windings of a barrel-type transformer for surges originating from either the low- or the high-voltage side.
2. To determine the model of an RTEmp-filled transformer and to predict the impulse voltage distribution along its windings.

A review of the literature concerning surge phenomena in transformers revealed that there is no information on the numerical analysis of impulse voltage distribution in the windings of barrel-type transformers. Furthermore, the reported methods of computation of circuit parameters are only applicable to disc-type windings.

The winding constants of a barrel-type transformer were identified and its model developed. The existing methods of calculating circuit constants of transformer windings were modified and used to determine the element values of the barrel-type transformer.

The impulse voltage distribution along the windings of the transformer was predicted by analyzing its circuit model through the use of the EMTP. To evaluate the accuracy of the model, ex-

perimental determination of the voltage stress distribution was carried out. Comparison of the experimental and theoretical results revealed that the model is reasonably accurate.

The sensitivity of the impulse response of the transformer to the following three design parameters was investigated:

1. Number of sections per coil.
2. Thickness of formel coating.
3. Clearance of coils from the tank wall.

It was found that the transformer having three sections per coil exhibits a more uniform impulse voltage distribution than the transformer of the same rating and construction, but with two sections per coil. The variation of the thickness of the formel coating and the clearance of the coils from the tank wall do not bring about significant changes in voltage stress distribution.

Prior to modelling the RTEmp-filled transformer, experiments were carried out to ascertain the breakdown and conduction characteristics of RTEmp fluid at various temperatures. The results revealed that RTEmp does not exhibit resistive conduction under impulse voltages. The voltage stress distribution along the windings of an RTEmp-filled transformer was computed. It was found that the responses to voltage surges, of a transformer filled with mineral oil and one filled with RTEmp are practically identical.

Surge transfer from the impulsed to the nonimpulsed winding was investigated. The results show that the voltages transferred from the high- to the low-voltage side are innocuous; while surge transfer in the reverse direction can be damaging to insulation on the high-voltage end.

The analysis of the transformer models using the EMTP was found to require much computer time and storage. A method of reducing the size of the electric circuit equivalent of the transformer was suggested and used. The results obtained by analyzing the simpler models compare reasonably well with those of the detailed model.

For further research, experimental determination of self- and mutual inductance values could be persued. In addition , the precise effect of the iron-core on inductance should be investigated.

Experimental determination of transferred surges should be carried out. The benefit of using a surge arrester on the low-voltage side is worth ascertaining.

Practical tests should be performed on the six-section transformer to determine whether it exhibits a more uniform voltage stress distribution than the four-section transformer.

BIBLIOGRAPHY

[1] K.W. Wagner, "The Progress of an Electromagnetic Wave in a Coil with Capacity between Turns," Electrotechnik und Maschinebau (Vienna, Austria), Vol. 33, 1915, p.89-107.

[2] R. Rudenberg, "Performance of Travelling Waves in Coils and Windings," AIEE Trans. ,Vol. 59, p. 1031-40, 1940.

[3] T.J. Lewis, "The Transient Behaviour of Ladder Networks of the Type Representing Transformer and Machine Windings, " Proc. IEE, Paper No. 1691S, October, 1954 (101,part II, p. 541).

[4] P.A. Abetti, "Transformer Models for the Determination of Transient Voltages," AIEE Trans. Vol. 72, p. 468-479, June 1953.

[5] P. Waldvogel and R. Rouxel, "A New Method of Calculating the Electrical Stresses in a Winding Subjected to a Surge Voltage," Brown Boveri Review, Vol. 43, p. 206, 1956.

[6] J.H. McWhirter, C.D. Fahrnkopf and J.H.L Steel, "Determination of Impulse Stresses within Transformer Windings by Computers," AIEE Trans. Vol. 75, p. 1267-74, February 1957.

[7] B.M. Dent, E.R. Hartill and J.G. Miles, "A Method of Analysis of Transformer Impulse Voltage Distribution using a Digital Computer," Proc. IEE, Vol. 105, p. 445-459, October 1958.

[8] Kasturi and G.R.K. Murty, "Computation of Impulse Voltage Stresses in Transformer Windings," Proc. IEE, Vol. 126, p. 397-400, May 1979.

[9] W.N. White, "Numerical Transient Voltage Analysis of Transformers and LRC Networks Containing Nonlinear

Resistive Elements," Power Industry Applications Conference, p.288-294, 1977.

[10] H.W. Dommel, "Digital Computer Solution of Electromagnetics Transients in Single- and Multiphase Networks," IEEE Trans. , Vol. PAS-88, APril 1969, p. 388-397.

[11] K.D. Beardsley, W.A. McMorris and H.C. Stewart, "Voltage Stresses in Distribution Transformers Due to Lightining Currents in Low-voltage Circuits," AIEE Trans., Vol. 67, 1948, p.1632-1635.

[12] P.A. Abetti and H.F. Davis, "Surge Transfer in 3-Winding Transformers," AIEE Trans., p. 1395-1407. December 1954.

[13] A. Miki, T. Hosoya and K. Okuyama, "A Calculation Method for Impulse Voltage in Transformer Windings," IEEE Trans., Vol. PAS-97, May/June 1978, p. 930-939.

[14] C.J. McMillen, C.W. Schoendube and D.W. Caverly, " Susceptibility of Distribution Transformers to Low-voltage Side Lightining Surge Failure," 1982 IEEE, Paper No. 82 WM 093-3.

[15] H. William Hayt, "Engineering Electromagnetics, McGraw-Hill ,1981, p. 161.

[16] K. Okuyama, "A Numerical Analysis of Impulse Voltage Distribution," J. Inst. Elec. Engrs., Japan, Vol. 87, p. 80-88, 1967.

[17] Y. Kawaguchi, "Calculation of Circuit Constants for Computing Internal Oscillating Voltage in Transformer Windings, Electrical Engineering in Japan, Vol. 89, p. 44-53, 1969.

[18] P.I. Fergestad and T. Henriksen, "Inductances for the

Calculation of Transient Oscillations in Transformers," IEEE PES Summer Meeting and EHV/UHV Conference, Vancouver, B.C. , Canada, July 1973, Paper T 73 3944, P. 510-516 .

[19] L.F. Blume and A. Boyajian, "Abnormal Voltages within Transformers," AIEE Trans. , Vol. 38, p. 577-620, 1919.

[20] Bureau of Standards Journal of Research, Vol. 3, 1929, p. 188.

[21] F.W. Grover, "Inductance Calculations: Working Formulas and Tables," Dover, 1962.

[22] R.C. Degeneff and W.N. Kennedy, "Reducing Storage and Saving Computation Time with a Generalization of the Dommel (BPA) Solution Method," IEEE Summer Power Meeting, 1975, San Francisco, California.

[23] H. Bedrich, P. Bedrich and V. Karel, "Influence of the Shape of the Voltage Wave on the Internal Stresses of a Transformer, "Acta Technica Csav, p. 672-677, 1978.

[24] The British Electrical and Allied Industries Research Association,"Surge Phenomena, Seven Years' Research for the Central Electricity Board (1933-1940)," p. 277-305, 1941.

Appendix A

THE FORTRAN COMPUTER PROGRAM USED TO COMPUTE WINDING RESISTANCE

```
C  CALCULATION  OF  WINDING  RESISTANCE FOR THE FOUR-SECTION
C  TRANSFORMER; THE ONE AVAILABLE FOR IMPULSE TESTS.
C  IN  THIS  METHOD  THE FORMULA  'R=PL/A'IS USED FOR DC
C  RESISTANCE; A=AREA,L=LENGTH,P=RESISTIVITTY
      REAL*8 XH1,XH2,A,P,DELTA,R(11),WL,S,RT,TOT,PI,SE,RD,F,
     &RMP(11),PHO
C  DIMENSIONS  ARE  GIVEN  IN CENTIMETRES
C  RESISTANCE IS GIVEN IN OHMS.
C  XH1 AND XH2 ARE RESPECTIVELY THE WIDTH AND LENGTH OF A TURN;
C  ASSUMED TO BE RECTANGULAR.
      XH1=0.13851636D0*100.D0
      XH2=0.26.234136*100.D0
C  A=CROSS-SECTIONAL AREA OF CONDUCTOR WIRE
      A=0.0636D0*0.0885D0*2.54D0*2.54D0
C  RD=  RADIUS OF ROUND WIRE HAVING THE SAME CROSS-SECTIONAL AREA
C   AS THE ACTUAL WIRE
      RD=0.1075125D0
      PI=3.14159265D0
C  SE= NUMBER OF TURNS PER CENTIMETRE
      SE=4.139483D0
C  P=RESISTIVITY OF FLATTENED ALUMINIUM
      P=3.52D-6
```

```
      PHO=3520.D0
C  S=RADIAL INCREMENT FROM ONE LAYER TO THE NEXT
      S=0.19558D0
      DELTA=2.D0*S
C  RT=46=NUMBER OF TURNS IN EACH OF THE INNERMOST NINE LAYERS
      RT=46.D0
C  F=DOMINANT FREQUENCY,IN HZ, OF A 1/50US WAVE.
      F=2.5D5
      WRITE(6,14)
14    FORMAT(25X,'   DC  RESISTANCE          IMPULSE  RESISTANCE')
      TOT=0.D0
      I=1
C  WL=PERIMETER OF TURN
15    WL=2.D0*(XH1+XH2)
C  R(I) CONTAINS DC RESISTANCE
C  RMP(I) CONTAINS IMPULSE RESISTANCE
      R(I)=(P*WL*RT)/A
C  IN THE NEXT STEP DC RESISTANCE IS MODIFIED TO YIELD IMPULSE
C  RESISTANCE.
      RMP(I)=R(I)*((1.D0)+(4.D0*PI*(RD**3)*(SE**2)*
     &DSQRT(PI*2.D0*PI*F/(2.D0*PHO))))
      TOT=TOT+R(I)
      WRITE(6,16) I,R(I),RMP(I)
16    FORMAT(25X,I2,3X,D14.7,10X,D14.7)
      XH1=XH1+DELTA
      XH2=XH2+DELTA
      I=I+1
```

```
      IF(I.LE.9) GO TO 15
      IF(I.NE.10) GO TO 17
C RT=27=NUMBER OF TURNS IN TENTH LAYER
      RT=27.D0
      GO TO 15
17    IF(I.GT.11) GO TO 18
C  RT=26=NUMBER OF TURNS IN THE ELEVENTH LAYER
      RT=26.D0
      GO TO 15
  18  WRITE(6,19) TOT
19    FORMAT('1',10X,D14.7)
      STOP
      END
$ENTRY
/*
```

Appendix B

CALCULATION OF THE CONSTANTS CHARACTERISING IMPULSE WAVE SHAPES

Impulse voltage can be expressed as:

$$E(t) = E(e^{-at} - e^{-bt}) \quad (1)$$

In which E, a, b are constants.

Let t1 be the time at which the maximum voltage E1 is reached and t2 be the time taken for E1 to fall to its half-value E2.

Let k = b/a.

Relation (1) can be used to write:

$$E1 = E(e^{-at1} - e^{-bt1}) \quad (2)$$

$$E2 = E(e^{-at2} - e^{-at2}) \quad (3)$$

The slope of the wave is zero at t1 when maximum voltage occurs.

Therefore,

$$0 = dE(t)/dt = E(-ae^{-at1} + be^{-bt1}) \quad (4)$$

Introducing b = ka in relations (2), (3), and (4) yields:

$$E1 = Ee^{-at1} [1 - e^{-(k-1)at1}] \quad (5)$$

$$E2 = Ee^{-at2} [1 - e^{-(k-1)at2}] \quad (6)$$

$$0 = Eae^{-at1} [1 - ke^{-(k-1)at1}] \quad (7)$$

Dividing (7) by a gives:

$$0 = Ee^{-at1} - kEe^{-kat1} \quad (8)$$

(5) - (8) yields:

$$(k-1)e^{-kat1} = E1/E$$

Therefore,

$$e^{-kat1} = E1/[E(k-1)] \quad (9)$$

Comparing (9) and (5) , it follows that:

$$E1/E = e^{-at1} - e^{-kat1}$$

From (9) ,

$$E1/E = (k-1)e^{-kat1}$$

Hence,

$$E1/E = (k-1)e^{-kat1} = e^{-at1} - e^{-kat1}$$

Therefore,

$$ke^{-kat1} - e^{-kat1} = e^{-at1} - e^{-kat1}$$

Hence,

$$e^{-(k-1)at1} = 1/k$$

Raising the above expression to power -1/(k-1) yields:

$$e^{-at1} = k^{-1/(k-1)} \quad (10)$$

Raising (10) to power k gives:

$$e^{-akt1} = k^{-k/(k-1)}$$

By comparing the above expression with (9) it can be noted that:

$$k^{-k/(k-1)} = E1/[E(k-1)] \quad (11)$$

From (5),

$$k^{-t2/[t1(k-1)]} = e^{-at2}$$

Introducing the above relationship into (11) yields:

$$E2/E = k^{-t2/[t1(k-1)} - k^{-kt2/[t1(k-1)]} \quad (13)$$

From relations (12) and (13),

$$E2/E1 = (1/2)(k-1)k^{-k/(k-1)} = k^{-t2/\{t1(k-1)\}}\,[1 - k^{-t2/t1}] \quad (14)$$

From (10) it follows:

$$a = [1/\{t1(k-1)\}]\ln(k) \quad (15)$$

$$b = ak = [k/\{t1(k-1)\}]\ln(k) \quad (16)$$

From equation (11),

$$E = [E1/(k-1)]k^{k/(k-1)} \quad (17)$$

To get the value of k, it is necessary to solve equation (14). In this expression,

$$1 >> k^{-t2/t1}$$

Therefore,

$$E2/E1 = (1/2) = [1/(k-1)]k^{-\{k-(t2/t1)\}/(k-1)} \quad (18)$$

Taking natural logarithms,

$$\ln\{(k-1)/2\} = [\{k - (t2/t1)\}/(k-1)]\ln(k)$$

Therefore,

$$t2/t1 = k - [(k-1)\ln\{(k-1)/2\}/\ln(k)] \quad (19)$$

Equations (19) and (15) are plotted in combination as shown in in Fig. B1.

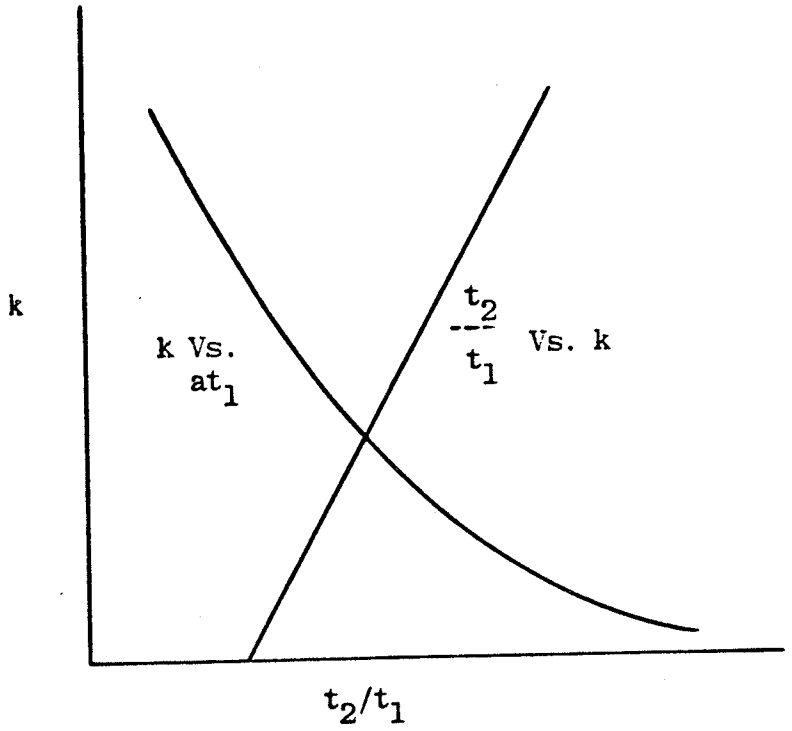

FIG. B1: Curves for deriving constants a and b from the ratio between the time to fall to half of the maximum value and the time to reach the peak (t2/t1).

The point of intersection of the two curves (Fig. B1) gives the required value of k.

Some impulse wave constants are given in Table B1 for the impulse

$$E(t) = E_1 (e^{-at} - e^{-bt})$$

Where the maximum value of E(t) is unity.

TABLE B1: Impulse wave constants

Wave shape	E_1	a	b
.25/500	1	1.386×10^{3}	4.134×10^{7}
.25/100	1.001	6.8×10^{3}	3.37×10^{7}
.25/50	1.003	1.4×10^{4}	2.95×10^{7}
.25/5	1.044	1.45×10^{5}	1.97×10^{7}
.25/1	1.48	1.056×10^{6}	9.62×10^{6}
.5/500	1	1.386×10^{3}	1.912×10^{7}
.5/100	1.004	6.6×10^{3}	1.5×10^{7}
.5/50	1.01	1.42×10^{4}	1.355×10^{7}
.5/5	1.11	1.6×10^{5}	8.15×10^{6}
.5/2	1.48	5.44×10^{5}	4.95×10^{6}
1/500	1	1.386×10^{3}	8.79×10^{6}

A 0.5/1 wave cannot be expressed as a double exponential [24].

Appendix C

THE FORTRAN COMPUTER PROGRAM USED TO COMPUTE INTERTURN CAPACITANCE

```
C THE COMPUTATIONS ARE FOR THE FOUR-SECTION TRANSFORMER; THE ONE
C AVAILABLE FOR TESTS
C  CALCULATION  OF INTERTURN CAPACITANCE AS A DISTRIBUTED
C  CAPACITANCE.
C  THE DIMENSIONS OF LENGTH ARE IN METRES
C  CAPACITANCE IS GIVEN IN FARADS.
C  D=THICKNESS OF FORMEL COATING
      REAL*8 D,EO,EF,PI,W,XH1,XH2,RM,PERI,CAP,DCF
      D=8.636D-5
C  EO=FREE SPACE PERMITTIVITY
      EO=8.854D-12
C  EF=DIELECTRIC CONSTANT OF FORMEL
      EF=3.D0
C  N=46=NUMBER OF TURNS IN EACH OF THE FIRST NINE LAYERS
      N=46
C  I IS THE INDICATOR FOR THE LAYER NUMBER
      I=1
      PI=3.14159265359D0
C  W=CONDUCTOR THICHNESS
      W=1.61544D-3
C  NL=NUMBER OF LAYERS IN EACH HV SECTION
      NL=11
```

```
C  INCREMENT IN WIDTH AND LENGTH OF A TURN FROM ONE LAYER TO THE
C  CONSECUTIVE ONE.
      DELTA=4.1656D-3
C  XH1 AND XH2 ARE RESPECTIVELY THE WIDTH AND LENGTH OF A TURN;
C  ASSUMED TO BE RECTANGULAR.
      XH1=(13.851636D-2)-DELTA
      XH2=(26.234136D-2)-DELTA
62    XH1=XH1+DELTA
      XH2=XH2+DELTA
C  PERI=PERIMETER OF A TURN
      PERI=2.D0*(XH1+XH2)
C  CAP=INTERTURN CAPACITANCE OF A LAYER.
      CAP=EO*EF*W*(N-1)*PERI/(D*N*N)
      WRITE(6,1) I,CAP
1     FORMAT(20X,I2,3X,D14.7)
      I=I+1
      IF(I.GT.NL) GO TO 80
      IF(I.GE.10) GO TO 2
      GO TO 62
C  N=27=NUMBER OF TURNS IN THE TENTH LAYER
C  N=26=NUMBER OF TURNS IN THE  ELEVENTH LAYER
2     N=27
      IF(I.EQ.11) N=26
      GO TO 62
80    STOP
      END
$ENTRY
```

Appendix D

FORTRAN PROGRAM USED TO CALCULATE LAYER-TO-LAYER CAPACITANCE

```
C  THE FOLLOWING COMPUTATIONS ARE FOR THE FOUR-SECTION
C TRANSFORMER; THE ONE AVAILABLE FOR TESTS.
C  CALCULATION OF LAYER-TO-LAYER CAPACITANCE
      REAL*8 S,G,HT,XH1,XH2,TG,DELTA,X1,X2,EO,EP,EF,DP,DF,C1,
     &C3,CE1,C12,C32,CE2,CLTL,HO.
C  THE DIMENSIONS OF LENGTH ARE GIVEN IN METRES
C  CAPACITANCE IS GIVEN IN FARADS
      ICR=1
C  S=RADIAL SEPARATION BETWEEN TWO CONSECUTIVE LAYERS
      S=2.12344D-3
C  G=RADIAL SEPARATION BETWEEN OUTER SIDE OF AN HV LAYER AND THE
C  INNER SIDE OF THE CONSECUTIVE LAYER.ED 2854
      G=5.0800D-4
      HT=0.111125D0
      HO=HT
C  XH1 AND XH2 ARE RESPECTIVELY THE WIDTH AND LENGTH OF A
C  TURN; ASSUMED TO BE RECTANGULAR.
      XH1=(13.851636D-2)
      XH2=(26.234136D-2)
      TG=2.D0*G
      DELTA=2.D0*S
1     I=ICR
```

```
      J=ICR+1
C  X1 AND X2 ARE RESPECTIVELY THE AVERAGE WIDTH AND LENGTH OF TWO
C  CONSECUTIVE LAYERS.
      X1=(XH1+XH1+TG)/2.D0
      X2=(XH2+XH2+TG)/2.D0
C  EO=FREE SPACE PERMITTIVITY
      EO=8.854D-12
C  EP=RELATIVE PERMITTIVITY OF EPOXY PAPER IMPREGNATED
C  WITH MINERAL OIL.
      EP=4.25D0
C  EF=RELATIVE PERMITTIVITY OF FORMEL
      EF=3.D0
C  DP=THICKNESS OF PAPER INSULATION BETWEEN TWO CONSECUTIVE
C  LAYERS.
      DP=2.54D-4
C  DF=FORMEL THICKNESS
      DF=4.318D-5
C  USE OF FORMULA 'C=EA/D'
      C1=(EO*EF*HT*X1)/DF
      C3=(EO*EP*HT*X1)/DP
C  CAPACITANCE OF ONE PLATE PAIR FOLLOWS NOW.
      CE1=(C1*C3)/((2.D0*C3)+C1)
      C12=(EO*EF*HT*X2)/DF
      C32=(EO*EP*HT*X2)/DP
C  CAPACITANCE OF SECOND PLATE PAIR FOLLOWS
      CE2=(C12*C32)/((2.D0*C32)+C12)
C  SUM OF CAPACITORS FOLLOWS
```

```
      CLTL=2.D0*(CE1+CE2)
      WRITE(6,3) I,J,CLTL
3     FORMAT(10X,I2,2X,I2,3X,D14.7)
      ICR=ICR+1
      IF(ICR.GT.10) GO TO 5
      XH1=XH1+DELTA
      XH2=XH2+DELTA
      IF(ICR.GT.9) GO TO 4
      GO TO 1
C THE HEIGHT OF THE 11TH LAYER IS 10.16CM
4     HT=(HT+10.16D-2)/2.D0
      GO TO 1
5     STOP
      END
$ENTRY
```

Appendix E

FORTRAN COMPUTER PROGRAM FOR CALCULATING SECTION-TO-SECTION CAPACITANCE

```
C  ORIGINAL MODEL;THE ONE AVAILABLE FOR TESTS.
C  COMPUTATION OF SECTION-TO-SECTION CAPACITANCES
      REAL*8 TH,AREA,EV,EO,S,XH1,XH2,PERI,AR(11),ARM,CM,CA,C(11),
     &DELTA
C  THE DIMENSIONS OF LENGTH ARE IN  METRES
C  CAPACITANCE IS GIVEN IN FARADS
C  TH=THICKNESS OF CONDUCTOR (UNCOATED)
      TH=0.0885*2.54*1.D-2
C  ARRAY  AR CONTAINS AREAS CONTRIBUTED BY EACH LAYER
C  AREA=TOTAL AREA CONTRIBUTED BY LAYERS
      AREA=0
      I=1
C NL=NUMBER OF LAYERS
      NL=11
C  EV=DIELECTRIC CONSTANT OF MINERAL OIL
C  EO=PERMITTIVITTY OF FREE SPACE
      EV=2.2
      EO=8.854D-12
C  S=SEPARATION BETWEEN TOP AND BOTTOM SECTIONS
      S=0.75*2.54*1.D-2
C  DELTA=INCREMENT  OF WIDTH AND LENGTH FROM ONE LAYER TO THE
C  CONSECUTIVE ONE (MOVING OUTWARDS)
```

```
      DELTA=0.41656D-2
C  XH1 AND XH2 REPRESENT THE LENGTH AND WIDTH OF LAYERS
      XH1=(13.851636D-2)-DELTA
      XH2=(26.234136D-2)-DELTA
1     XH1=XH1+DELTA
      XH2=XH2+DELTA
C  PERI=PERIMETER OF A TURN.
      PERI=2.D0*(XH1+XH2)
C  ARRAY AR CARRIES AREAS OF LAYERS.
      AR(I)=PERI*TH
      AREA=AREA+AR(I)
      I=I+1
      IF(I.LE.NL) GO TO 1
C  ARM=AREA OF EACH IMAGINARY PLATE
      ARM=XH1*XH2
C  CM=CAPACITANCE OF IMAGINARY PLATES
      CM=(EV*EO*ARM)/S
C  CA=CAPACITANCE ATTRIBUTED TO LAYERS
      CA=(CM*((AREA+ARM)/2.D0))/ARM
C C(I)=CAPACITANCE BETWEEN CORRESPONDING LAYERS
      DO 2 I=1,11
      C(I)=(CA*AR(I))/AREA
      WRITE(6,3) I,C(I)
3     FORMAT(20X,I2,2X,D14.7)
2     CONTINUE
      STOP
      END
```

Appendix F

THE FORTRAN COMPUTER PROGRAM FOR CALCULATING SELF-INDUCTANCE USING THE HEXAGONAL REPRESENTATION

```
C  THE MEANINGS OF THE SYMBOLS ARE AS IN RELATION (3.16) AND
C  FIG. 3.16.
C  THE TURNS ARE TAKEN IN PAIRS (FIG. 3.15).
C  IN THIS PROGRAM, THE LABELLING OF THE HEXAGON SEGMENTS IS
C  PRESERVED, BUT, ASA=Aa, ASB=Ab, ASC=ac, etc.
      REAL*8 DELTA,XH1,XH2,WD,XM1(11,46),AB,KOX,SBK,SBOX,KC,GC,OG,
     &OR,RSE,RSD,R2O,OW,R2S,MC,BC,CD,EF,FA,DE,VU,ZY,SEH,UA,XY,ZX,
     &H,BSB,ASA,DSD,ASC,BSA,ASB,RL,RM,V,DT1,ZL1,ZL2,ZMS,ZMC,SL1,
     &,C1,ZMM,ZE,BD,AD,BE,AE,BF,AF,CE,CF,DF,ZL,SUM,ZC,XZ(11),R1,R2
     &,DSQRT,DABS,BB,D,DS,OMG,MU,NU,Q1,Q2,Q3,Q4,Q5,Q6,Q7,Q8,Q9,Q10
     &,ZM,RL1,RLX,RJ1,RJ2,ST1,ST2,ST3,ST4,BSC,BSE,DT2,ASF,BSF,ASD,
      REAL*8 CSA,CSB,CSC,DT3,CSD,CSE,CSF,DT4,ESD,ESE,ESF,FSA,FSB
     &,FSE,FSF,ALFA,E,CHK,ZH,ZHB,ZMB,CRT,XG,ZR,QSC,OP,BP,SM1,R,R7,
     &R3,R4,Q11,ASE,BSD,FSC,FSD.
C  THE DIMENSIONS OF LENGTH ARE CENTIMETRES; THE VALUES OF
C  INDUCTANCE ARE IN MICROHENRIES.
C  I IS AN INDICATOR OF LAYER NUMBER.
      I=1
C  NT=46=NUMBER OF TURNS IN EACH OF THE INNERMOST NINE LAYERS.
      NT=46
      I1=1
      J1=2
```

```
C  NL=NUMBER OF LAYERS IN EACH HV SECTION.
      NL=11
      ID=0
C  DELTA=TWICE RADIAL INCREMENT FROM ONE LAYER TO THE NEXT.
      DELTA=4.1656D-1
      XH1=(14.174724D0)-DELTA
C  XH1 AND XH2 ARE RESPECTIVELY THE WIDTH AND LENGTH OF THE
C  RECTANGLE WHICH ENCLOSES THE HEXAGON (FI. 3.11).
      XH2=(26.557224D0)-DELTA
      WD=.233426D0
50    XH1=XH1+DELTA
      XH2=XH2+DELTA
      XM1(I1,J1)=0.D0
C  AB=STRAIGHT PORTION OF A TURN.
      AB=(18.D0/38.D0)*XH2
      R7=DSQRT(((XH1/2.D0)**2)+((XH2-((XH2-AB)/2.D0))**2))
      KOX=(XH2-AB)/2.D0
      SBK=XH1/2.D0
      SBOX=DSQRT((SBK**2)+(KOX**2))
      KC=(XH2-AB)/2.D0
C  KG=AB-SASB=0.0
      GC=KC
      OG=SBK
      QSC=XH2-((XH2-AB)/2.D0)
      OR=XH1
      RSE=0.D0
      RSD=AB
```

```
      R2O=XH2-((XH2-AB)/2.D0)
      OW=XH2
      R2S=AB
      MC=(XH2-AB)/2.D0
      BC=DSQRT(((XH1/2.D0)**2)+(MC**2))
      CD=BC
      EF=BC
      FA=BC
      DE=AB
      ZH=.371647073D0*BC
      ZHB=.371647073D0*BC
      ZM=AB+(2.D0*ZH)
      ZMB=AB+(2.D0*ZHB)
      CRT=(ZMB-ZM)/2.D0
      ZY=ZM+CRT
      XG=.334482365D0*BC
      ZR=.334482365D0*BC
      XY=XG+ZR
      ZX=DSQRT((XY**2)+(ZY**2))
      OP=0.D0
      BP=0.D0
      H=0.D0
444   H=H+WD
      XM1(I1,J1)=0.D0
      I=0
15    I=I+1
C  THE DIMENSIONS (R1, R2, R3, R4, D, V, M, L) AND ANGLE (e),
```

```
C  FIG. 3.16, FOR ANY PAIR OF SEGMENTS OF THE HEXAGONS ARE
C  DETERMINED  BY MOVING CONTROL TO STATEMENTS 1 TO 36 AS
C  ENCLOSED IN THE "GO TO" STATEMENT BELOW.
      GO TO (1,2,3,4,5,6,7,8,9,10,11,12,13,144,155,166,177,188,19,
     &2020,2121,22,2323,2424,25,26,27,28,29,30,31,32,33,34,35,36),
     &I
      JDUMMY=I+1
      GO TO 40
C  RL AND RM REPRESENT L AND M RESPECTIVELY.
200   Q1=(R2**2)-(R3**2)-(RL**2)
      Q2=(R4**2)-(R3**2)-(RM**2)
      Q4=2.D0*RL*RL
      Q5=2.D0*RM*RM
C  ALPHA=a IN RELATION 3.16.
      ALFA=((R4**2)-(R3**2)+(R2**2)-(R1**2))
      Q3=(4.D0*RL*RL*RM*RM)-(ALFA**2)
      Q6=(ALFA/(2.D0*RL*RM))
      CHK=DABS(Q6)
      IF(CHK.GT.1.D0) GO TO 69
      Q7=DSQRT(1.D0-(Q6*Q6))
C  MU=u
      MU=(RL*((Q5*Q1)+(ALFA*Q2)))/Q3
C  NU=v
      NU=(RM*((Q4*Q2)+(ALFA*Q1)))/Q3
      D=H
      DS=D*D
      IF(D.NE.0.D0) GO TO 777
```

```
      OMG=0.D0
      GO TO 778
C   OMG=
777   OMG=DATAN(((DS*Q6)+((MU+RL)*(NU+RM)*Q7*Q7))/(D*R1*Q7))-
     &DATAN(((DS*Q6)+((MU+RL)*NU*Q7*Q7))/(D*R2*Q7))
     &DATAN(((DS*Q6)+(MU*NU*Q7*Q7))/(D*R3*Q7))-
     &DATAN(((DS*Q6)+(MU*(NU+RM)*Q7*Q7))/(D*R4*Q7))
778   Q8=RM/(R1+R2)
      Q9=RL/(R1+R4)
      Q10=RM/(R3+R4)
      Q11=RL/(R2+R3)
C   ZM REPRESENTS M.
C   IMMEDIATELY BELOW, RELATION 3.16 IS APPLIED.
       ZM=((((MU+RL)*(DLOG((1.D0+Q8)/(1.D0-Q8))))
     &((NU+RM)*(DLOG((1.D0+Q9)/(1.D0-Q9))))-
     &(MU*(DLOG((1.D0+Q10)/(1.D0-Q10))))-
     &(NU*(DLOG((1.D0+Q11)/(1.D0-Q11)))))*0.001D0*Q6)-
     &(((OMG*D)/Q7)*.001D0*Q6)
      GO TO 250
 80   RL1=DABS((RL-RM)/2.D0)
      IF(RM.GT.RL) GO TO 700
      RLX=RM+RL1
      GO TO 1000
 700  RLX=RL+RL1
1000  RJ1=.002D0*RLX*(DLOG((RLX/V)+DSQRT(1.D0+((RLX/V)**2)))-
     &DSQRT(1.D0+((V/RLX)**2))+(V/RLX))
      IF(RL1.EQ.0.D0) GO TO 64
```

```
      RJ2=.002*RL1*(DLOG((RL1/V)+DSQRT(1.D0+((RL1/V)**2)))-
     &DSQRT(1.D0+((V/RL1)**2))+(V/RL1))
      GO TO 650
64    RJ2=0.D0
650   ZM=(RJ1-RJ2)*((-1)**IM)
      IF(I.EQ.1) GO TO 70
      IF(I.EQ.4) GO TO 71
      IF(I.EQ.8) GO TO 72
      ST4=ZM
      GO TO 250
70    ST1=ZM
      GO TO 250
71    ST2=ZM
      GO TO 250
72    ST3=ZM
250   IDUMMY=I+1
      IF(ID.EQ.0) GO TO 251
      ZE=ZE+ZM
      GO TO 433
C  THE MUTUAL-INDUCTANCES ARE BEING SUMMED UP.
251   XM1(I1,J1)=XM1(I1,J1)+ZM
      GO TO 15
1     BSB=H
      ASA=BSB
      DSD=BSB
      ASC=DSQRT((H**2)+(OG**2)+(QSC**2))
      BSA=DSQRT((H**2)+(AB**2))
```

```
      ASB=BSA
      RL=AB
      RM=AB
      V=H
      DT1=V
      IM=2
      GO TO 80
2     BSC=DSQRT((H**2)+(OG**2)+(((XH2-AB)/2.D0)**2))
      R1=BSC
      R2=BSB
      R3=ASB
      R4=ASC
      RM=BC
      GO TO 200
4     BSE=ASD
      RM=DE
      V=DSQRT((H**2)+(XH1**2))
      DT2=V
      IM=1
      GO TO 80
5     ASF=BSC
      BSF=ASC
      R1=BSF
      R2=BSE
      R3=ASE
      R4=ASF
      RM=EF
```

```
      GO TO 200
3     ASD=DSQRT((H**2)+(OR**2)+(RSD**2))
      ASE=DSQRT((H**2)+(OR**2)+((RSE/2.D0)**2))
      BSD=ASE
      R1=BSD
      R2=BSC
      R3=ASC
      R4=ASD
      RM=CD
      GO TO 200
6     R1=BSA
      R2=BSF
      R3=ASF
      R4=ASA
      RM=FA
      GO TO 200
7     CSA=DSQRT((H**2)+(R2O**2)+(SBK**2))
      CSB=DSQRT((H**2)+(SBK**2)+(KOX**2))
      R1=CSB
      R2=CSA
      R3=BSA
      R4=BSB
      RL=BC
      RM=AB
      GO TO 200
8     CSC=H
      RM=BC
```

```
      IM=2
      V=H
      DT3=V
      GO TO 80
 9    CSD=CSB
      R1=CSD
      R2=CSC
      R3=BSC
      R4=BSD
      RM=CD
      GO TO 200
 10   CSE=DSQRT((H**2)+((XH1/2.D0)**2)+((AB+((XH2-AB)/2.D0))**2))
      R1=CSE
      R2=CSD
      R3=BSD
      R4=BSE
      RM=DE
      GO TO 200
 11   CSF= DSQRT((H**2)+(OW**2))
      RM=EF
      IM=1
      V= DSQRT((H**2)+(ZX**2))
      DT4=V
      GO TO 80
 12   R1=CSA
      R2=CSF
      R3=BSF
```

```
      R4=BSA
      RM=FA
      GO TO 200
13    DSA=BSE
      DSB=BSD
      R1=DSB
      R2=DSA
      R3=CSA
      R4=CSB
      RL=CD
      RM=AB
      GO TO 200
144   DSC=BSC
      R1=DSC
      R2=DSB
      R3=CSB
      R4=CSC
      RM=BC
      GO TO 200
155   ZM=ST3
      GO TO 250
166   DSE=BSA
      R1=DSE
      R2=DSD
      R3=CSD
      R4=CSE
      RM=DE
```

```
      GO TO 200
177   DSF=BSF
      R1=DSF
      R2=DSE
      R3=CSE
      R4=CSF
      RM=EF
      GO TO 200
188   ZM=ST4
      GO TO 250
 19   ESA=ASE
      ESB=DSA
      ZM=ST2
      RL=DE
      GO TO 250
2020  ESC=DSF
      R1=ESC
      R2=ESB
      R3=DSB
      R4=DSC
      RM=BC
      GO TO 200
2121  DSD=BSB
      ESD=DSE
      R1=ESD
      R2=ESC
      R3=DSC
```

```
      R4=DSD
      RM=CD
      GO TO 200
22    ESE=BSB
      DSD=BSB
      ZM=ST1
      GO TO 250
2323  ESF=DSC
      R1=ESF
      R2=ESE
      R3=DSE
      R4=DSF
      RM=EF
      GO TO 200
2424  R1=ESA
      R2=ESF
      R3=DSF
      R4=DSA
      RM=FA
      GO TO 200
25    FSA=CSB
      FSB=CSA
      R1=FSB
      R2=FSA
      R3=ESA
      R4=ESB
      RL=EF
```

```
      RM=AB
      GO TO 200
26    FSC=CSF
      ZM=ST4
      GO TO 250
27    FSD=CSE
      R1=FSD
      R2=FSC
      R3=ESC
      R4=ESD
      RM=CD
      GO TO 200
28    FSE=CSD
      R1=FSE
      R2=FSD
      R3=ESD
      R4=ESE
      RM=DE
      GO TO 200
29    FSF=CSC
      ZM=ST3
      GO TO 250
30    R1=FSA
      R2=FSF
      R3=ESF
      R4=ESA
      RM=FA
```

```
      GO TO 200
31    R1=ASB
      R2=ASA
      R3=FSA
      R4=FSB
      RL=FA
      RM=AB
      GO TO 200
32    R1=ASC
      R2=ASB
      R3=FSB
      R4=FSC
      RM=BC
      GO TO 200
33    ZM=ST4
      GO TO 250
34    R1=ASE
      R2=ASD
      R3=FSD
      R4=FSE
      RM=DE
      GO TO 200
35    R1=ASF
      R2=ASE
      R3=FSE
      R4=FSF
      RM=EF
```

```
      GO TO 200
36    ZM=ST3
      GO TO 250
40    J1=J1+1
      IF(J1.LE.NT) GO TO 444
C MIN SELF  INDUCTANCES  FOLLOW NOW
C  THESE ARE TEH SELF-INDUCTANCES OF THE STRAIGHT CONDUCTOR
C  SEGMENTS CALCULATED BY USING RELATION 3.15.
      ZL1=.002D0*BC*((DLOG((2.D0*BC)/.386334D0))+.498141187D0)
      ZL2=.002D0*AB*((DLOG((2.D0*AB)/.386334D0))+.498141187D0)
      ZMS=(4.D0*ZL1)+(2.D0*ZL2)
C  SELF TERMS  NOW  FINISHED
      ZMC=0.D0
      IC=1
401   IF(IC.EQ.1) GO TO 402
      IF(IC.EQ.2) GO TO 403
      IF(IC.EQ.3) GO TO 404
      IF(IC.EQ.4) GO TO 405
      IF(IC.EQ.5) GO TO 406
      SL1=EF
      SM1=FA
      R=XH1
      E=((SL1**2)+(SM1**2)-(R**2))/(2.D0*SL1*SM1)
      GO TO 400
402   SL1=FA
      SM1=AB
      R=R7
```

```
      E=((SL1**2)+(SM1**2)-(R**2))/(2.D0*SL1*SM1)
      GO TO 400
403   SL1=AB
      SM1=BC
      R=R7
      E=((SL1**2)+(SM1**2)-(R**2))/(2.D0*SL1*SM1)
      GO TO 400
404   SL1=BC
      SM1=CD
      R=XH1
      E=((SL1**2)+(SM1**2)-(R**2))/(2.D0*SL1*SM1)
      GO TO 400
405   SL1=CD
      SM1=DE
      R=R7
      E=((SL1**2)+(SM1**2)-(R**2))/(2.D0*SL1*SM1)
      GO TO 400
406   SL1=DE
      SM1=EF
      R=R7
      E=((SL1**2)+(SM1**2)-(R**2))/(2.D0*SL1*SM1)
400   C1=1.D0+(SM1/SL1)+(R/SL1)
      ZMM=.001D0*SL1*(E)*(DLOG(C1/(1.D0-(SM1/SL1)+(R/SL1)))
     &((SM1/SL1)*(DLOG(C1/((SM1/SL1)+(R/SL1)-1.D0)))))
      ZMC=ZMC+ZMM
      IC=IC+1
      IF(IC.LE.6) GO TO 401
```

```
      GO TO 407
C  THIS PART IS OVER
407   ZE=0.D0
C  ID DETERMINES WHETHER WE ARE USING THE LOOP FOR INCLINED
C  FILAMENTS THE FIRST OR THE SECOND CASE
      ID=1
      BD=XH1
      H=0.D0
      AC=R7
      AD=DSQRT((AB**2)+(XH1**2))
      BE=AD
      AE=XH1
      BF=AC
      AF=BC
      CE=AC
      CF=XH2
      DF=AC
      IX=0
433   IX=IX+1
      GO TO (415,416,417,418,419,420,421,422,423),IX
C  ALL TERMS  HAVE NOW BEEN FOUND
      ZL=(ZMS+(2.D0*ZMC)+(2.D0*ZE))*NT
      IF(I1.LE.9) GO TO 465
      IF(I1.EQ.10) GO TO 466
      SUM=0.D0
      DO 467 JC=1,24
      J2=JC+1
```

```
C  SUM IS THE TOTAL OF THE SELF-INDUCTANCES OF TURN SEGMENTS.
467    SUM=SUM+(2.D0*(NT-JC)*XM1(I1,J2))
       GO TO 475
465    SUM=0.D0
       DO 450 JC=1,44
       J2=JC+1
450    SUM=SUM+(2.D0*(NT-JC)*XM1(I1,J2))
       GO TO 475
466    SUM=0.D0
       DO 468 JC=1,25
       J2=JC+1
468    SUM=SUM+(2.D0*(NT-JC)*XM1(I1,J2))
C  ZC=SUM OF THE MUTUALS.
475    ZC=SUM+(2.D0*(XM1(I1,NT)))
C XZ IS THE TOTAL SELF INDUCTANCE
C  EQUATION 3.14 IS BEING APPLIED.
       XZ(I1)=ZC+ZL
       WRITE(6,451) I1,XZ(I1)
451    FORMAT(10X,I2,2X,D14.7)
       I1=I1+1
       ID=0
       J1=2
       IF(I1.GT.NL) GO TO 68
       IF(I1.LE.9) GO TO 50
       IF(I1.GT.10) GO TO 455
       NT=27
       GO TO 50
```

```
455    NT=26
       GO TO 50
C AB,CD
415    R1=BD
       R2=BC
       R3=AC
       R4=AD
       RL=AB
       RM=CD
       GO TO 200
C AB,DE
416    R1=BE
       R2=BD
       R3=AD
       R4=AE
       RM=DE
       V=XH1
       GO TO 80
C AB,EF
417    R1=BF
       R2=BE
       R3=AE
       R4=AF
       RM=EF
       GO TO 200
C BC,DE
418    R1=CE
```

```
      R2=CD
      R3=BD
      R4=BE
      RL=BC
      RM=DE
      GO TO 200
C BC,EF
419   R1=CF
      R2=CE
      R3=BE
      R4=BF
      RM=EF
      V=DT4
      GO TO 80
C BC,FA
420   R1=AC
      R2=CF
      R3=BF
      R4=AB
      RM=AF
      GO TO 200
C CD,EF
421   R1=DF
      R2=DE
      R3=CE
      R4=CF
      RL=CD
```

```
      RM=EF
      GO TO 200
C CD,FA
422   R1=AD
      R2=DF
      R3=CF
      R4=AC
      RM=AF
      V=DT4
      GO TO 80
C DE,FA
423   R1=AE
      R2=EF
      R3=DF
      R4=AD
      RL=DE
      RM=AF
      GO TO 200
 69   WRITE(6,601) IX,I1,J1,RL,RM,R1,R2,R3,R4,ID
 601  FORMAT(5X,I2,2X,I2,2X,I2,2X,D14.7,2X,D14.7,2X,D14.7,2X,D14.7
     &,2X,D14.7,2X,D14.7,2X,I1)
 68   STOP
      END
 $ENTRY
```

Appendix G

THE FORTRAN PROGRAM FOR COMPUTING SELF-INDUCTANCE USING THE CIRCULAR REPRESENTATION DEPICTED IN FIG. 3.13

```
C  THE COMPUTATIONS ARE FOR THE THE FOUR-SECTION TRANSFORMER;
C  THE ONE AVAILABLE FOR TESTS.
C  CALCULATION OF SELF INDUCTANCE FOR HV USING
C  NAGAOKA'S FORMULA ,GROVER'S EQN.(118),PAGE 143; THIS IS GIVEN
C  AS RELATION 3.18 IN THIS THESIS.
C  L=0.002(PI*PI)*A(2*A/B)*(N*N)*K
C  THE DIMENSIONS OF LENGTH ARE IN CENTIMETRES; THE INDUCTANCE
C  VALUES ARE IN MICROHENRIES.
C  A=RADIUS OF CIRCULAR REPRESENTATION OF A TURN (FIG.3.13)
C  B=HEIGHT
      REAL*8 ST1(101),STK(101),DELTA,PI,XH2,AOB,A,B,RK,XC,XL,RL
C  MATRIX STK CONTAINS THE VALUES OF k GIVEN AS A FUNCTION OF 2a/b.
C  THE VALUES OF 2a/b ARE CONTAINED IN MATRIX ST1.
C  IMMEDIATELY BELOW, THE TABLE OF k IS READ IN.
      READ,(STK(I),I=1,101)
      IJ=1
      ST1(1)=0.D0
11    IJ=IJ+1
      IF(IJ.GT.101) GO TO 8
      ST1(IJ)=ST1(IJ-1)+0.01D0
      GO TO 11
```

```
C  XH2=LENGTH OF A TURN; DENOTED BY X IN FIG. 3.8.
8      XH2=(26.234136D0)
       I=1
C  NL=NUMBER OF LAYERS IN EACH HV SECTION.
       NL=11
C  DELTA=TWICE RADIAL SEPARATION BETWEEN TWO CONSECUTIVE LAYERS.
       DELTA=0.41656D0
       PI=3.14159265359D0
C  N=46=NUMBER OF TURNS IN THE FIRST NINE LAYERS.
       N=46
       B=11.111125D0
3      A=(DSQRT(2.D0))*(9.D0/38.D0)*XH2
       AOB=B/(2.D0*A)
       IT=1
C  BELOW THE CONSTANT k IS FOUND BY INTERPOLATION IN THE TABLE.
2      IF(AOB.LE.ST1(IT)) GO TO 1
       IT=IT+1
       IF(IT.LE.101) GO TO 2
       GO TO 10
1      XC=ST1(IT)-AOB
       XL=ST1(IT)-ST1(IT-1)
C  RK REPRESENTS k.
       RK=STK(IT)-((STK(IT)-STK(IT-1))*(XC/XL))
       RL=0.004D0*PI*PI*A*A*N*N*RK/B
       WRITE(6,12) I,RL
12     FORMAT(20X,I2,2X,D14.7)
       I=I+1
```

```
      IF(I.GT.NL) GO TO 10
      IF(I.EQ.NL) GO TO 5
      IF(I.EQ.10) GO TO 7
      GO TO 6
C  N=26 FOR THE ELEVETH LAYER AND 27 FOR THE TENTH.
7     N=27
      B=B*(27.D0/46.D0)
      GO TO 6
5     B=B*(26.D0/27.D0)
6     XH2=XH2+DELTA
      GO TO 3
10    STOP
      END
$ENTRY
C The data which is supposed to follow is given in Table
  36 [21].
```

Appendix H

EMTP COMPANION NETWORK MODELS

The Capacitor Model

Consider a capacitive branch j,k shown in Fig. H1. For a capacitor,

$$ej(t) - ek(t) = (1/C)\int ij,k(t)dt$$

Carrying out integration from the known state at time $(t - dt)$ to the unknown state at t:

$$ej(t) - ek(t) = (1/C)\int_{t-dt}^{t} ij,k(t)dt + ej(t-dt) - ek(t-dt) \qquad (1)$$

Applying the trapezoidal rule of integration to the integral in relation (1) yields:

$$ej(t) - ek(t) = (dt/2C)\{ij,k(t) - Ij,k(t-dt)\}$$

Therefore,

$$ij,k(t) = (2C/dt)\{ej(t) - ek(t)\} + Ij,k(t-dt) \qquad (2)$$

with the current source Ij,k known from the past history:

$$Ij,k(t-dt) = -ij,k(t-dt) - (2C/dt)\{ej(t-dt) - ek(t-dt)\} \qquad (3)$$

The equivalent impedance network corresponding to equation (3) is shown in Fig. H2.

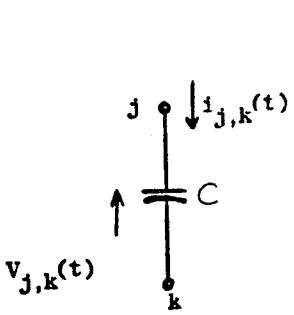

FIG. H1: Capacitive Branch

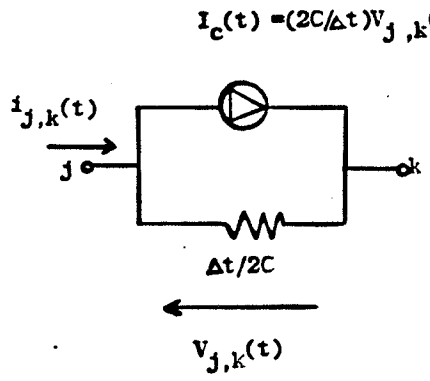

FIG. H2: Capacitor Model

Inductor Model

For the inductance L of a branch j,k (Fig. H3) the following relationship holds:

$$ej(t) - ek(t) = L[(dij,k(t)/dt]$$

Integrating from the known state at t-dt to the unknown state at t gives:

$$ij,k(t) = ij,k(t-dt) + (1/L)\int_{t-dt}^{t}(ej - ek)dt \qquad (4)$$

Using the trapezoidal rule of integration yields:

$$(1/L)\ (ej-ek)dt = (dt/2L)[\{ej(t)-ek(t)\} -\{ej(t-dt)-ek(t-dt)\}]$$

Substituting for the integral in (4) yields:

$$(1/L)\ (ej -ek)dt = (dt/2L)[\{ej(t) -ek(t)\} - \{ej(t-dt) - ek(t-dt)\}]$$

$$(dt/2L)[ej(t) - ek(t)] + Ij,k(t-dt) \qquad (5)$$

where the equivalent source is known from the past history:

$$Ij,k(t-dt) = ij,k(t-dt) + (dt/2L)\{ej(t-dt) - ek(t-dt)\} \qquad (6)$$

The equivalent impedance network corresponding to relation (6) is depicted in Fig. H4.

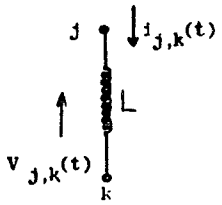

FIG. H3: Inductor

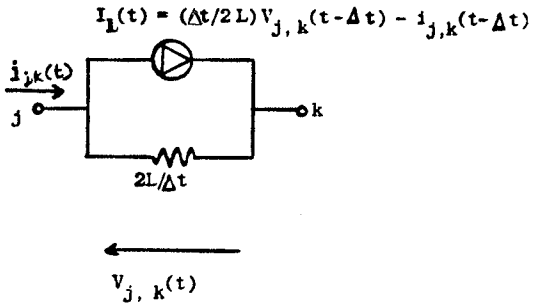

FIG. H4: Inductor Model

Appendix I

SIMPLIFICATION OF THE EQUIVALENT CIRCUIT OF THE TRANSFORMER

Consider two identical series-connected circuit segments depicted in Fig. I1(a). The two segments are equivalent to the network shown in Fig. I1(b).

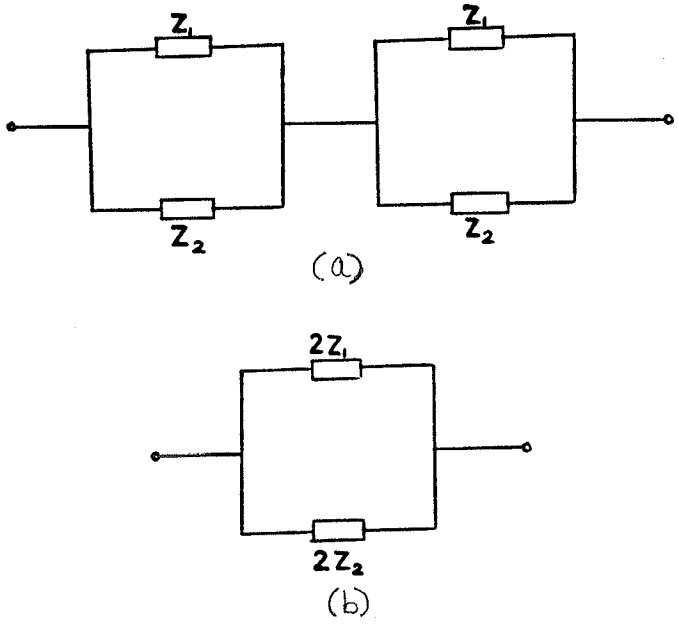

FIG. I1:

(a) Two Identical Series-connected Circuit Segments

(b) Simplified Equivalent Network

For the network portions of the transformer shown in Fig. I2, it has been assumed that the two consecutive layers are identical, that is, Ri = Rj, Li = Lj and Ci = Cj.

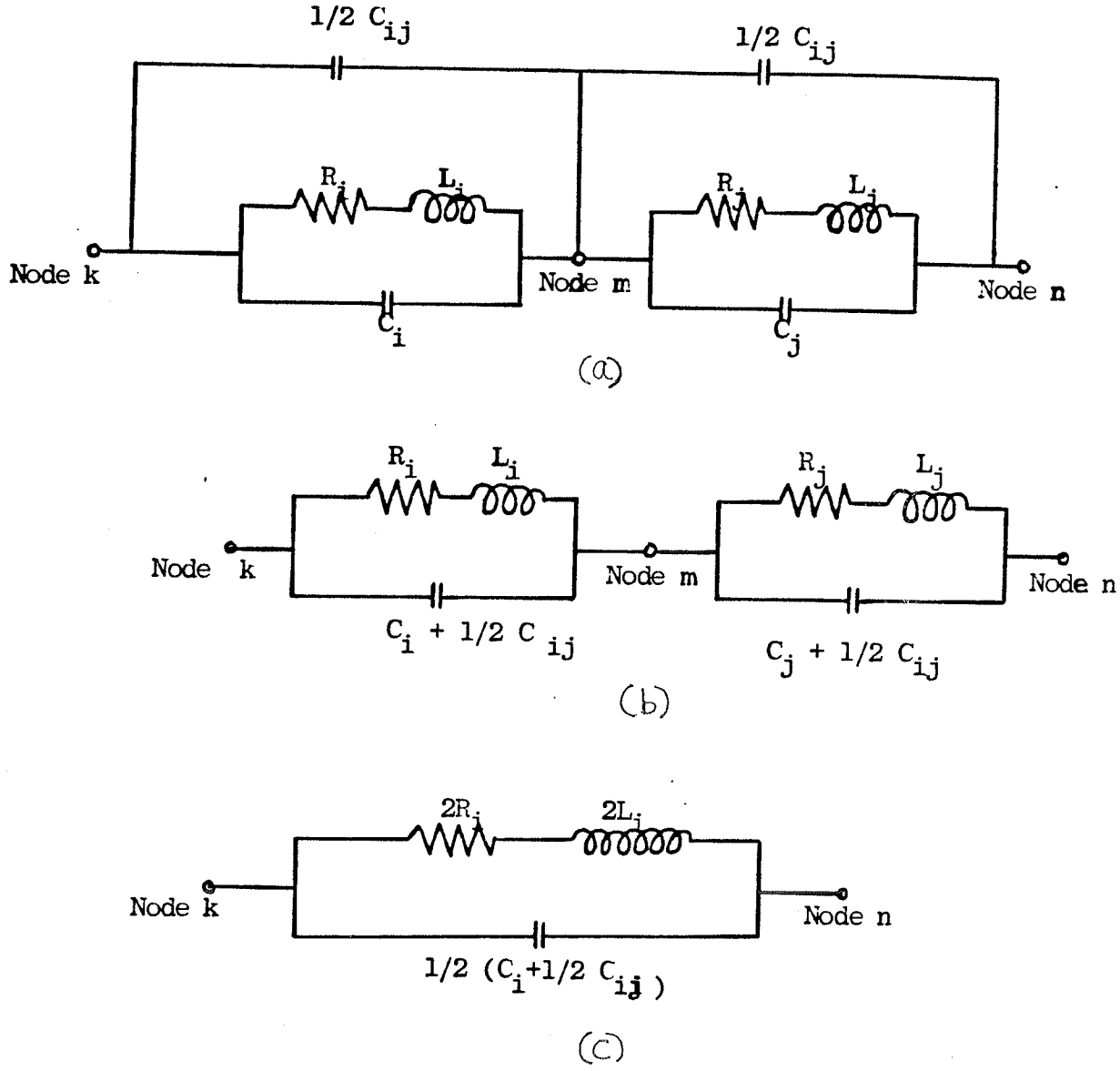

FIG. I2:

(a) Electric Network Equivalent of two consecutive Transformer Layers

(b) Simplified Equivalent Network

(c) Further Simplified Equivalent Network

Let Z be the equivalent impedance between nodes k and n. At an angular frequency w, and if there is no mutual coupling between the inductors,

$$Z = \frac{2\{(R \pm jwL)\,1/jwC\}}{R + jwL + 1/jwC} = \frac{(2R \pm 2jwL)\,2/jwC}{2R + 2jwL + 2/jwC} \qquad (1)$$

Therefore, combining the two circuit portions, shown in Fig. I2(a), involves doubling the inductance and resistance values and halving the figure of capacitance. If there is mutual coupling (Mij) between the inductive elements, the inductance value of the equivalent circuit, shown in Fig. I2(c), is given by:

$$L = 2(Li \pm Mij)$$

The positive sign is used for positive coupling and the negative sign applies in the case of negative coupling.

The results of the computation of the transformer winding constants (Chap. III) revealed that there is no significant difference between the values of circuit elements of any two consecutive layers, except for the ninth and tenth layers because the number of turns in each of the two outermost layers (tenth and eleventh) is much less than that in each of the first nine layers. Therefore, the above method of reducing the equivalent networks of identical layers can be used in the simplification of the electric circuit segments of the transformers.

One section of the high-voltage winding is shown in Fig. 2.3. But, the section-to -section and layer-to-earth capacitances are so small (less than 5 pF) that they can be neglected to obtain the network shown in Fig. I3. In fact the results of the EMTP simulation carried out with and without accounting for these capacitors are virtually identical.

In order to illustrate the simplification of the network in Fig. I3, consider the first three and last two layers. The circuit in Fig. I4 is replaced by its equivalent, depicted in Fig. I5, by carrying out star-to-delta transformation on the first and last layers. By suitably combining the capacitive elements in Fig. I5, the circuit shown in Fig. I6 is obtained. The circuit representations of layers (marked 1 and 11 in Fig. I6), are then paired as indicated by the double-headed arrows. Since voltage stresses are generally most severe in layers closest to the line end and those nearest to the low-voltage winding (practically at ground potential), it is essential that the impulse voltage distribution in these layers is predicted very accurately. Hence, the layers marked 1, 10 and 11 in Fig. I6 were not paired.

The network obtained after the circuit reduction is given in Fig. I7. Further simplification of the network is carried out by pairing the circuit segments of Fig. I7 as indicated by the arrows. This simplification leads to a circuit representation shown in Fig. I8.

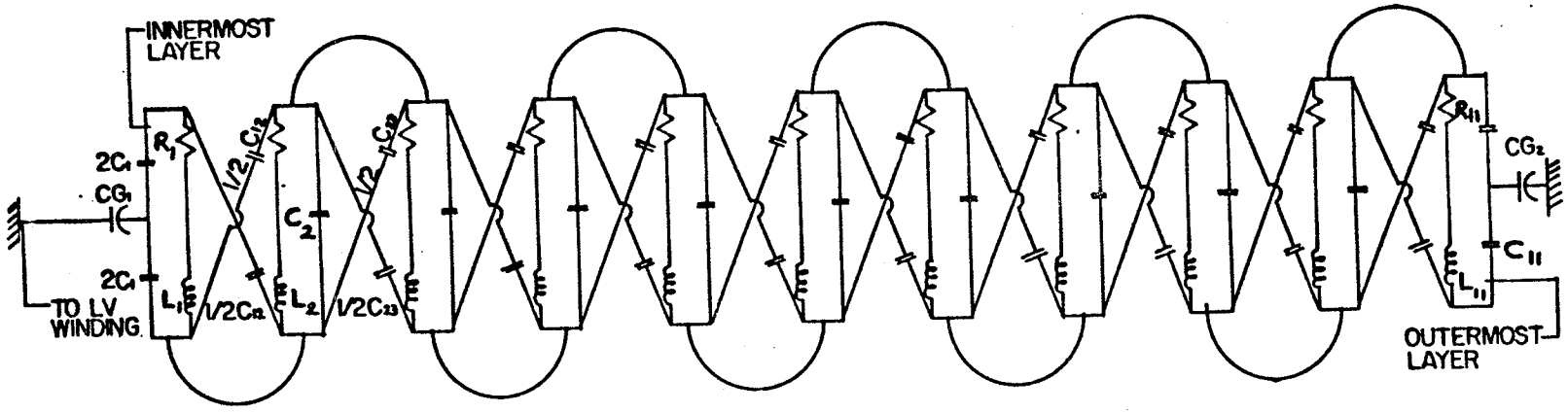

FIG. I3: Electrical network equivalent of a transformer section; section-to-section and layer-to-earth capacitances excluded.

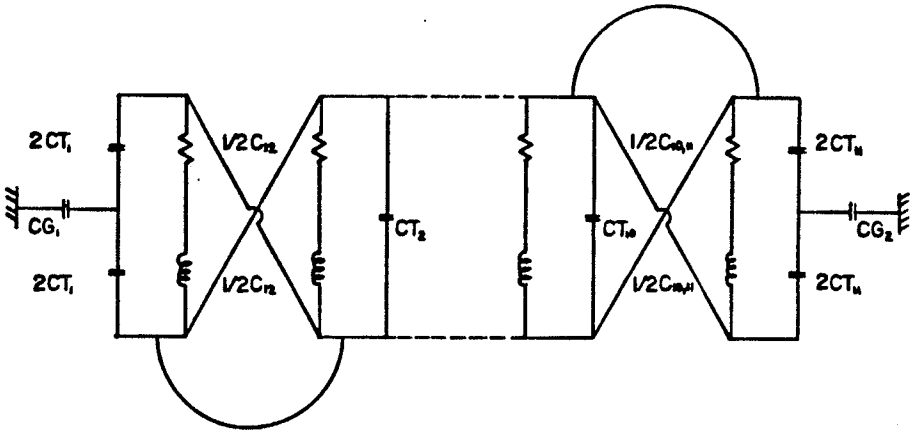

FIG. I4 : Innermost three and outermost two layers of the transformer section.

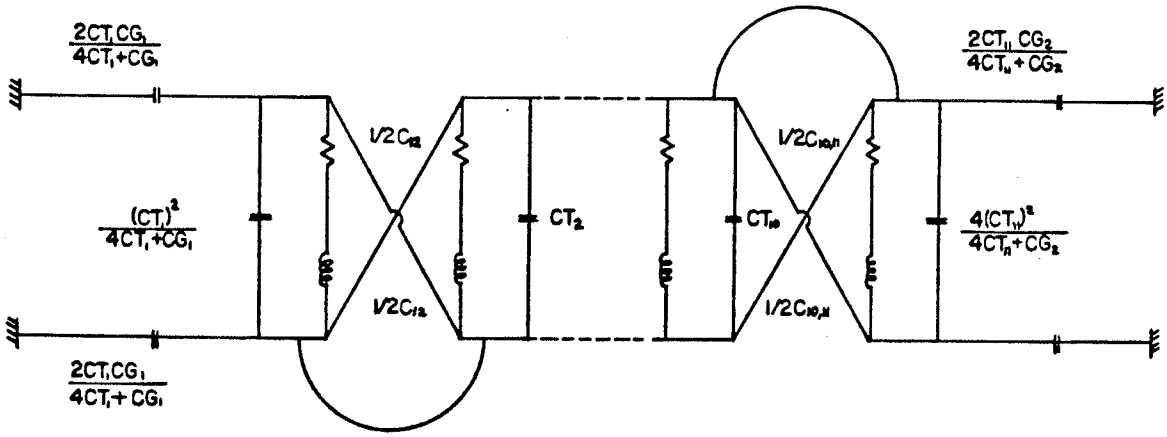

FIG. I5: Application of star-delta transformation to innermost and outermost layers in Fig. I4.

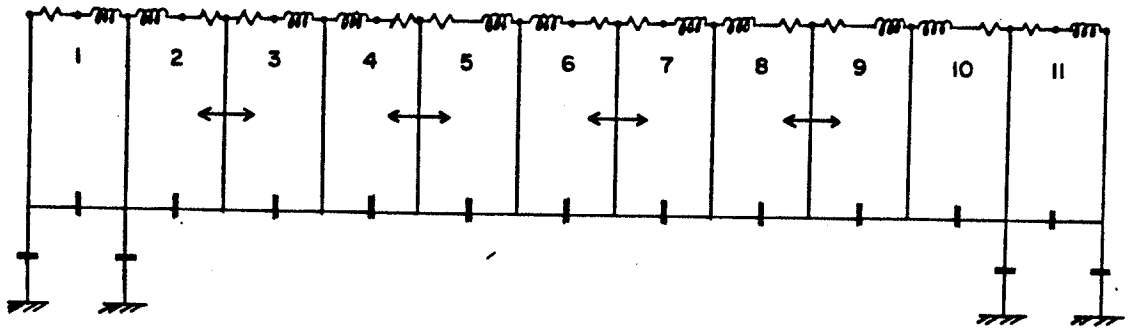

FIG. I6: Network obtained by combining the capacitive elements in Fig. I5.

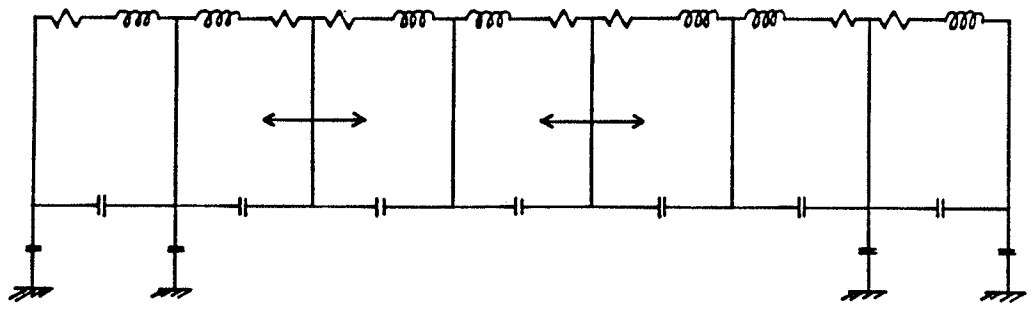

FIG. I7: Reduced network.

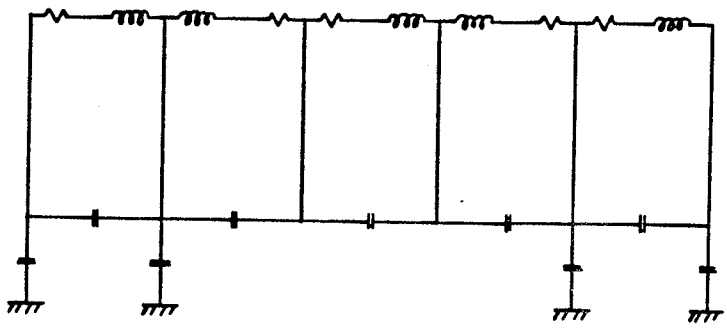

FIG. I8: Further reduced network.

Appendix J

THE EMTP JOB FORMAT

A problem to be solved by the EMTP must be described in a data set composed of the following parts, in the order as listed:

1. Cards to begin new data case.
2. Specially-requested extension to miscellaneous data cards.
3. Cards which define Transient Analysis of Control Systems, TACS, if any.
4. Cards for linear and nonlinear branches, transformers, and transmission lines (or cables), terminated by a blank card.
5. Cards for electric-network switches, diodes, AC/DC converter valves, switched-resistance elements, and switched-inductance elements, terminated by a blank card.
6. Source cards for electric network voltage sources, current sources, and dynamic synchronous machines. These are also terminated by a blank card.
7. Cards for overriding the internally-calculated initial conditions which come from the phasor steady-state network solution.
8. Node-voltage output specification cards.
9. Cards for specifying type 1-10 EMTP source functions point-by-point. There is one card at each time-step, terminated by a "9999" card.

10. Batch-mode plotting cards, terminated by a blank card.
11. "BEGIN NEW DATA CASE" card, terminated by a blank card.

Appendix K

PROPERTIES OF RTEmp

RTEmp fluid is a high fire point liquid dielectric-coolant formulated for use in transformers or other apparatus where its electrical and thermal properties are advantageous. It is a high molecular weight, paraffinic hydrocarbon material. Its biodegradability and low toxity have made it eminently satisfactory to environmentalists. It is fully miscible and compatible with mineral oils.

Its principle applications are as a dielectric-coolant in transformers, as a retrofill and makeup fluid for askarel transformers, and as a dielectric in switching equipment. In Tables K1-K3, some properties of RTEmp fluid are listed.

TABLE K1: Electrical properties of RTEmp fluid

Property	Temperature	Value
Dielectric strength (ASTM D-877) (kV)	25 °C	43
Dielectric constant	25 °C	2.38
Power factor (%)	25 °C	$<10^{-3}$
	100 °C	0.4
Volume resistivity (ASTM D-1169) Ω cm	25 °C	8×10^{12}

TABLE K2: Physical and chemical properties of RTEmp

Property	Temperature	Value
Specific gravity	25°C	0.877
Interfacial tension (dyne/cm)	25°C	38
Neutralization number (mgKOH/gram)		$<5X10^{-3}$
Viscosity (centistokes)	0°C	2750
	25°C	350
	50°C	85
	100°C	16
	150°C	5.5

TABLE K3: Thermal properties of RTEmp

Property	Value
Flash point (ASTM D-92) (°C)	285
Fire point (ASTM D-92) (°C)	312
Auto-ignition (°C)	540
Pour point (ASTM D-97) (°C)	-30
Thermal conductivity (cal./(sec.cm^2°C/cm)) 25°C	$3.1X10^{-4}$
Specific heat (cal./gm/°C) 25°C	0.46
Coefficient of expansion (cc/cc/°C) 25°C	$7.5x10^{-4}$